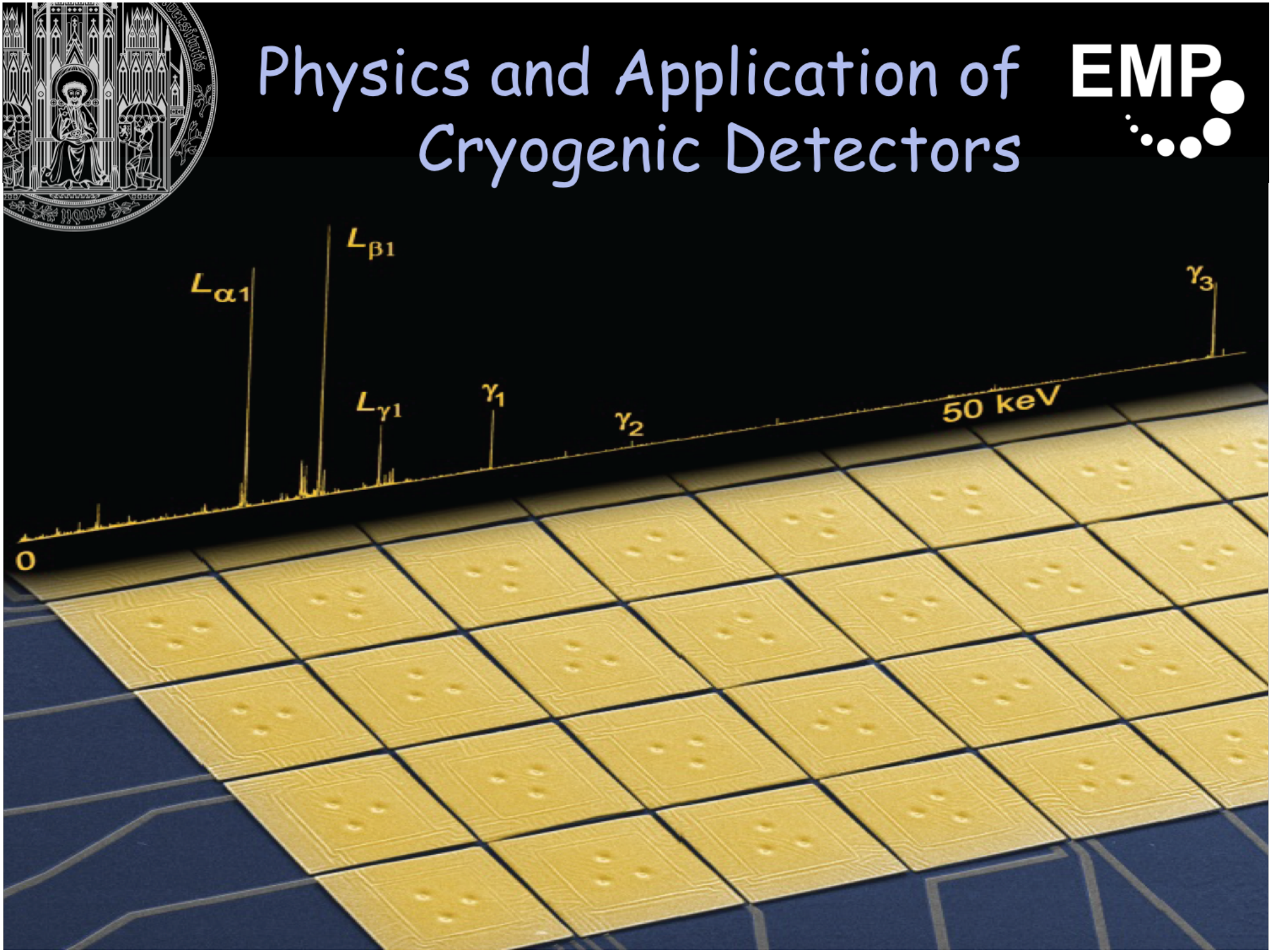
Physics and Application of
Cryogenic Detectors
EMP
$L_{\beta 1}$
$L_{\alpha 1}$
$L_{\gamma 1}$
γ_1
γ_2
γ_3
50 keV
0

History of Cryogenic Particle Detectors

~1845	Mayer, Joule	heat is a form of energy
1876	Langley	bolometer for ir-observations of sun
1903	Curie, Laborte	calorimetric detection of radioactivity
1935	Simons	cryogenic calorimeters
1939	Andrews	superconducting transition calorimeter
1949	Andrews, Fowler, Williams	detection of single α particle with a superconducting calorimeter
•		
•		
•		
1984	Fiorini, Niinikoski, Moseley, Mather, McCammon	modern type cryogenic particle detectors
today		over 500 scienties are working in this field

S.P. Langley (1834-1906)

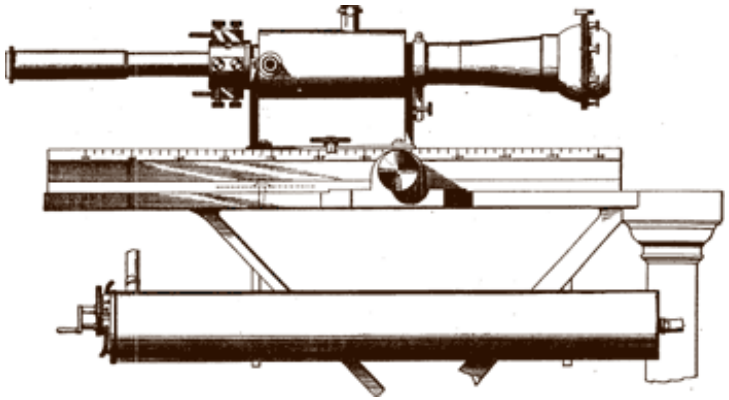

What Can One Measure With Low Temperature Detectors?

Photons

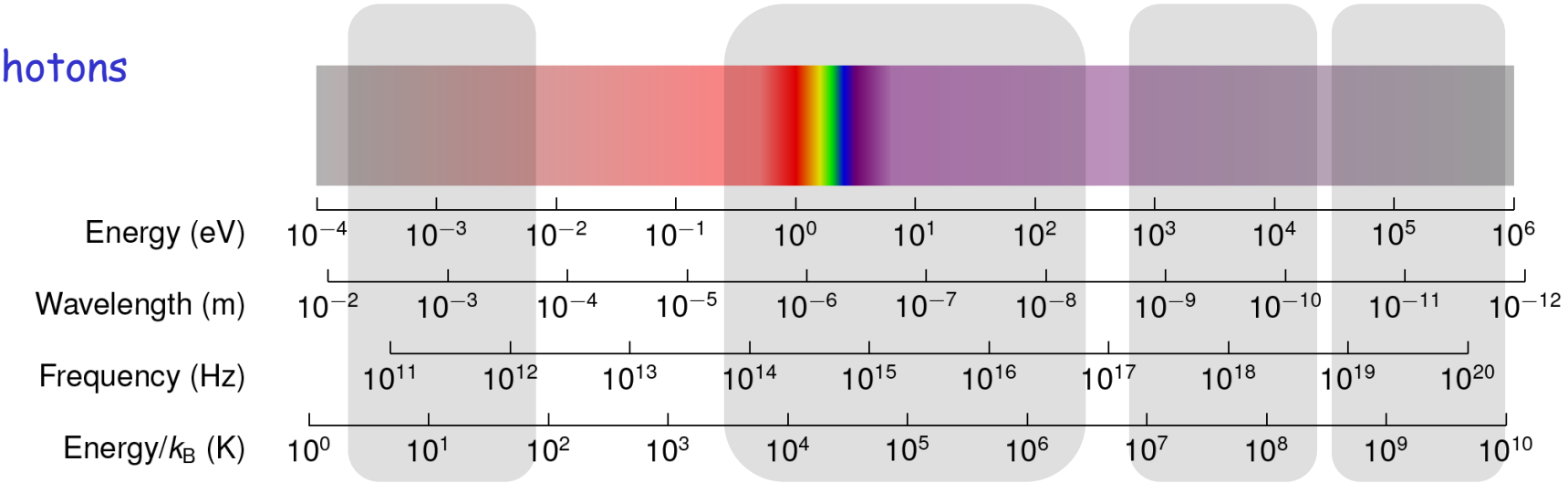

Matter

Mass Spectrometry (Mass 1 – 106 u, Energy 1 – 300 keV)
Heavy Ion Physics (^{4}He – ^{238}U, E 0.1 – 400 MeV/u)
α-particles (1 – 10 MeV)
β-particles
Neutinos

Other

Dark Matter (WIMPs)
Axions
Dark Photons
Primordial Gravity Waves ...

Applications:

nuclear physics, neutrino mass, WIMPs,
nuclear forensic, double beta decay,
metrology, atomic physics,
material analysis, mass spectrometry,
α,β,γ spectroscopy, astronomy, ...

Detector Concepts: Calorimeters

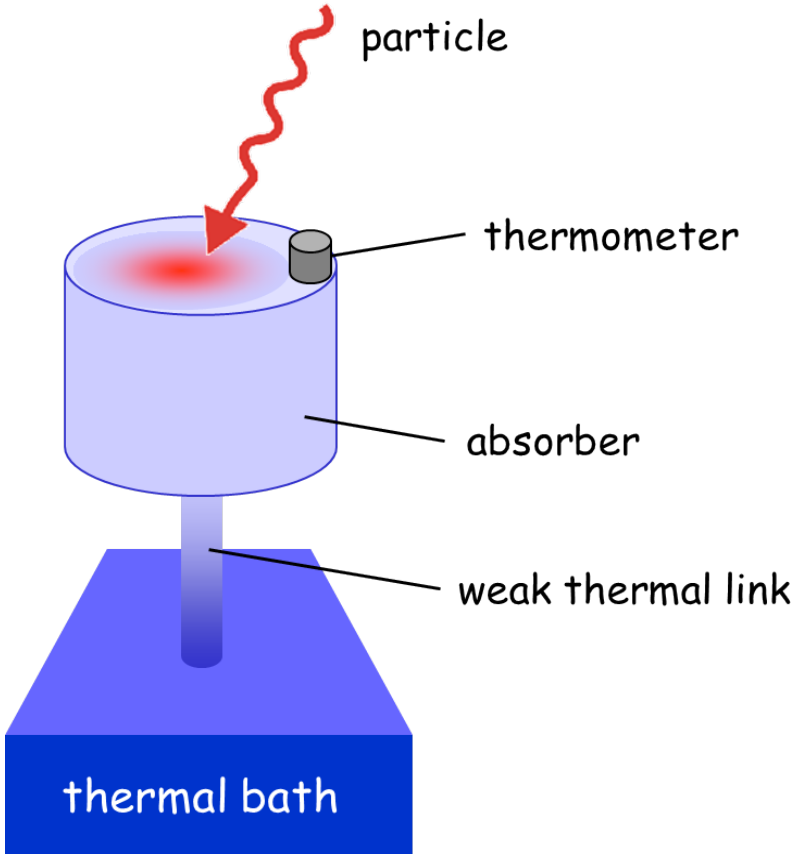

$$\delta T = \frac{E}{C_{\mathrm{tot}}}$$

C_{tot} : phonons
electrons
spins
tunneling states
quasi particles

Thermal relaxation time:

$$\tau = \frac{C_{\mathrm{tot}}}{G}$$

Thermal conductance

Detector Concepts: Calorimeters

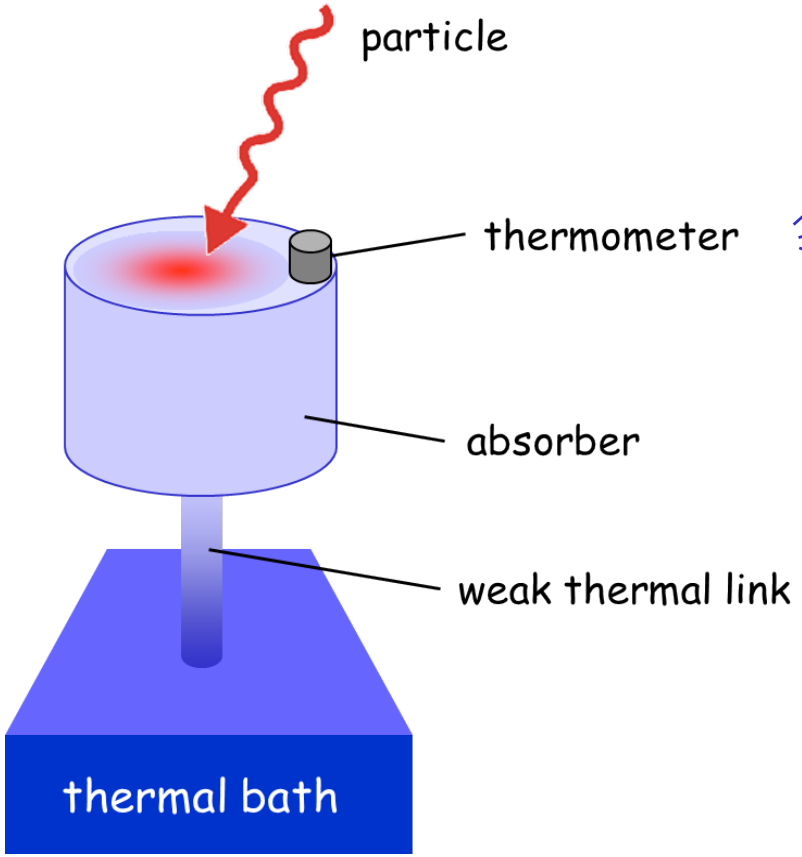

TES Transition Edge Sensors

MMC Metallic Magnetic Calorimeter

NTD Semiconductor Thermistors

Single Event

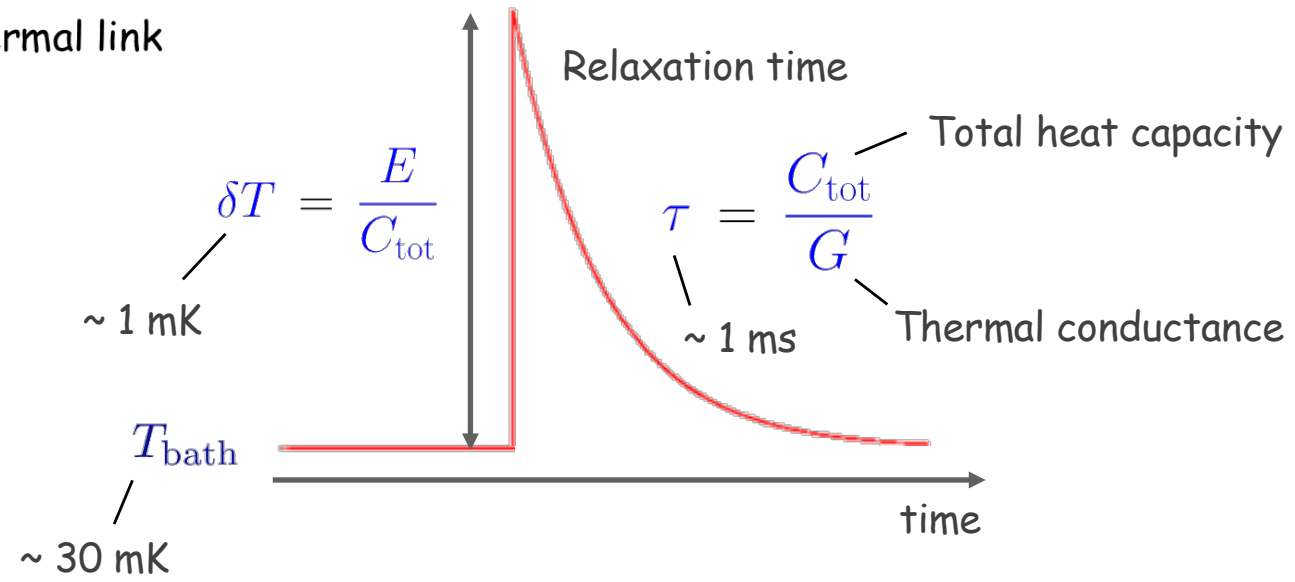

Ideal Calorimeter

- canonical ensemble
- ideal energy measurement $E(t)$:
  arbitrarily fast and accurate

response function:

$$|\widetilde{E}(f)| = E_0 \frac{2\tau}{\sqrt{1+(2\pi f\tau)^2}}$$

spectral noise density:

$$\sqrt{S_E(f)} = \sqrt{k_B C T^2}\,\frac{2\sqrt{\tau}}{\sqrt{1+(2\pi f\tau)^2}}$$

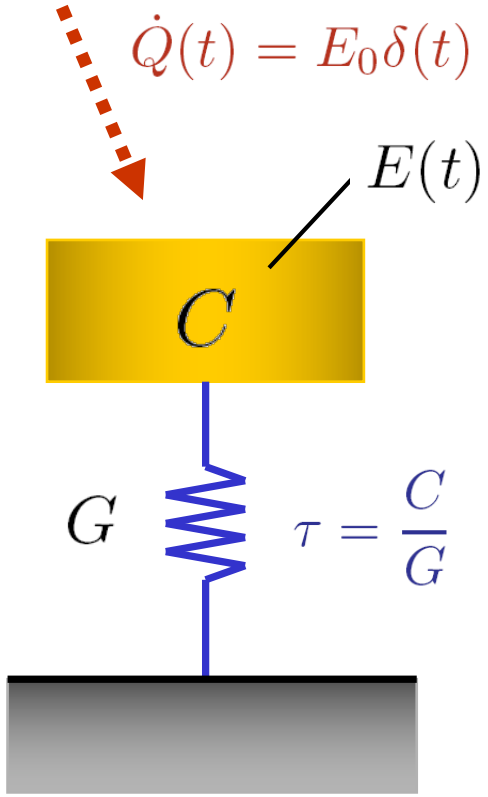

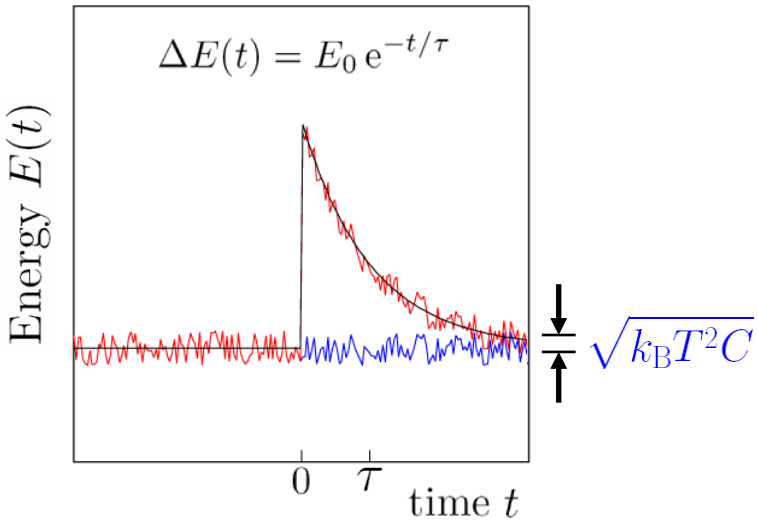

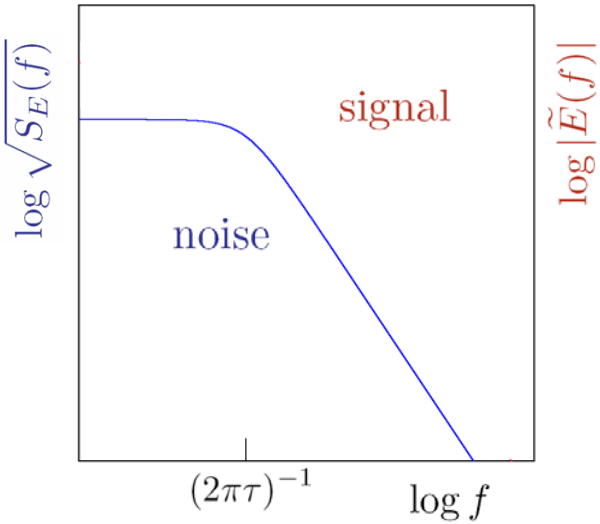

- signal to noise ratio independent of frequency

$$SNR = \frac{\sqrt{S_E(f)}\;\Delta f}{|\widetilde{E}(f)|\;\;\Delta f} = \text{const.}$$

- infinite bandwidth: $\Delta E \to 0$!

FiniteThermometer-Absorber Coupling

$$C_{\rm a}\frac{{\rm d}T_{\rm a}}{{\rm d}t} = -(T_{\rm a}-T_{\rm t})G_{\rm at} - (T_{\rm a}-T_{\rm b})G_{\rm ab} - P_{\rm at}(t) - P_{\rm ab}(t) + \dot{Q}(t)$$

$$C_{\rm t}\frac{{\rm d}T_{\rm t}}{{\rm d}t} = -(T_{\rm t}-T_{\rm a})G_{\rm at} + P_{\rm at}(t)$$

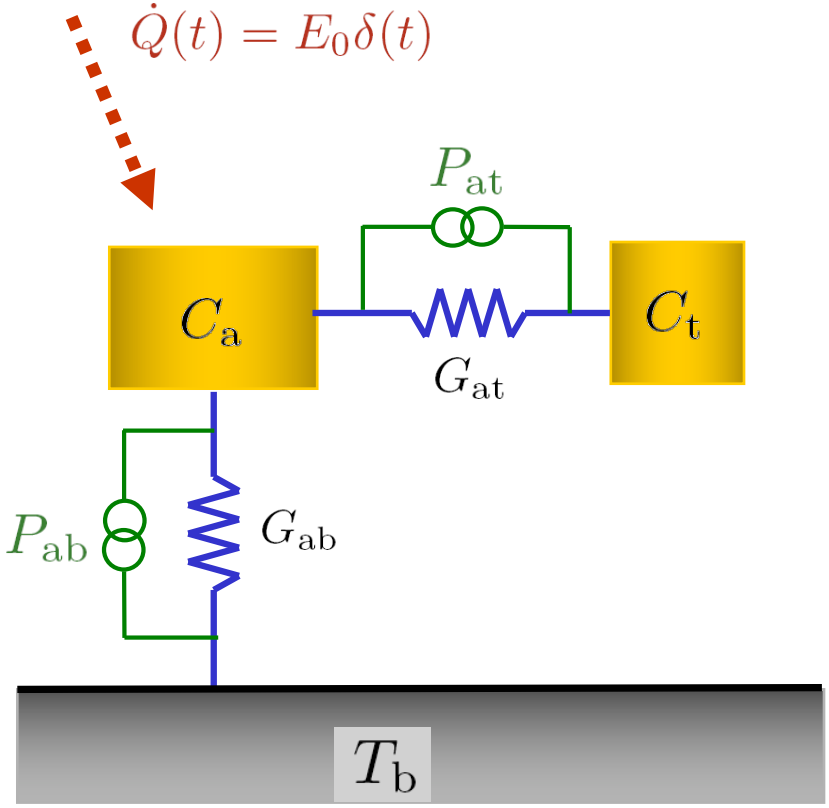

Signal: $G_{\rm ab} \ll G_{\rm at}$, $P_{\rm at} = P_{\rm ab} = 0$

$$E_{\rm t}(t) = E_0\frac{C_{\rm t}/G_{\rm ab}}{\tau_1-\tau_0}\left[{\rm e}^{-t/\tau_1} - {\rm e}^{-t/\tau_0}\right]$$

$$\tau_0 = \frac{1}{G_{\rm at}}\left(\frac{C_{\rm a}C_{\rm t}}{C_{\rm a}+C_{\rm t}}\right)$$

$$\tau_1 = \frac{1}{G_{\rm ab}}(C_{\rm a}+C_{\rm t})$$

Noise: $\dot{Q}(t) = 0$

$$S_{E{\rm t}}(f) = k_{\rm B}C_{\rm t}T^2\left[\left(1-\frac{C_{\rm t}}{C_{\rm a}+C_{\rm t}}\right)\frac{4\tau_0}{1+(2\pi f\tau_0)^2} + \left(\frac{C_{\rm t}}{C_{\rm a}+C_{\rm t}}\right)\frac{4\tau_1}{1+(2\pi f\tau_1)^2}\right]$$

Finite Thermometer-Absorber Coupling

$$E_t(t) = E_0 \frac{C_t/G_{ab}}{\tau_1 - \tau_0}\left[e^{-t/\tau_1} - e^{-t/\tau_0}\right]$$

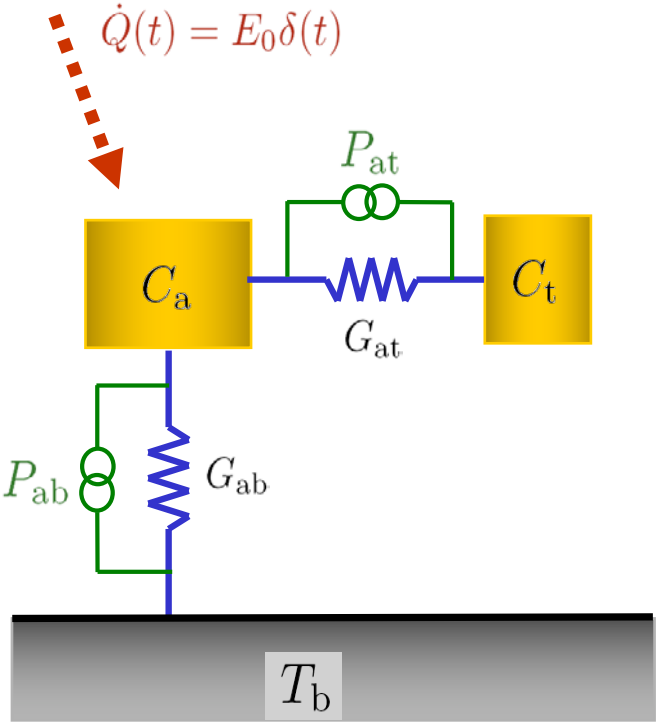

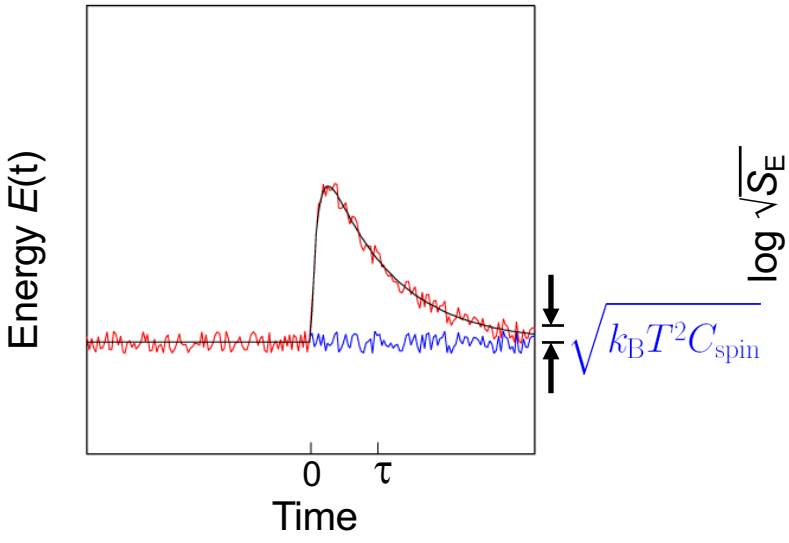

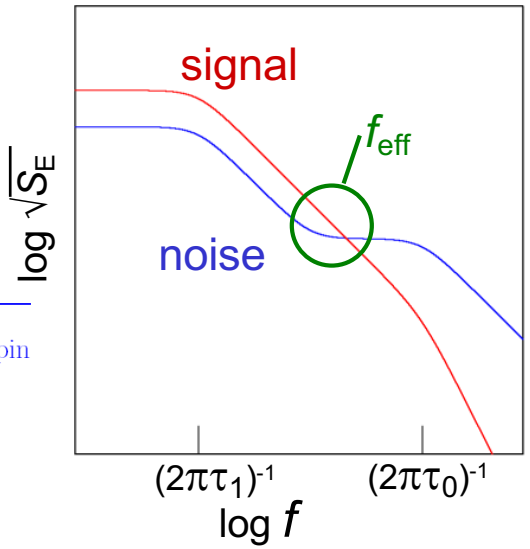

- signal to noise ratio frequency dependent
- optimal bandwidth $f_{eff}(C_a, C_t, \tau_0, \tau_1)$
- finite energy resolution ΔE_{FWHM}

Theoretical Resolution – Noise Sources

SNR frequency dependent

$$SNR^2(t) = \frac{SNR^2(f \to 0)}{1 + (f/f_{\mathrm{eff}})}$$

energy resolution:

$$\Delta E_{\mathrm{rms}} = \sqrt{\int_0^\infty SNR^2(f)\,\mathrm{d}f}$$

$$\Delta E_{\mathrm{rms}} = \sqrt{4k_{\mathrm{B}}T^2C_{\mathrm{a}}}\left[\frac{G_{\mathrm{ab}}}{G_{\mathrm{at}}} + \frac{G_{\mathrm{ab}}^2}{G_{\mathrm{at}}^2}\right]^{-1/4}$$

additional noise sources:

- preamplifier noise: white noise, 1/f noise, …
- Johnson noise
- discret noise sources: vibrations, electrical interference, ….

- excess noise: additional unexplained noise

Semiconducting Thermistors

S.H. Moseley, J.C. Mather, D. McCammon, J. Appl. Phys. 56, 1257 (1984)

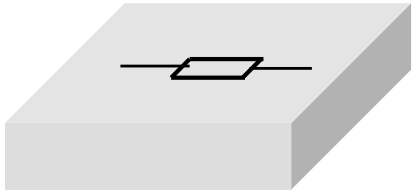

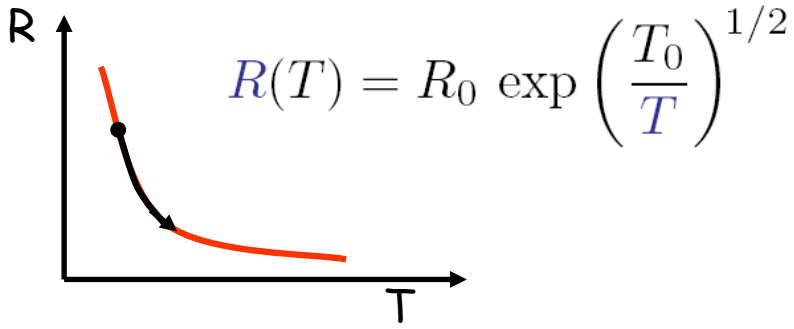

Si – ion-implanted (P,B)

Ge NTD (Neutron-Transmutation-Doped)

High impedance device

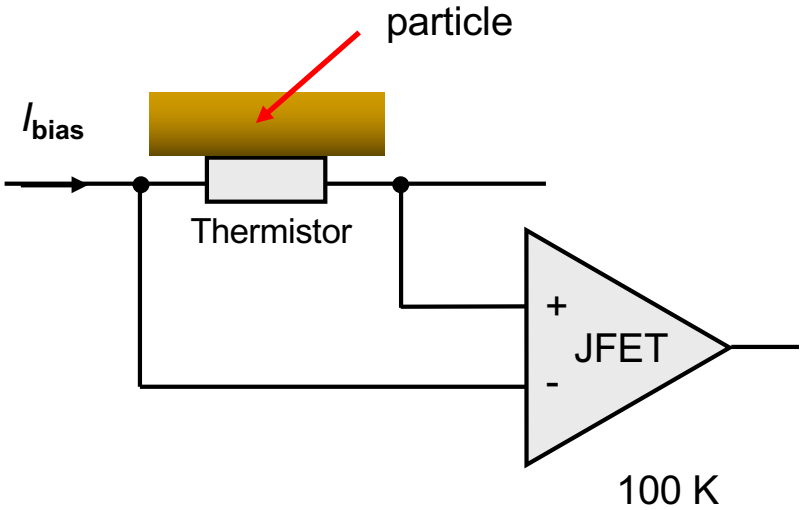

Main applications:

X-ray detection

dark matter detection

rare event search in nuclear physics

Hopping Conduction – Variable Range Hopping

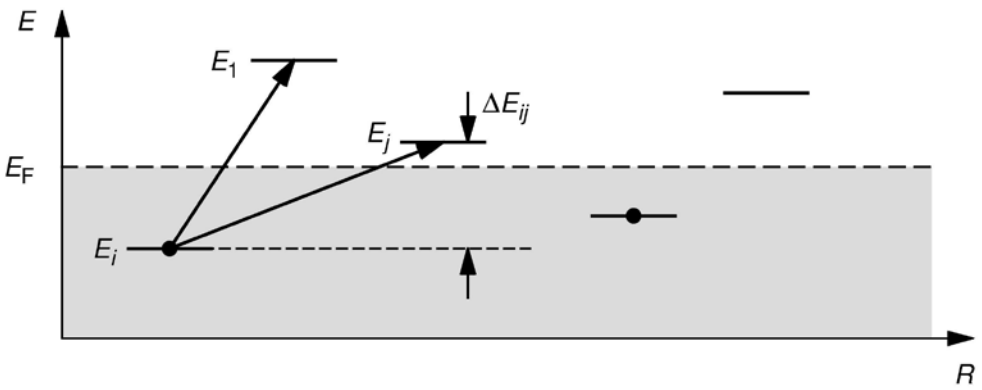

probability of hopping

$$P_{ij} = \nu_0 \exp\left(-\frac{\Delta E_{ij}}{k_B T} - 2\alpha R_{ij}\right)$$

wave function overlapp

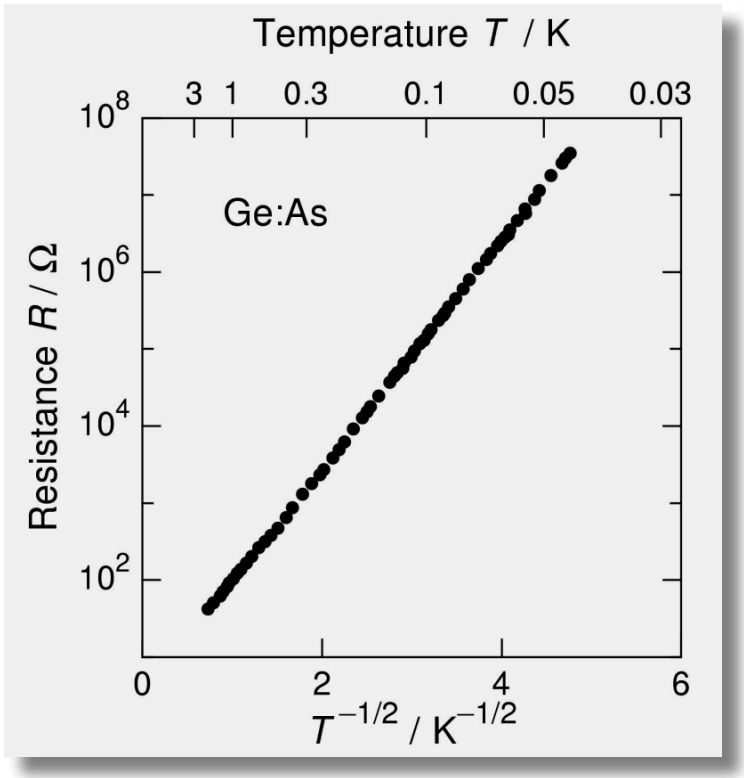

W. Schoepe

$$R(T) = R_0 \exp\left(\frac{T_0}{T}\right)^p$$

1/4 constant density of states

1/2 Coulomb gap

T_0 ~ doping density

Resolution at 6 keV

implanted Si, HgTe absorber
0.4 mm x 0.4 mm

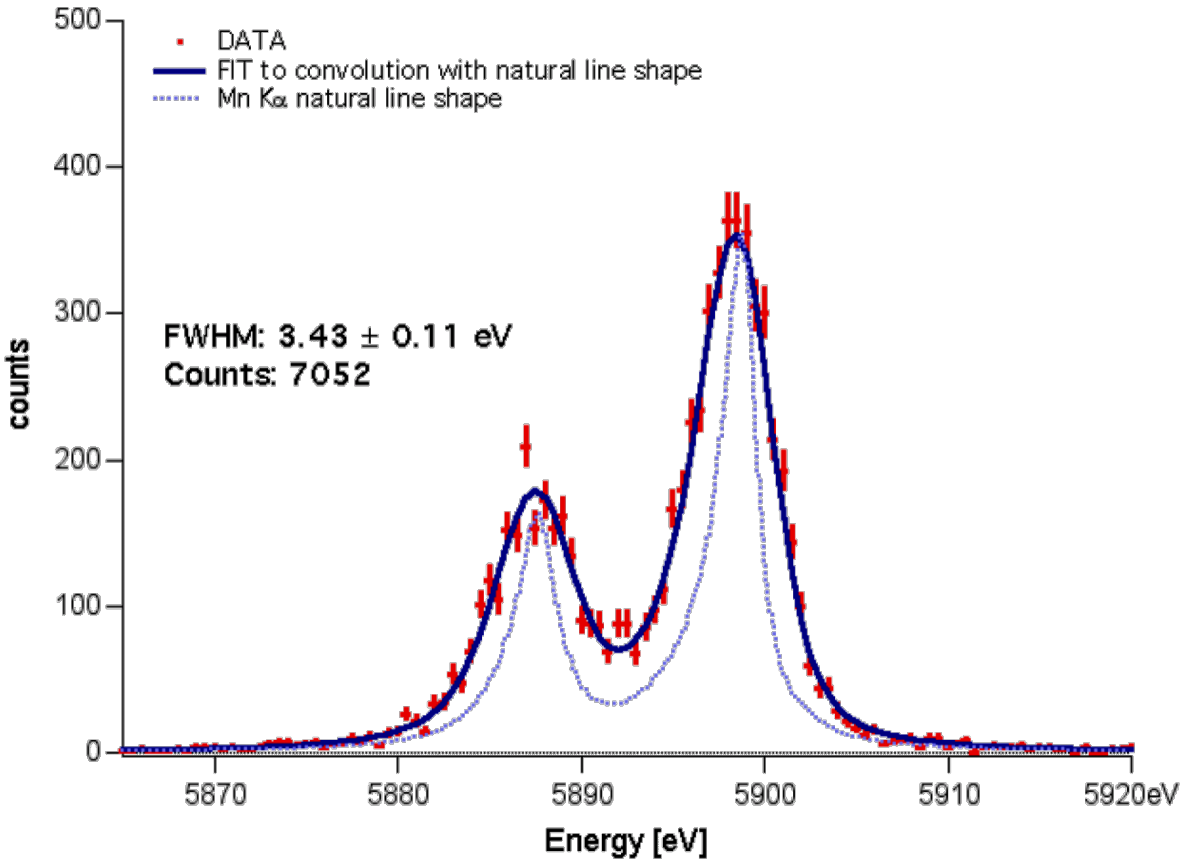

3.4 eV at 5.9 keV

→ $\Delta E / E < 1$ ‰

Quantum efficiency: ~ 100%

F. S. Porter et al. 2009

X-Ray Astronomy with Thermistors

Hitomi Focal Plane Detector: SXS

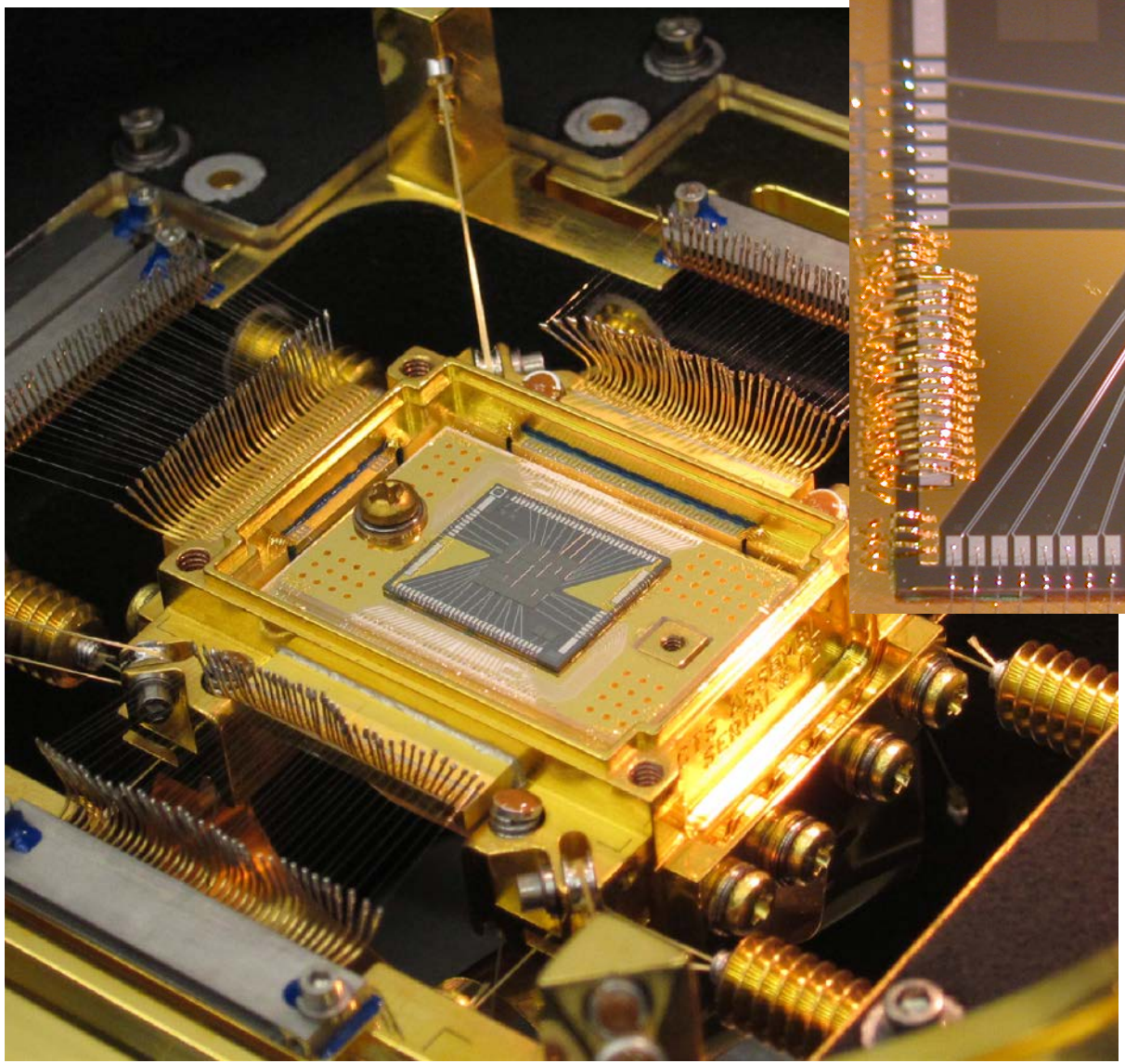

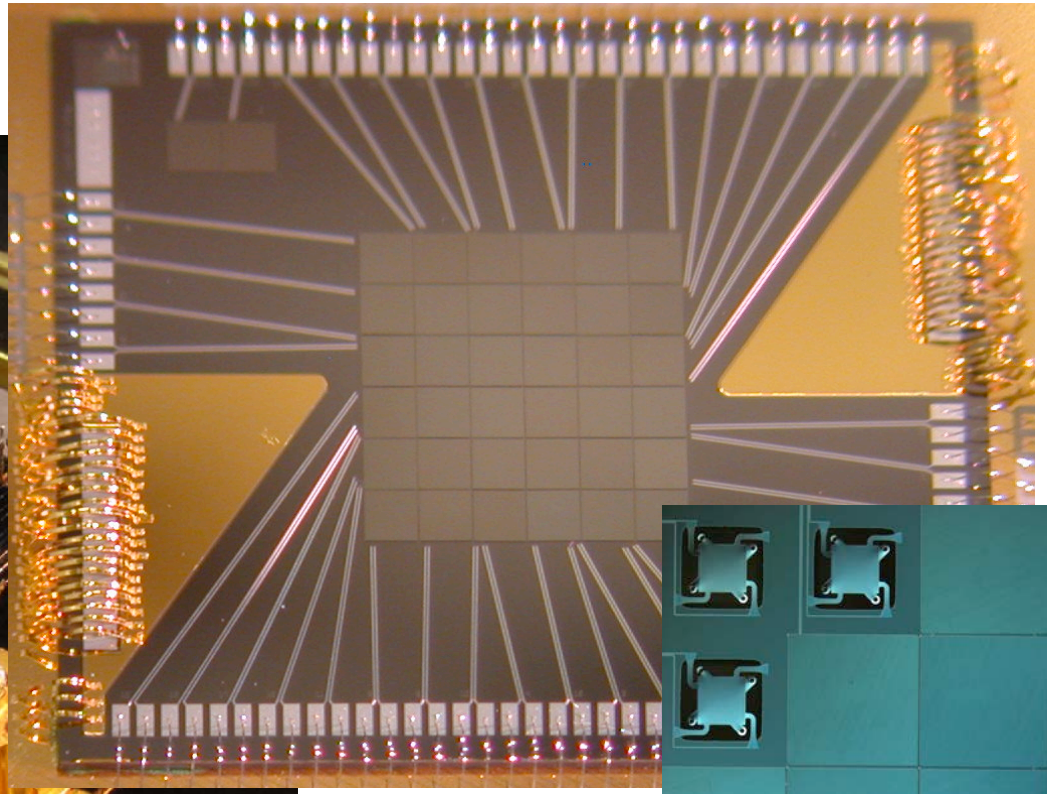

6 x 6 array

~ 4.2 eV resolution

implanted Si, HgTe absorber
0.8 mm x 0.8 mm

X-Ray Astronomy with Thermistors

He-Dewar holdtime > 3 years !

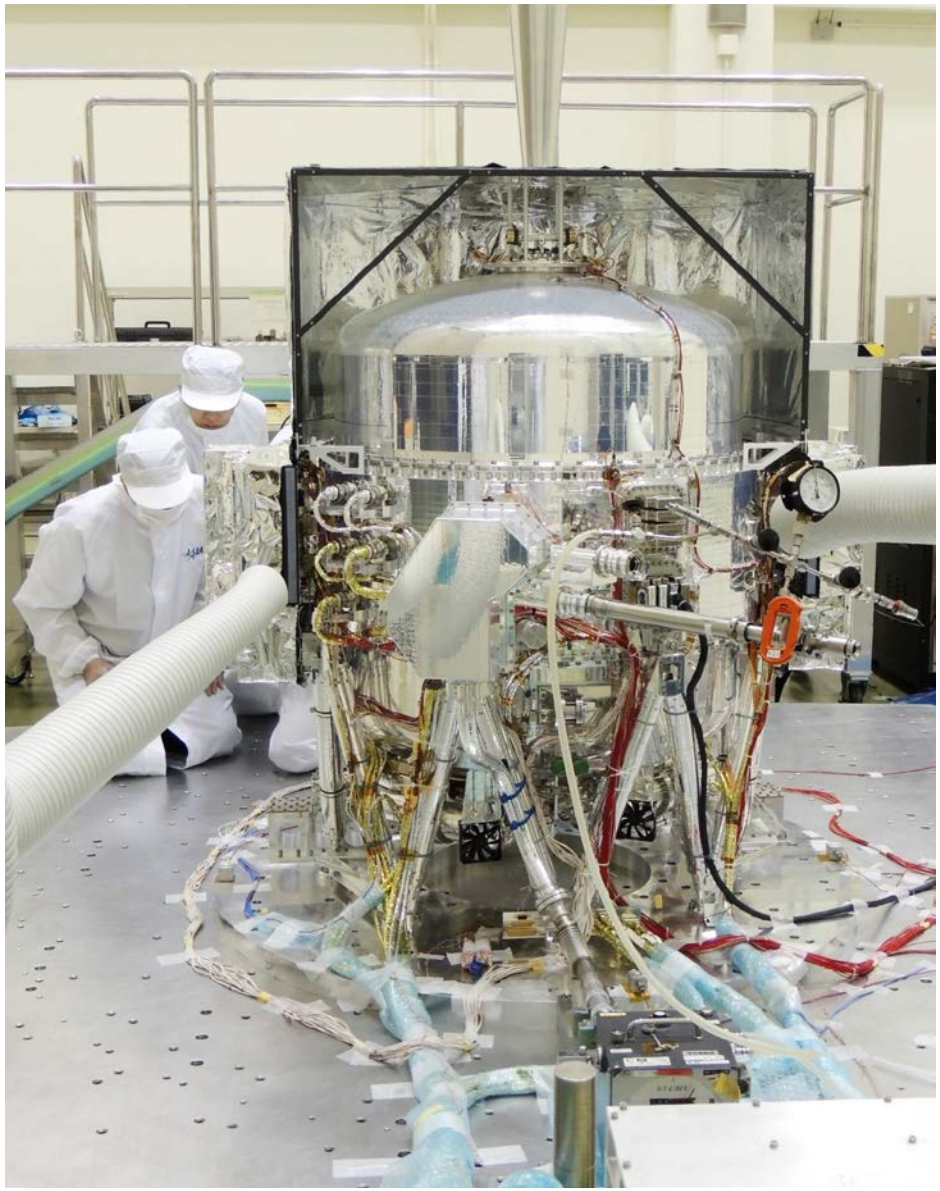

X-Ray Astronomy with Thermistors

Hitomi Satellit

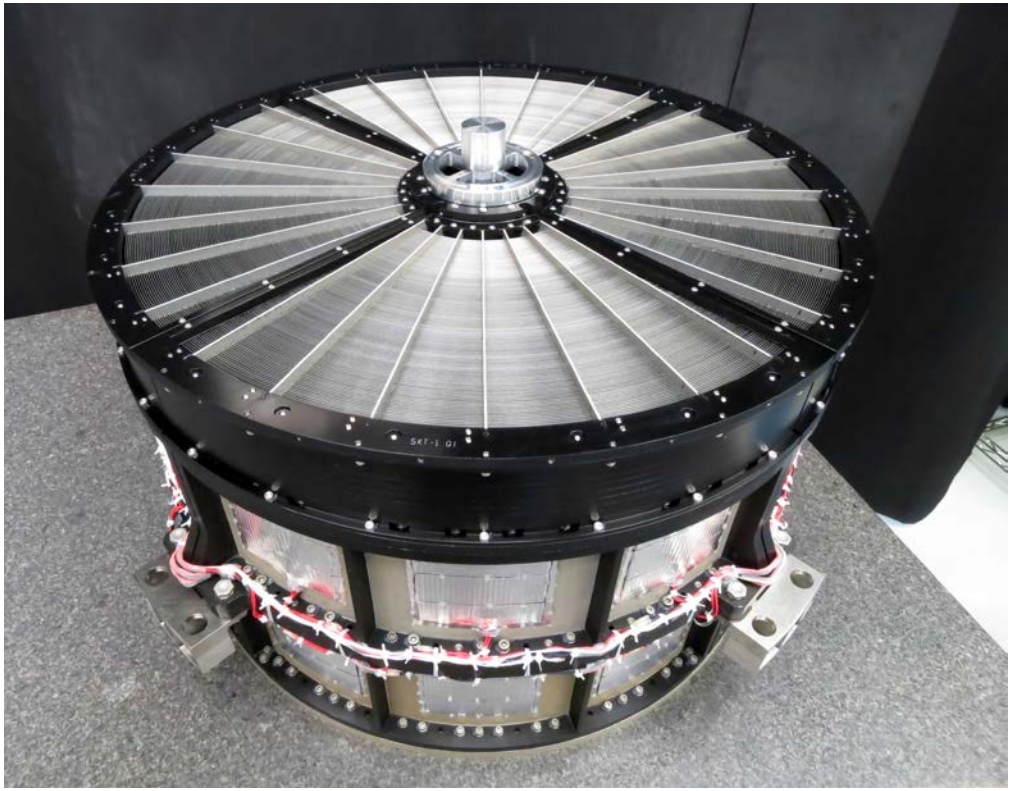

Hitomi Satellit

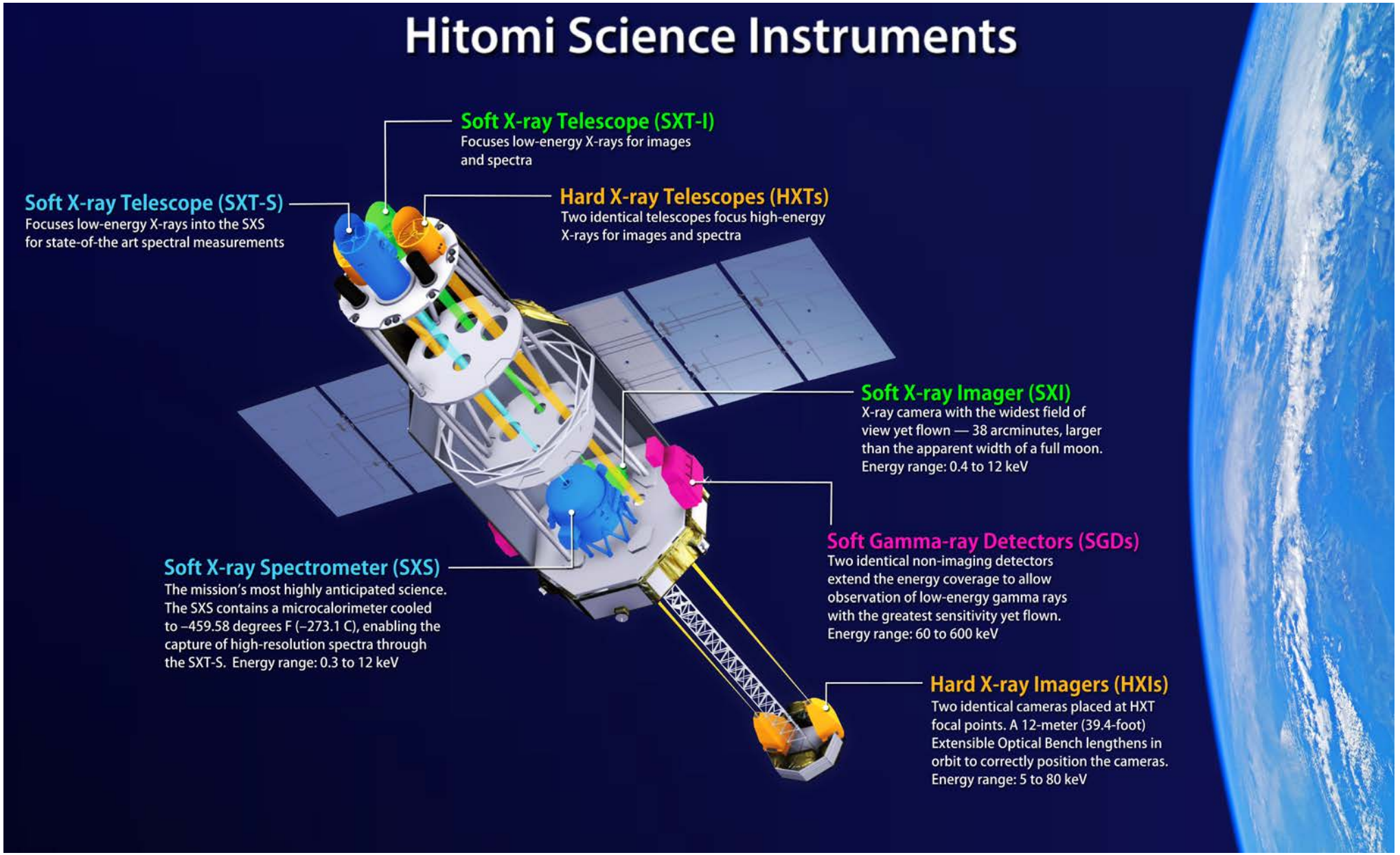

Hitomi Satellit: Persus Cluster Data

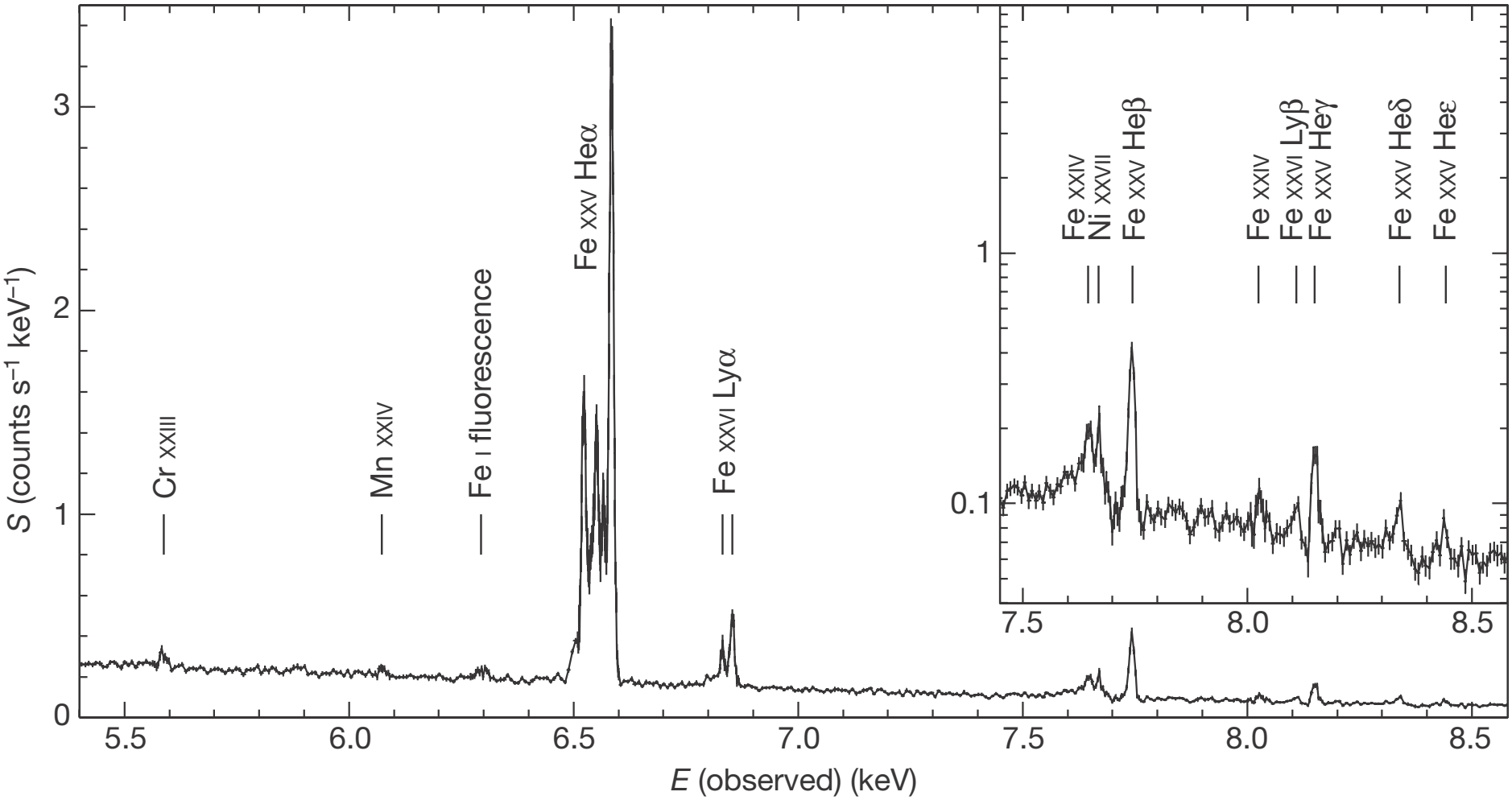

Z = 0,01756

Hitomi Satellit: Persus Cluster Data

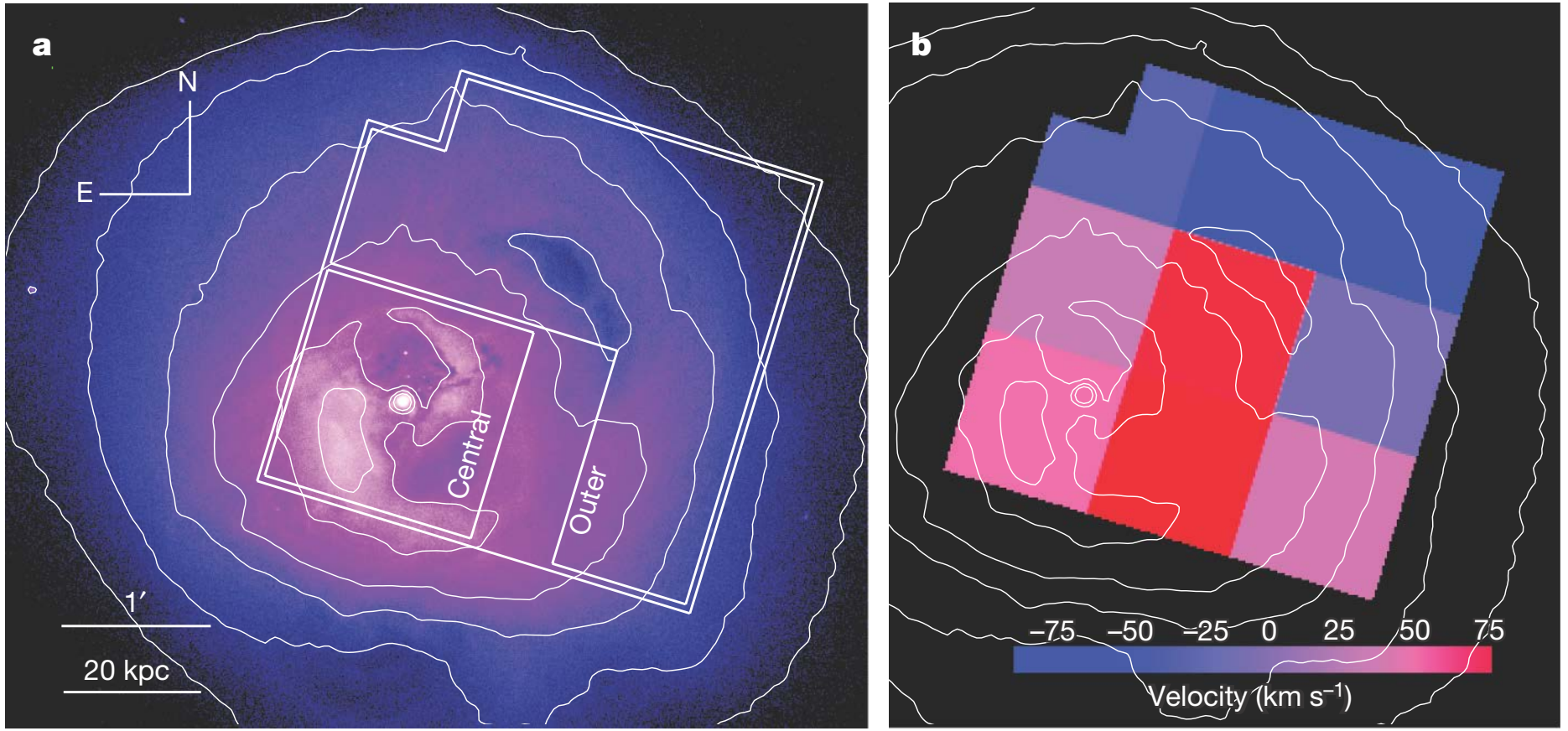

Superconducting Transition Edge Sensors (TES)

Donald. H. Andrews, American Philosophical Society Year Book, 132 (1938)
D. H. Andrews, et al., Rev. Sci. Instrum. **13**, 281 (1942)

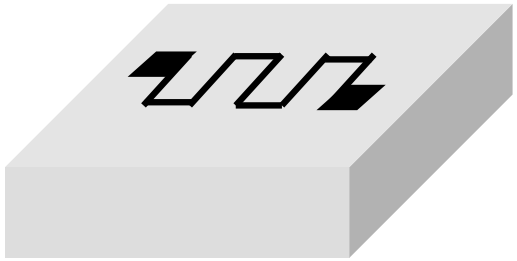

$$\alpha = \frac{\mathrm{d}\log R}{\mathrm{d}\log T}$$

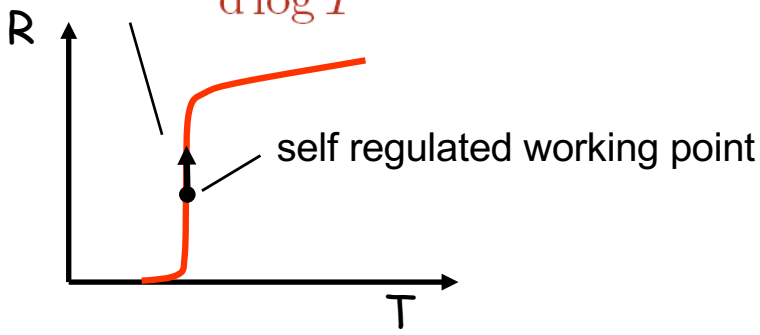

Materials Mo/Cu
Ir/Au
W

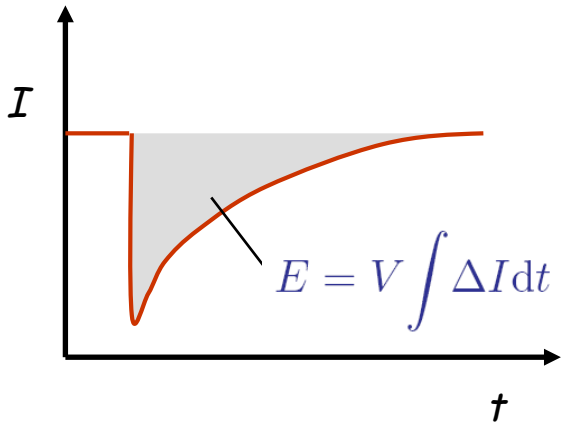

Electro-thermal feedback

K. D. Irwin, Appl. Phys. Lett. **66**, 1945 (1995)

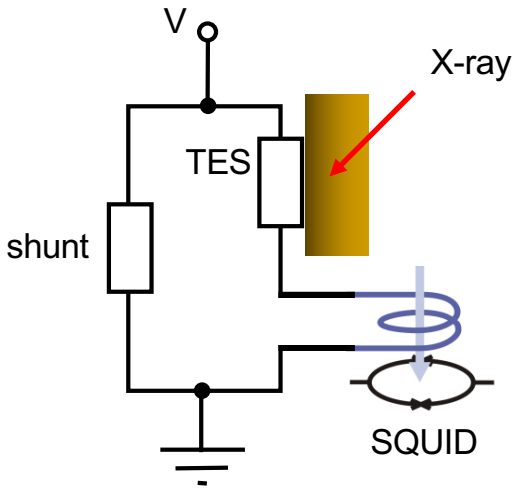

heat input:

→ R_{TES} goes up

→ joule heating decreases

fast response time

$$\tau_{\mathrm{eff}} = \frac{\tau}{1+\alpha/n}$$

$$G \propto T^{n}$$

Excess Noise

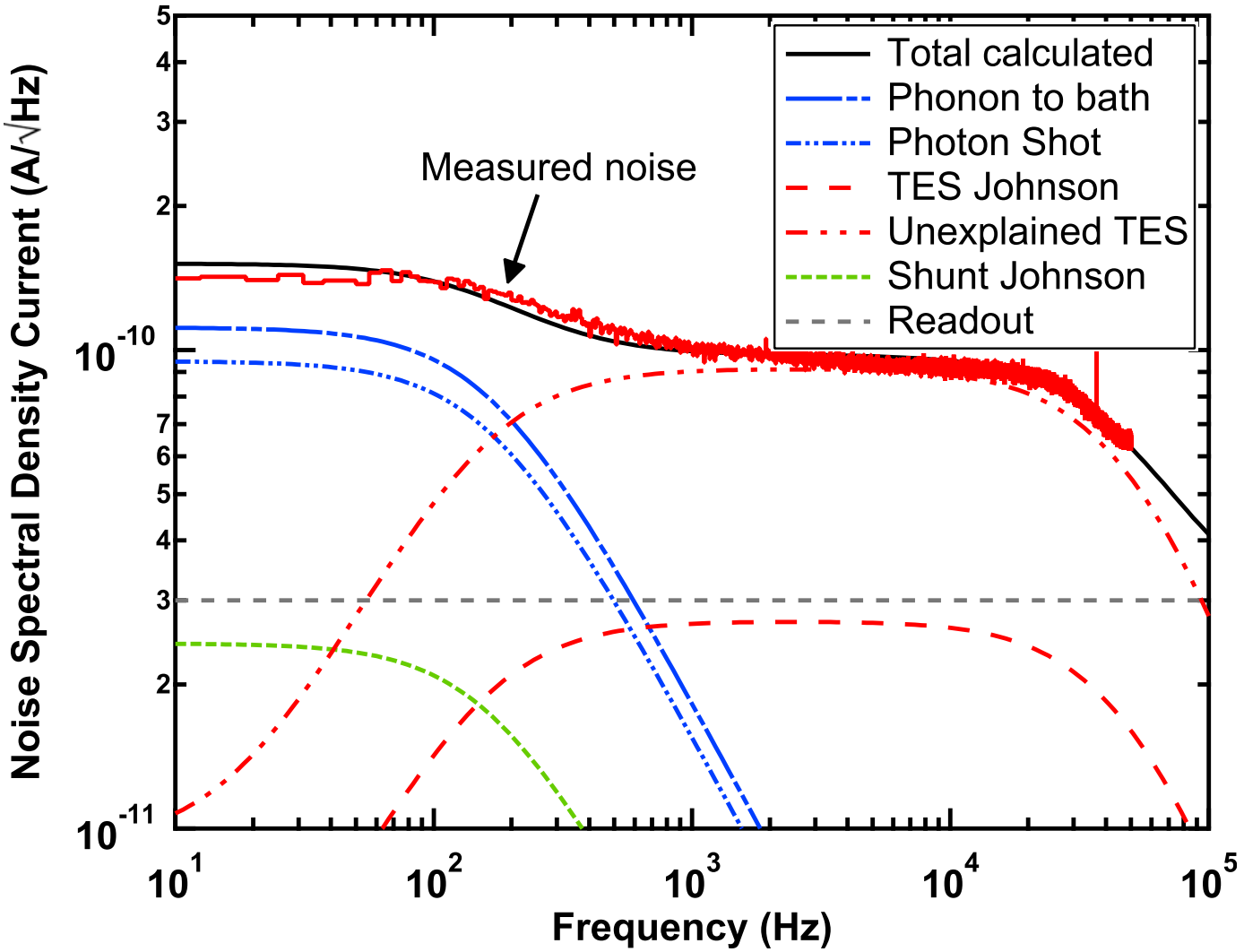

Smith *et al.* , J. Appl. Phys. 114, 074513 (2013)

Empirical Reduction of Excess Noise

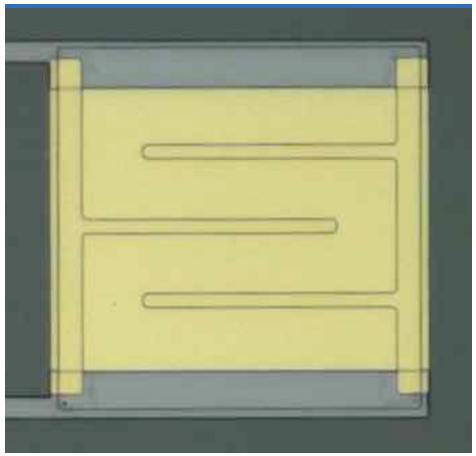

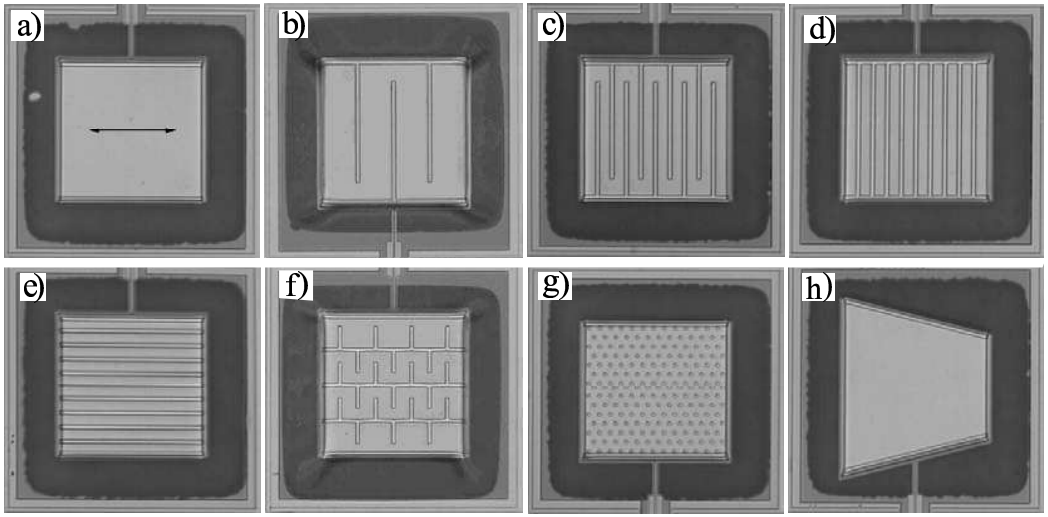

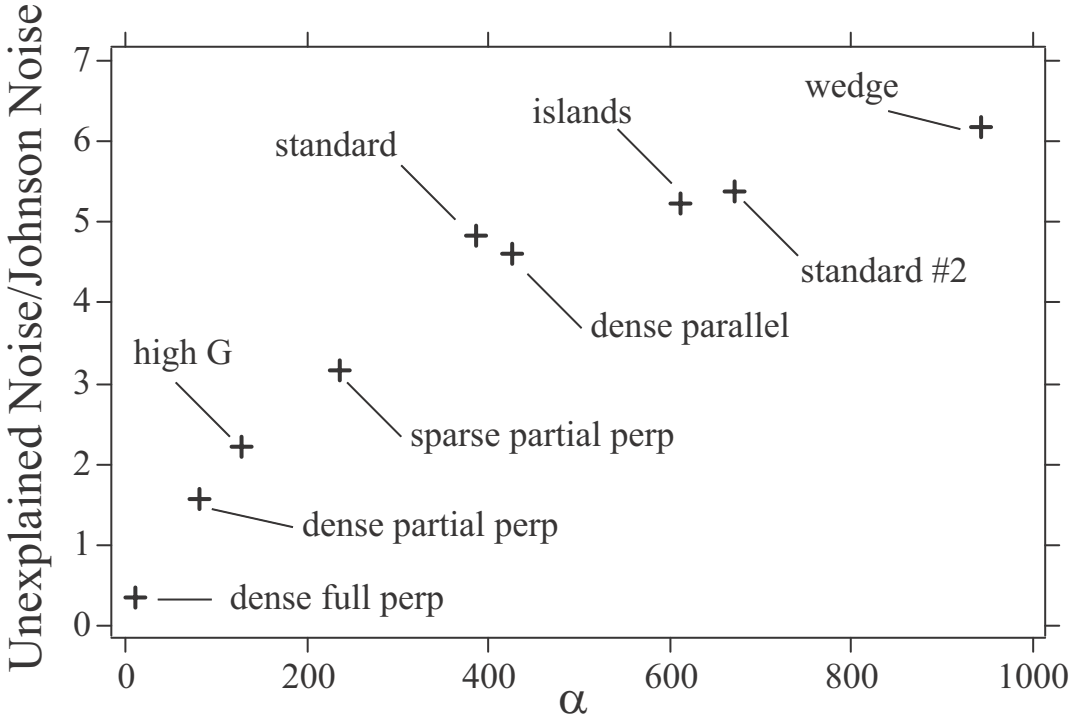

Performance of X-ray TES Detectors

57 μm x 57 μm x 4.5 μm Au absorbers

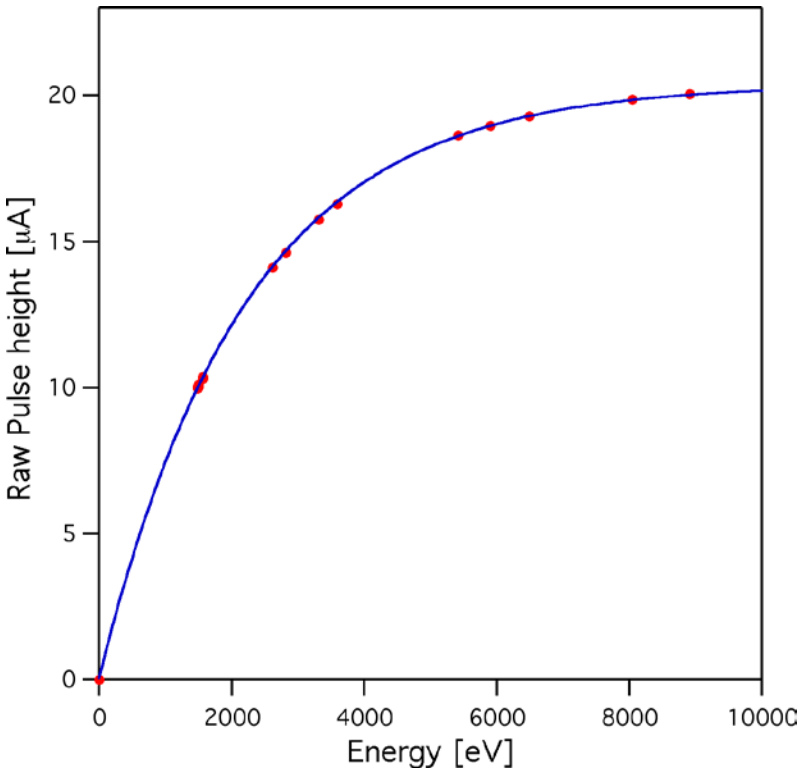

non-linearity

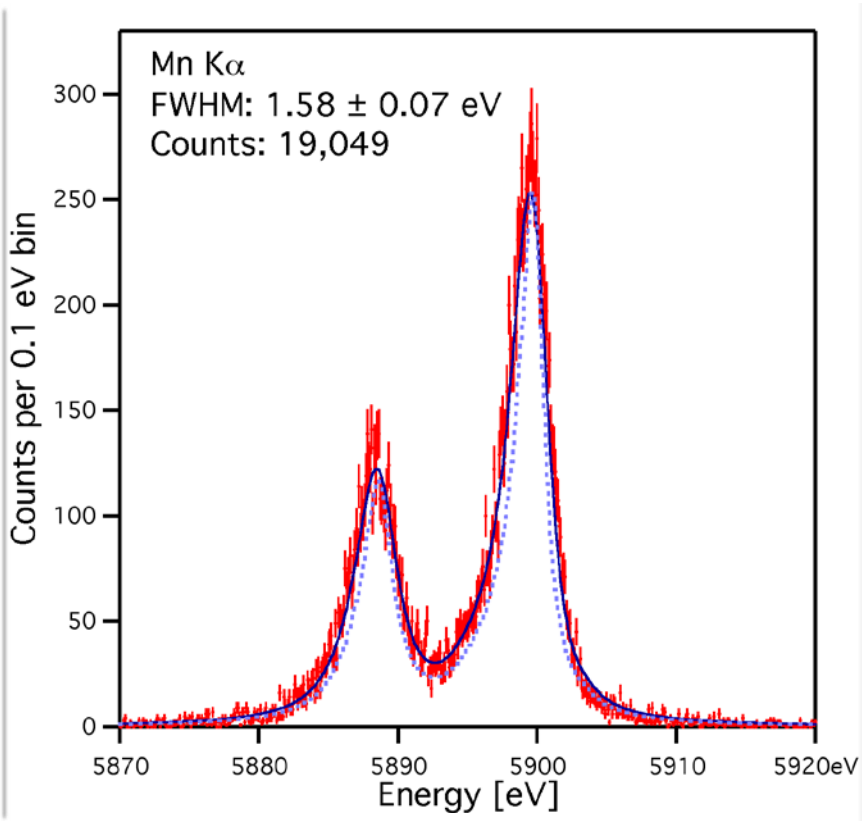

ΔE_{FWHM} = 1.58 eV at 5.9 keV

Proximity Induced Weak Link Effect

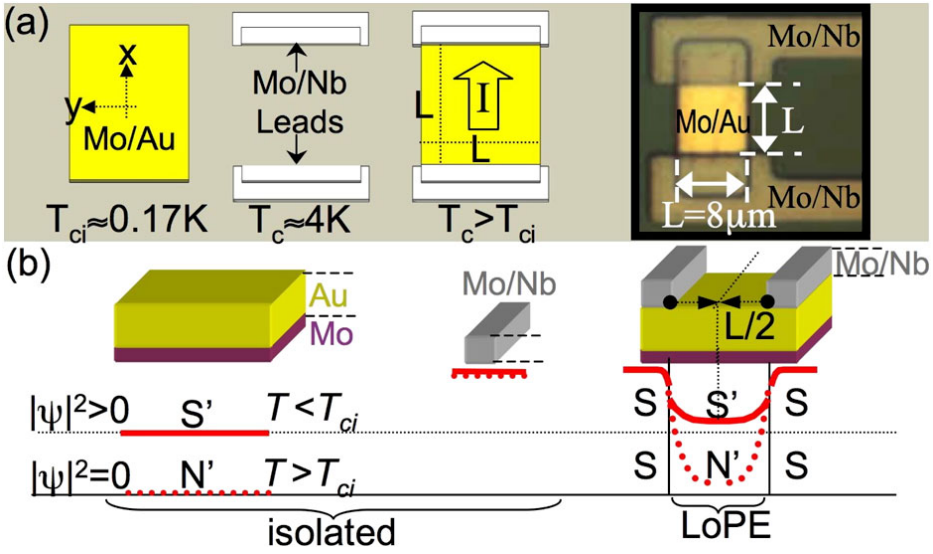

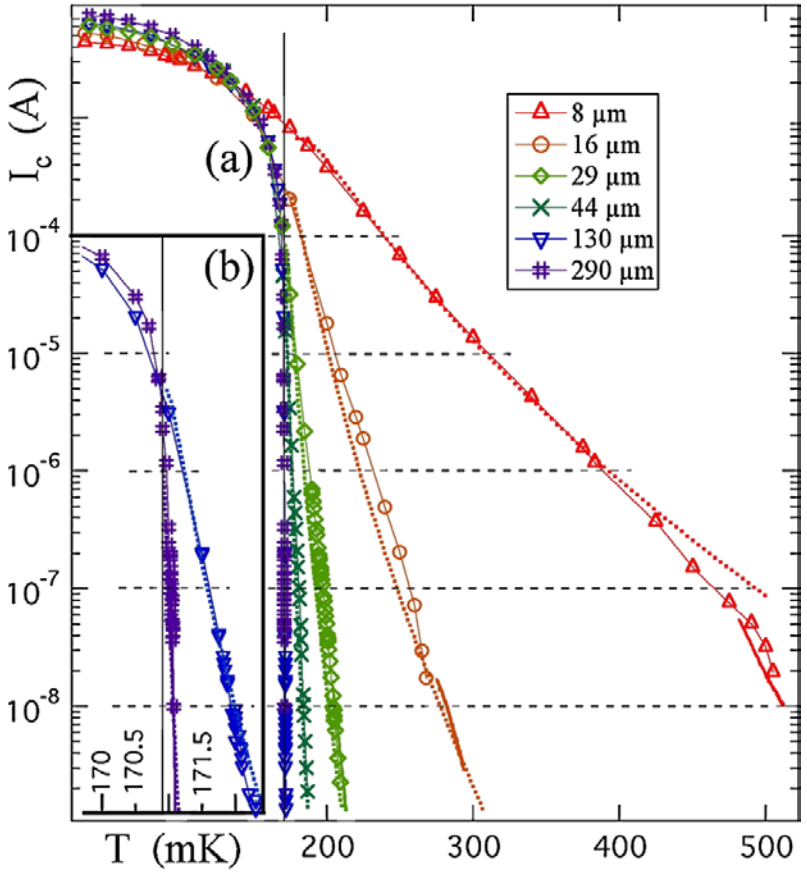

Superconducting leads influence TES through proximity effect

J. E. Sadleir, *et al.*, PRL **104**, 047003 (2010)

Proximity Induced Weak Link Effect

$$I_C(B) = I_C(0)\frac{\chi^2}{\chi^2\left(\pi\frac{B}{B_0}\right)^2}\left|\frac{\pi\frac{B}{B_0}\sin\left(\pi\frac{B}{B_0}\right)}{\chi\tanh(\chi)} + \cos\left(\pi\frac{B}{B_0}\right)\right|$$

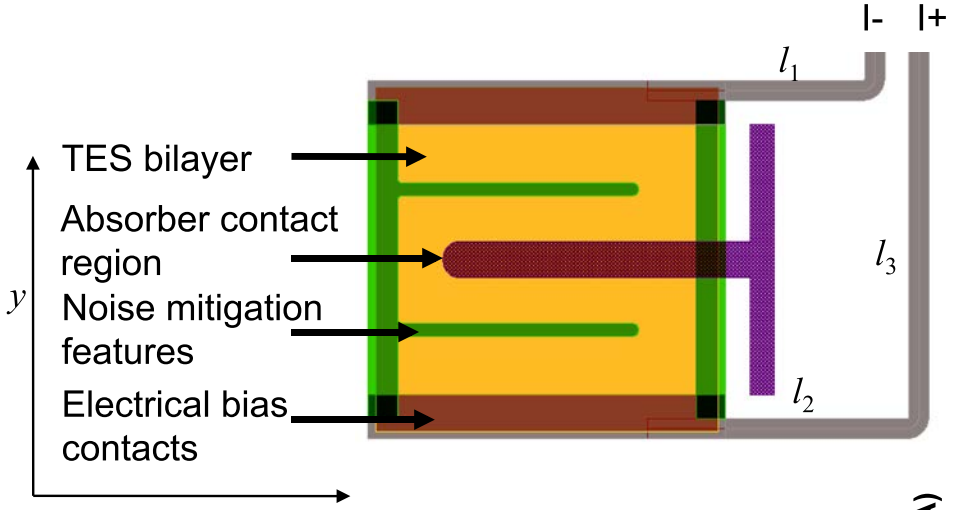

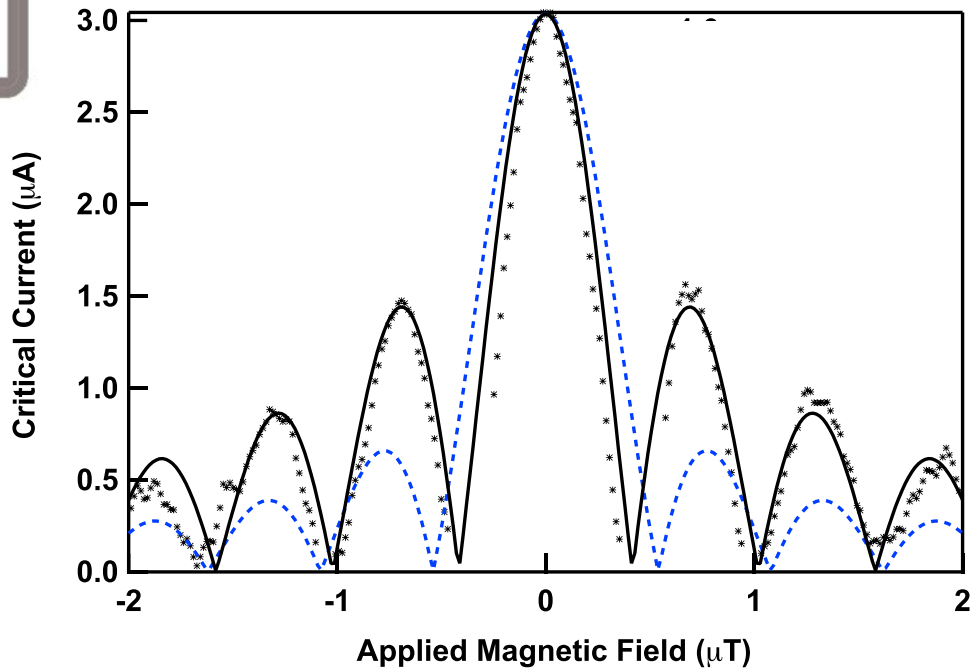

Cosmic Microwave Background

Cosmic Microwave Background Detection

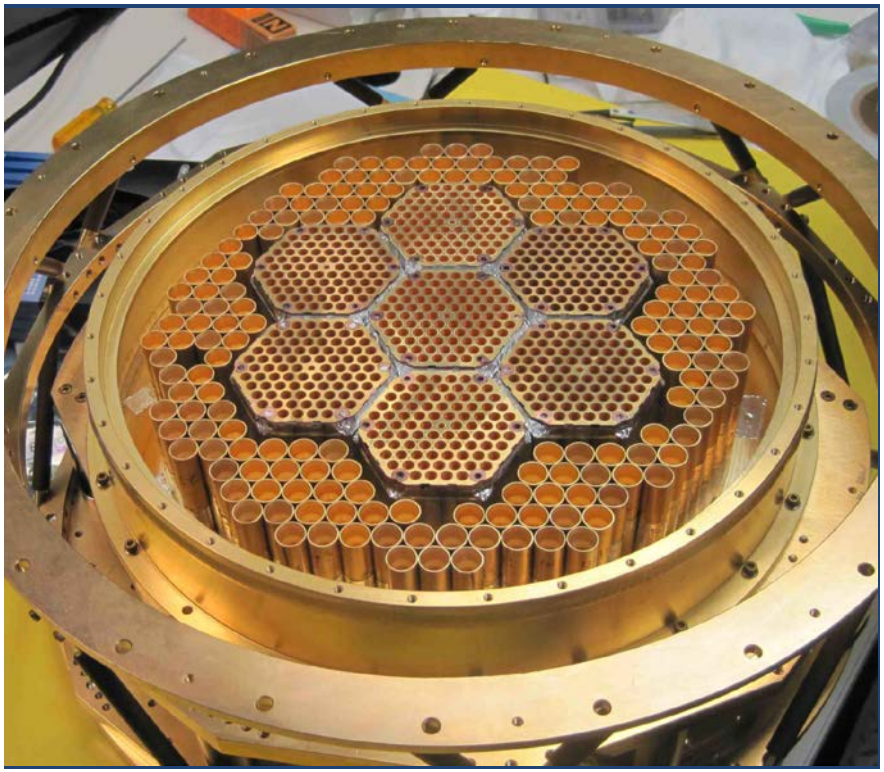

South Pole Telescope

95 GHz, 150 GHz, and 220 GHz

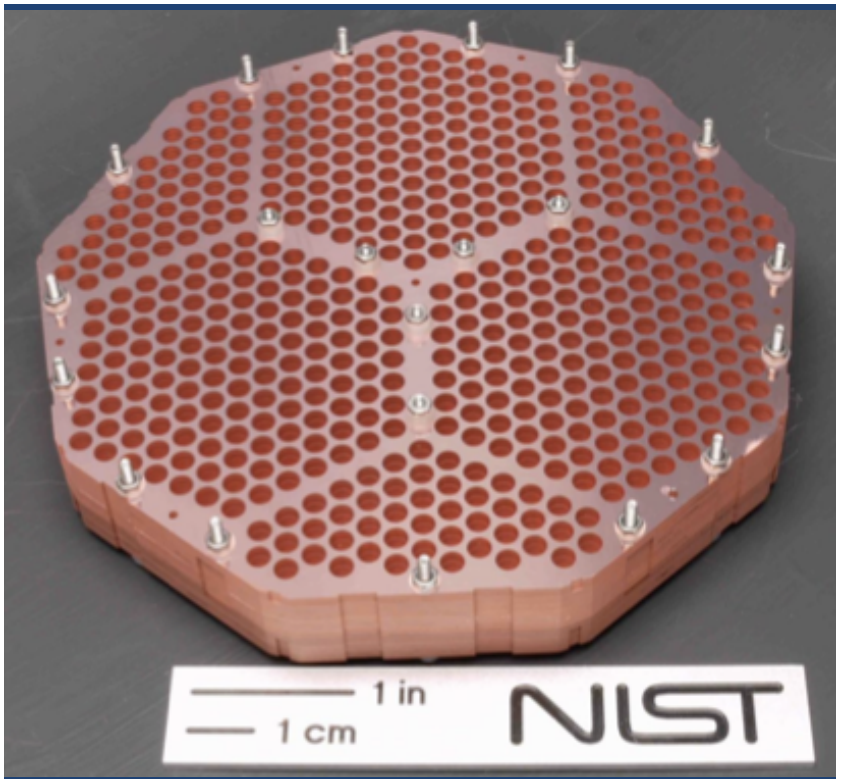

Atacama Cosmology Telescope

145 GHz und 280 GHz

Cosmic Microwave Background Detection

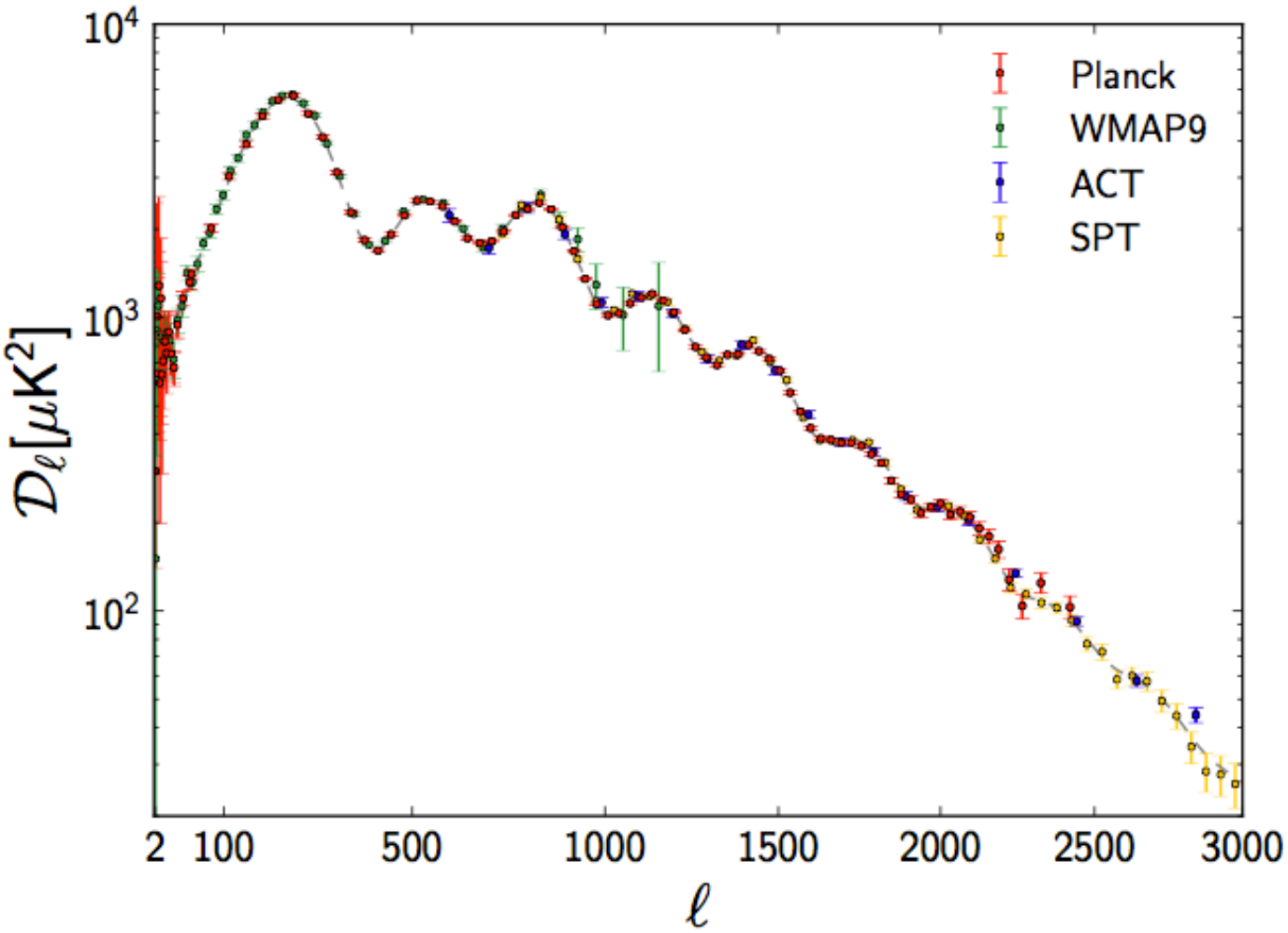

Cosmic Microwave Background Detection

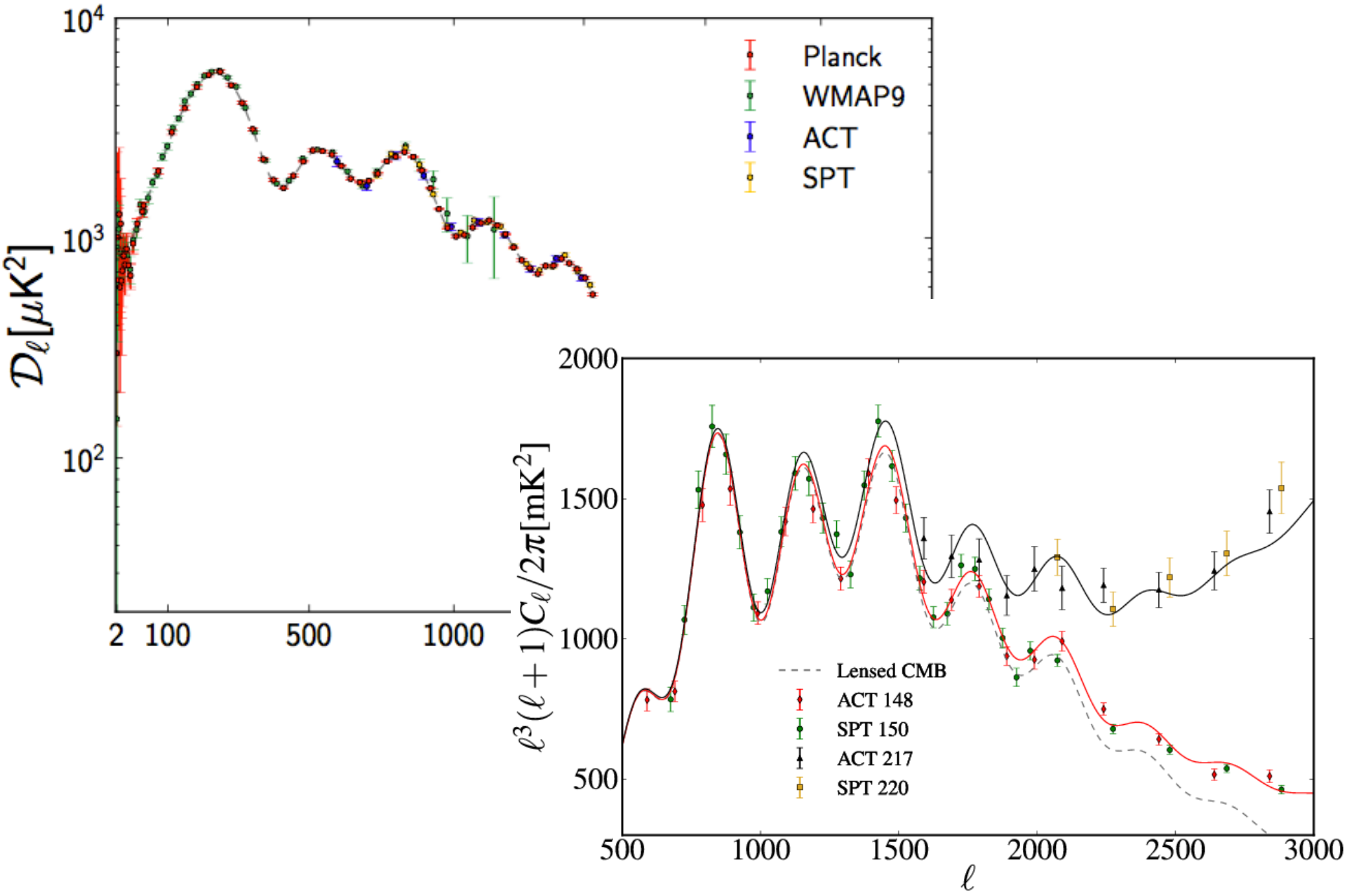

Millimeter Wave Astronomy

SCUBA 2 Detector: 32 x 40 arrays

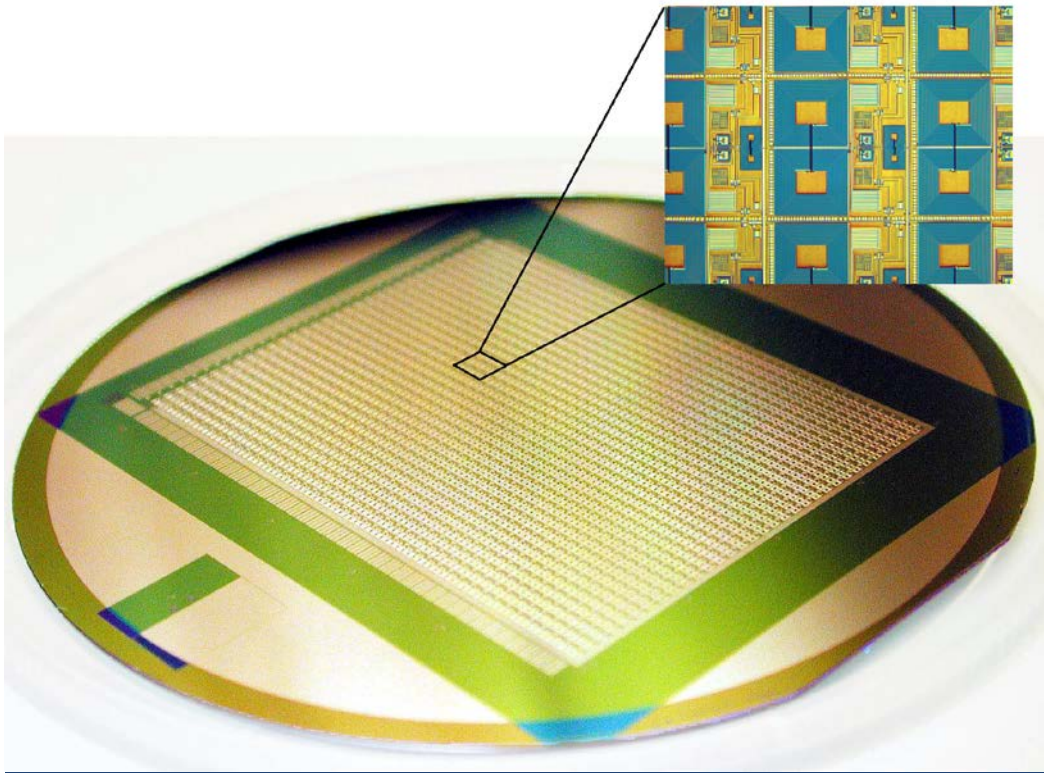

SQUID Wafer

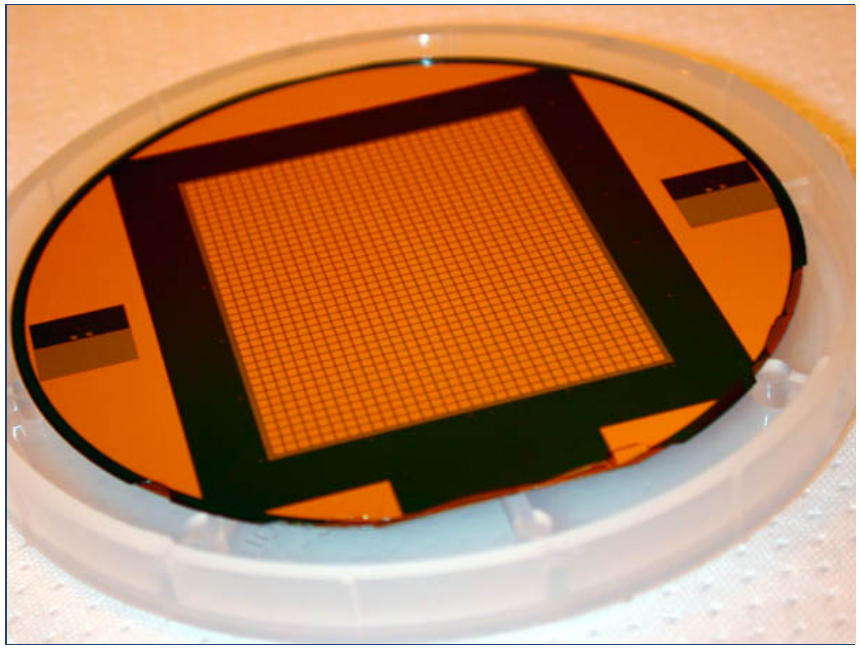

Detector Wafer

Millimeter Wave Astronomy

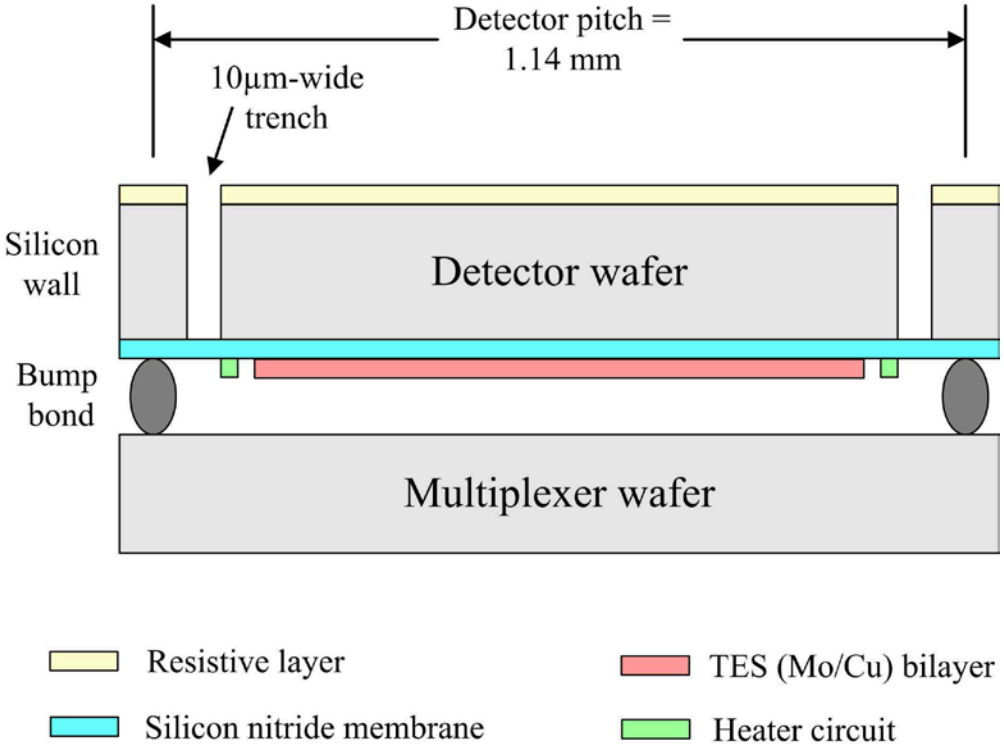

bump bonding

time domain multiplexing

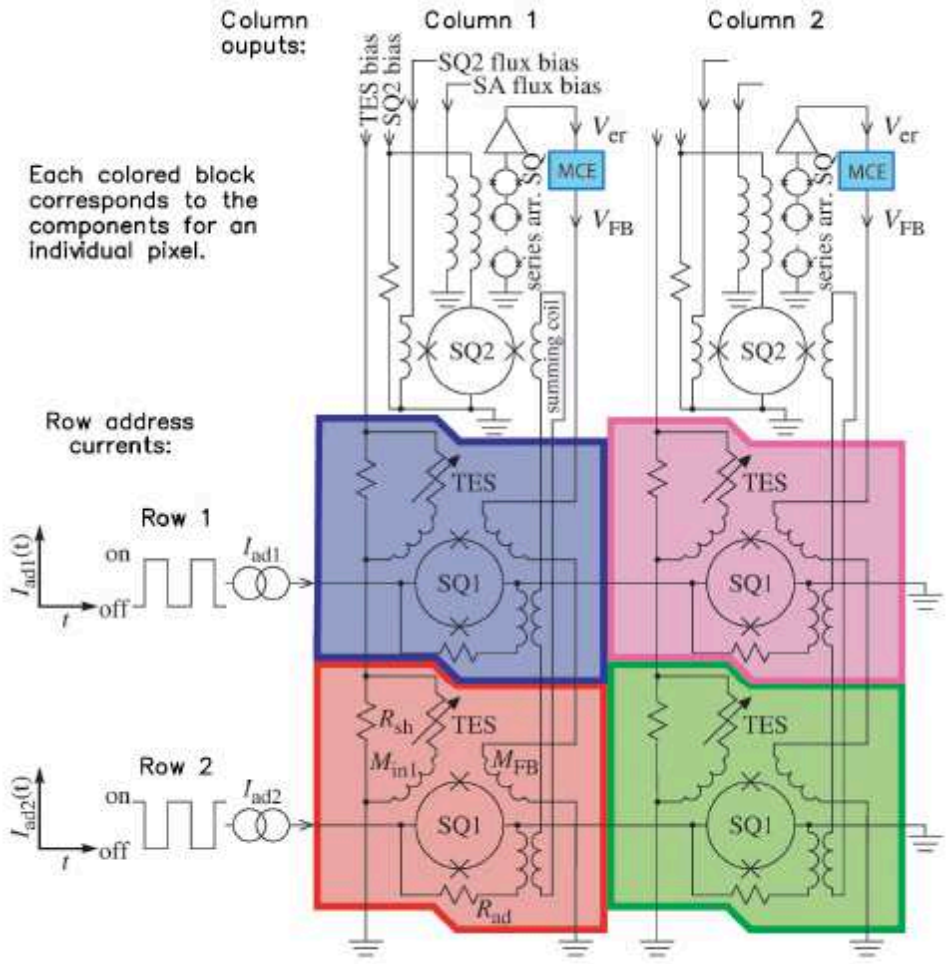

Millimeter Wave Astronomy

5,120 pixels at 450 um

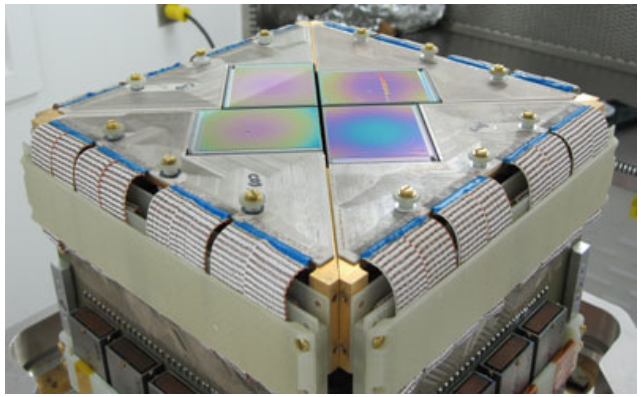

5,120 pixels at 850 um

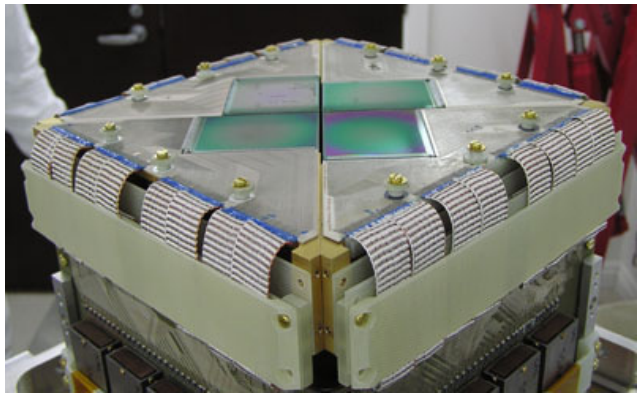

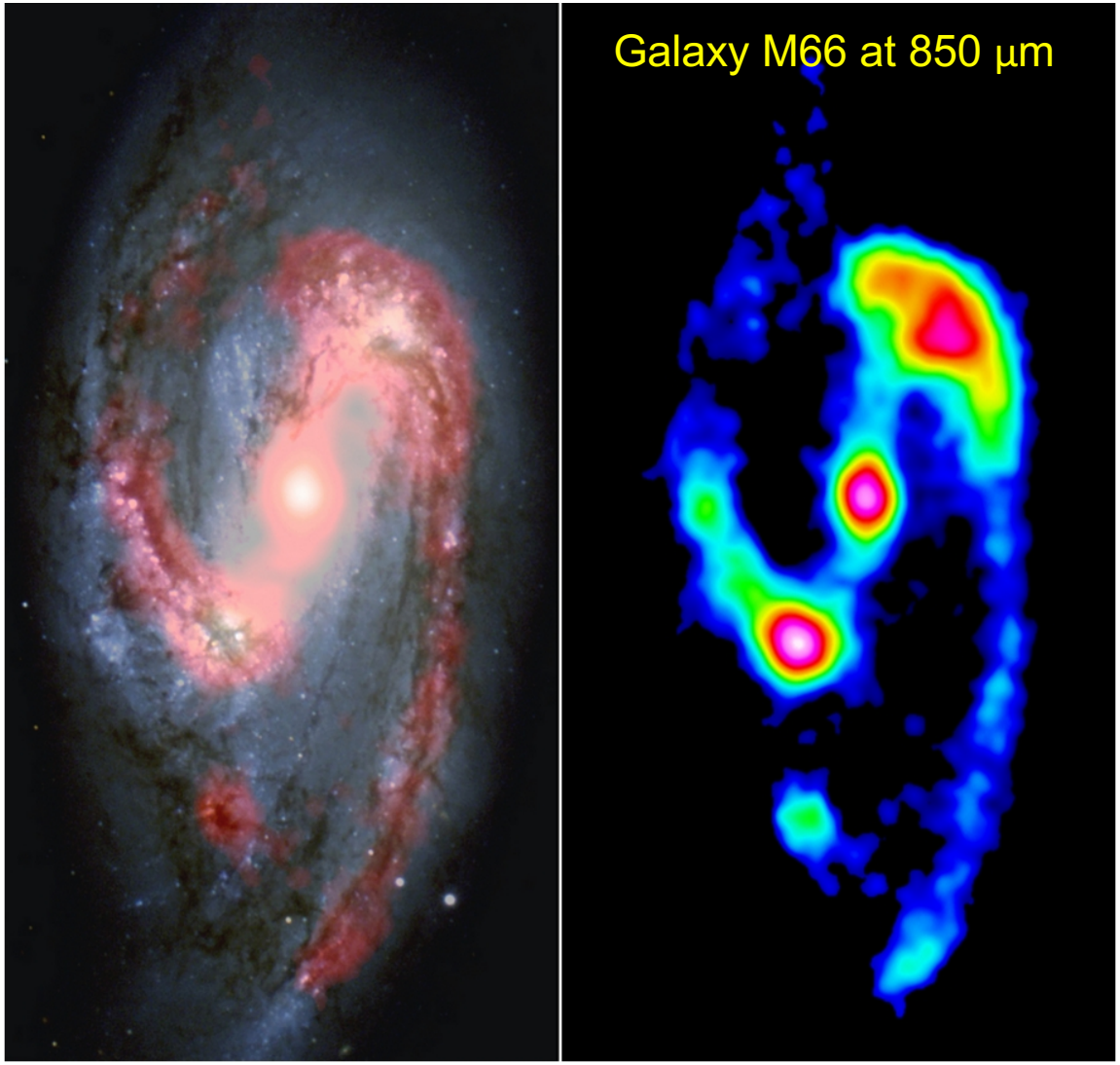

Metallic Magnetic Calorimeter (MMC)

S.R. Bandler, C. Enss, R.E. Lanou, H.J. Maris,
T. More, S.F. Porter, G.M. Seidel
J. Low Temp. Phys. **93**, 709-714 (1993)

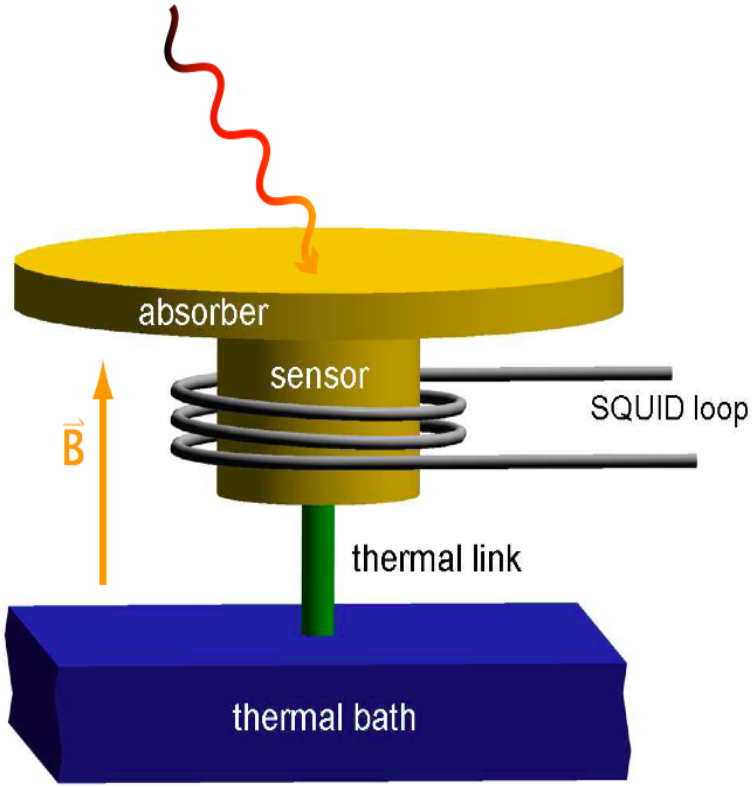

paramagnetic sensor:

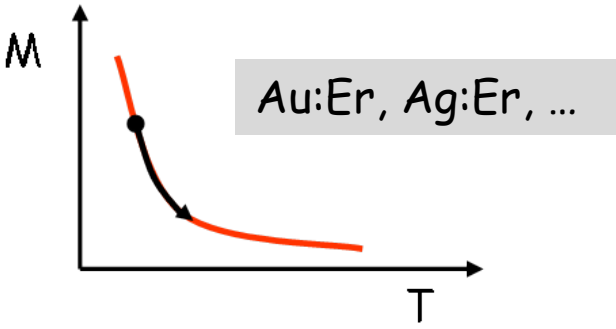

signal size:

$$\delta M = \frac{\partial M}{\partial T}\delta T = \frac{\partial M}{\partial T}\frac{E_\gamma}{C_{\mathrm{tot}}}$$

energy resolution:

$$\Delta E_{\mathrm{FWHM}} \simeq 2{,}36\sqrt{4k_{\mathrm{B}}C_{\mathrm{Abs}}T^2}\sqrt{2}\left(\frac{\tau_0}{\tau_1}\right)^{1/4}$$

main difference to resistive calorimters:

no dissipation in the sensor
no galvanic contact to the sensor

A. Fleischmann, Adv. Solid State Phys. **41**, 577 (2001)

Magnetism of Sensor Material: **Au**:Er

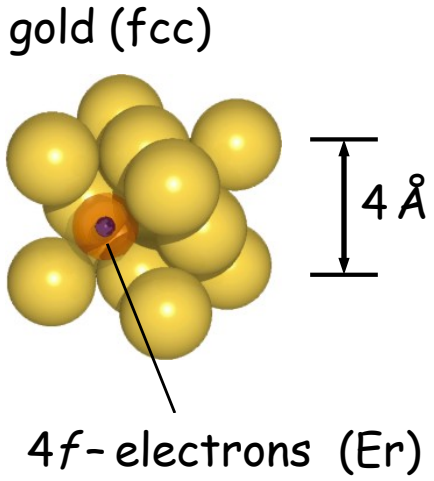

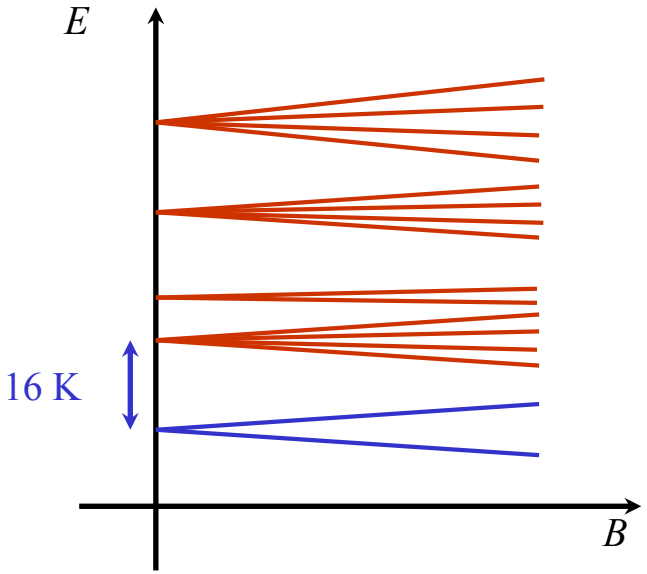

Rare earth ions in metals

- 4*f* - shell partially filled

angular momentum & magnetic moment

Er^{3+}: $J = 15/2$ → 16 levels

- crystal field splitting

Magnetic Susceptibility of **Au**:Er

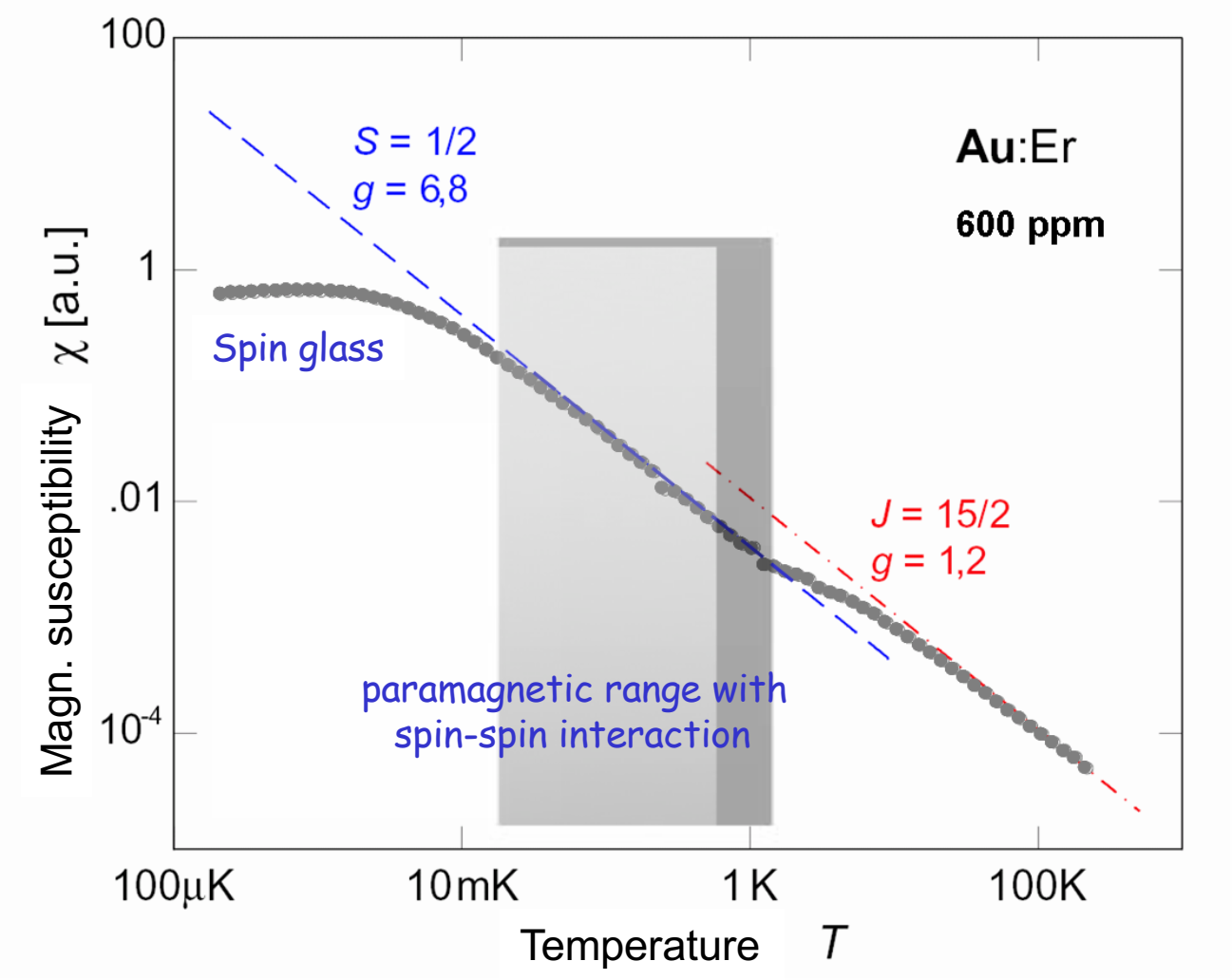

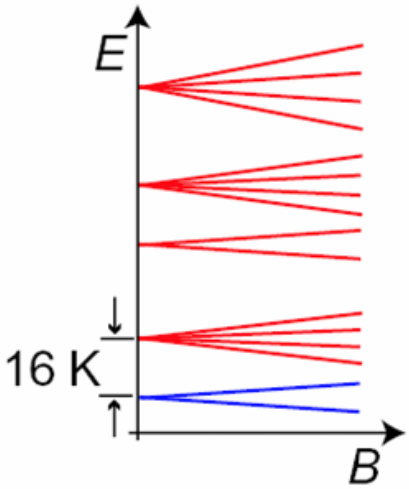

Γ_7 -Kramers doublet

two level system

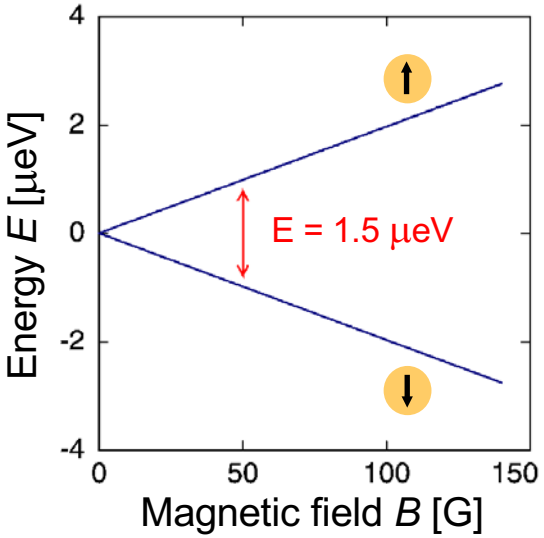

50 G → E = 1.5 μeV

100 keV → 10^{11} spin flips (!)

$$\delta\Phi_S \propto \frac{\partial M}{\partial T}\frac{1}{C_{tot}}\delta E$$

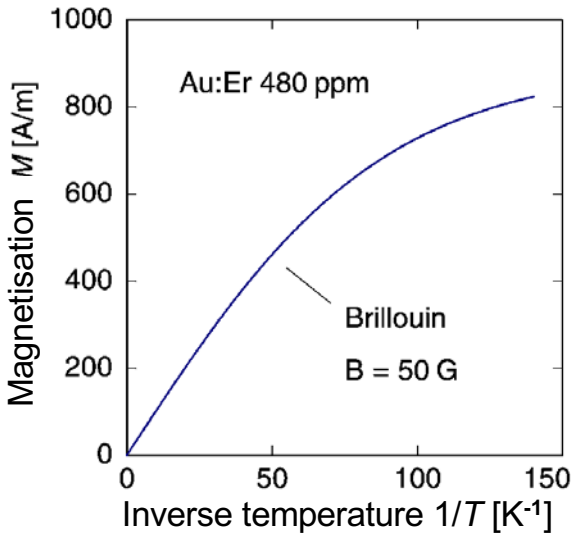

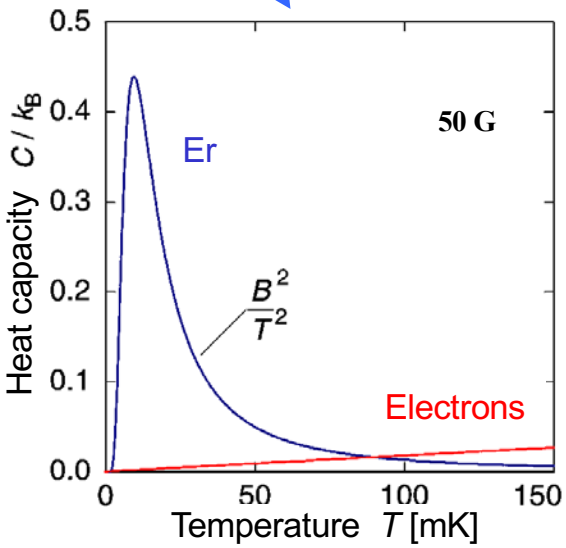

Interaction Between Er^{3+}- ions

dipole-dipole interaction

RKKY interaction — indirect exchange interaction
decreases with $1/r^3$
spatial oscillations

$$H_{ij} = \underbrace{\Gamma_{\mathrm{RKKY}}}_{\alpha\Gamma_{\mathrm{dipole}}} (\boldsymbol{S}_i \cdot \boldsymbol{S}_j)\ F\left(2k_{\mathrm{F}} r_{ij}\right)$$

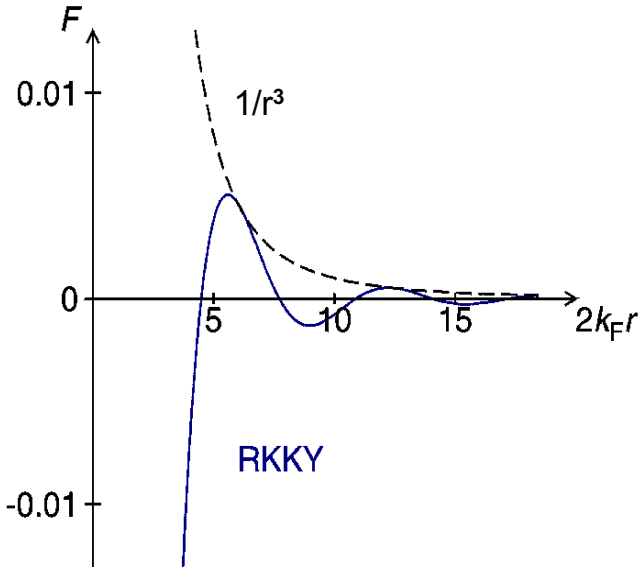

mean field approximation

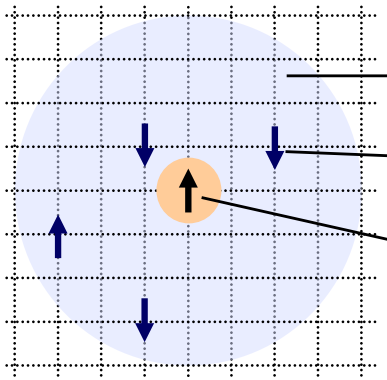

radius $7\,a_0$

0 ... 5 spins in field B_0

spin in field

$B_{\mathrm{eff}} = B_0 + B_{\mathrm{M}}$

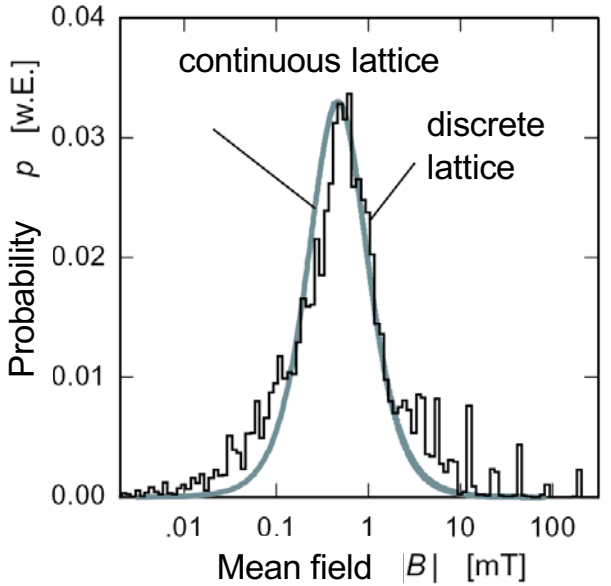

Calculation of $C(B,T)$ and $M(B,T)$

Magnetization and Heat Capacity

$$\delta\Phi_S \propto \frac{\partial M}{\partial T}\,\frac{1}{C_{tot}}\,\delta E$$

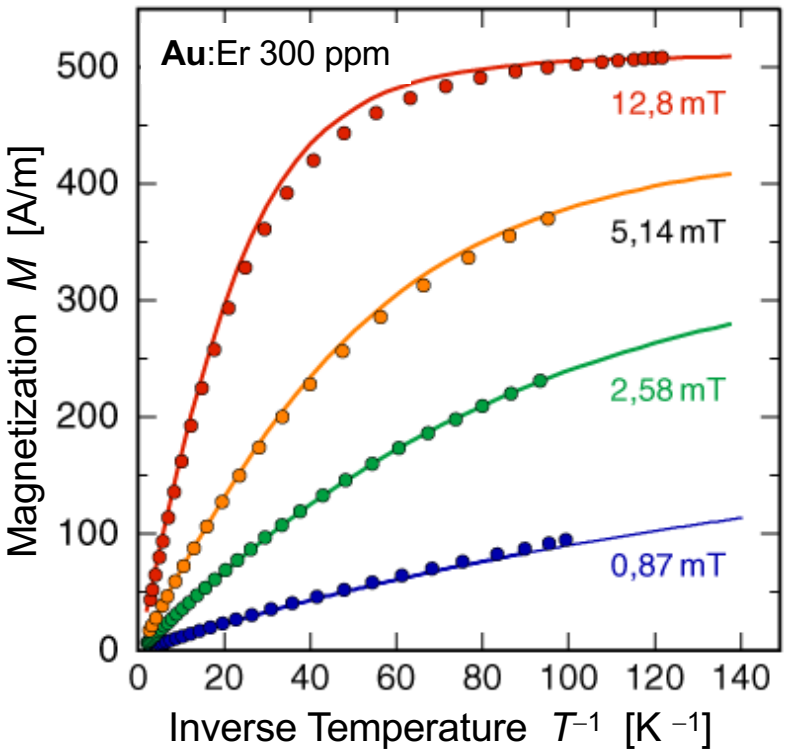

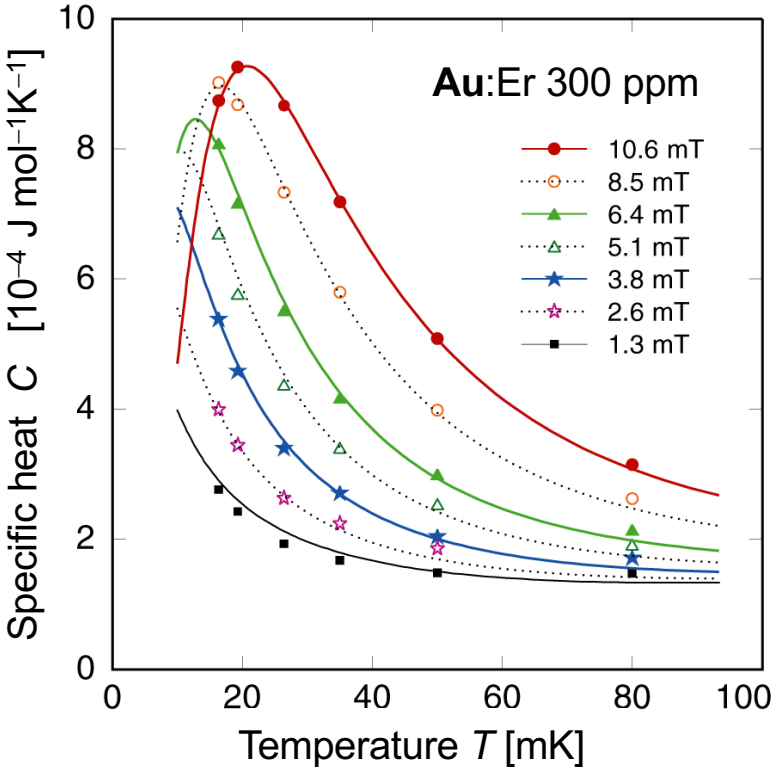

Calorimeter Signal

$$\delta\Phi_S = f(r,h)\frac{\partial M}{\partial T}\frac{1}{C_{tot}}\delta E$$

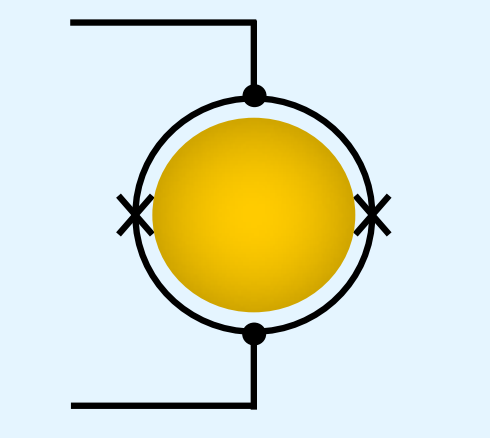

122 keV in **Au**:Er 300ppm

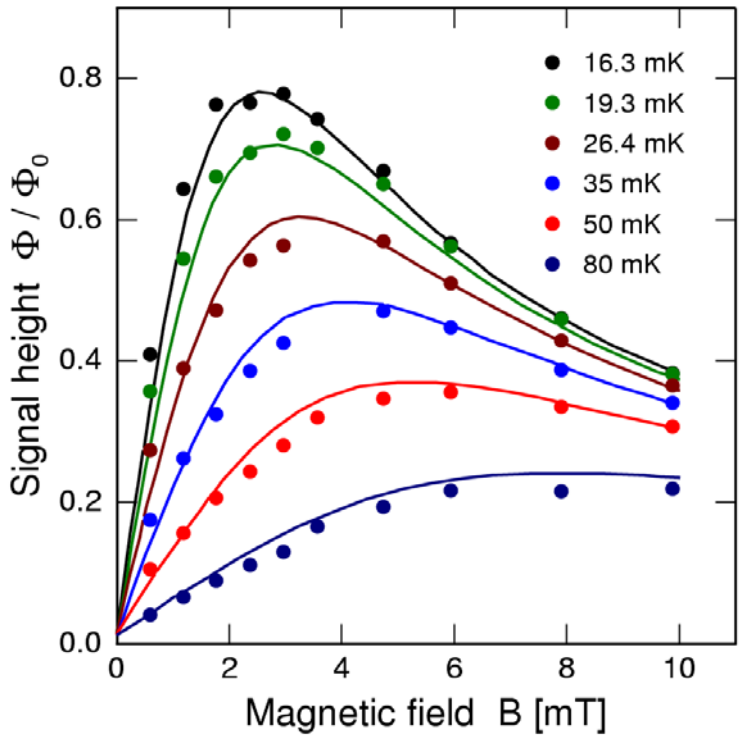

- satisfying agreement of theory and experiment
- signal size can be predicted!
- optimal detector design?

$$S_{max}(C_a, g, \alpha, T, x, r, h, B)$$

MMCs: Geometries

double meander:

- planar *T*-sensor
- superconducting meander shaped pickup loop
- B-field generated by persistent current
- transformer coupled to SQUID

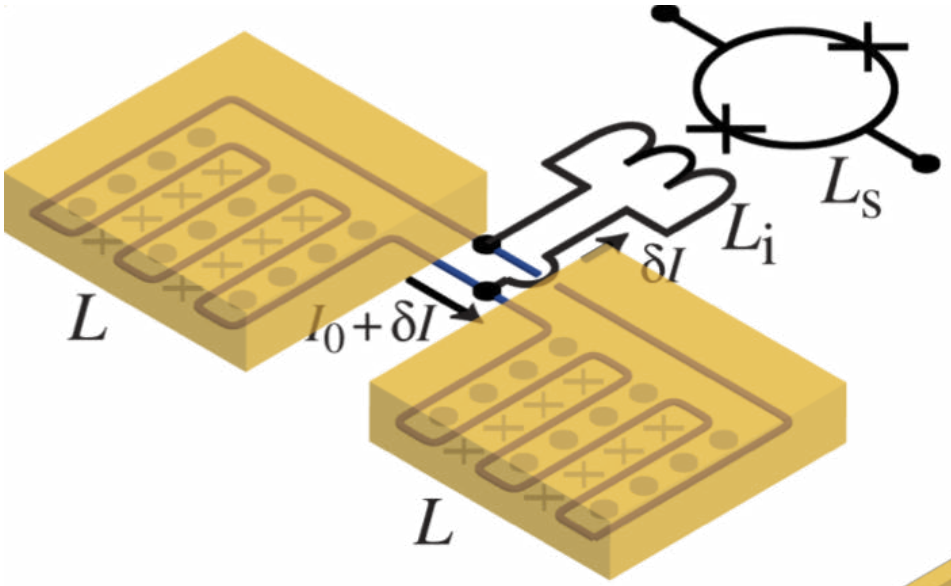

sandwich geometry:

- best magn. flux coupling,
- planar sensor
- sandwiched between stripline

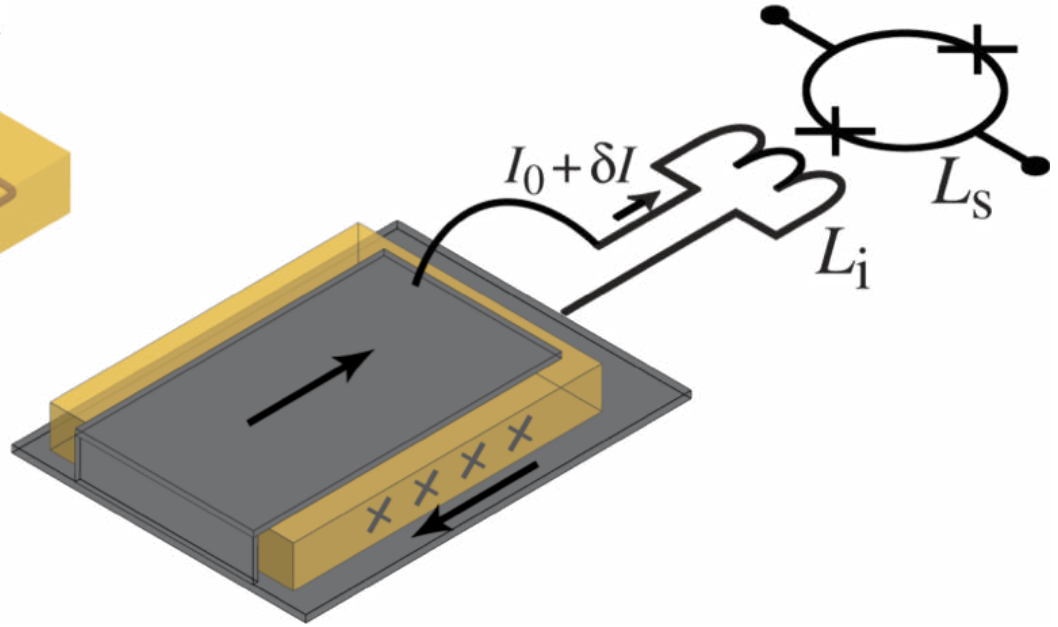

Readout Scheme For Magnetic Calorimeters

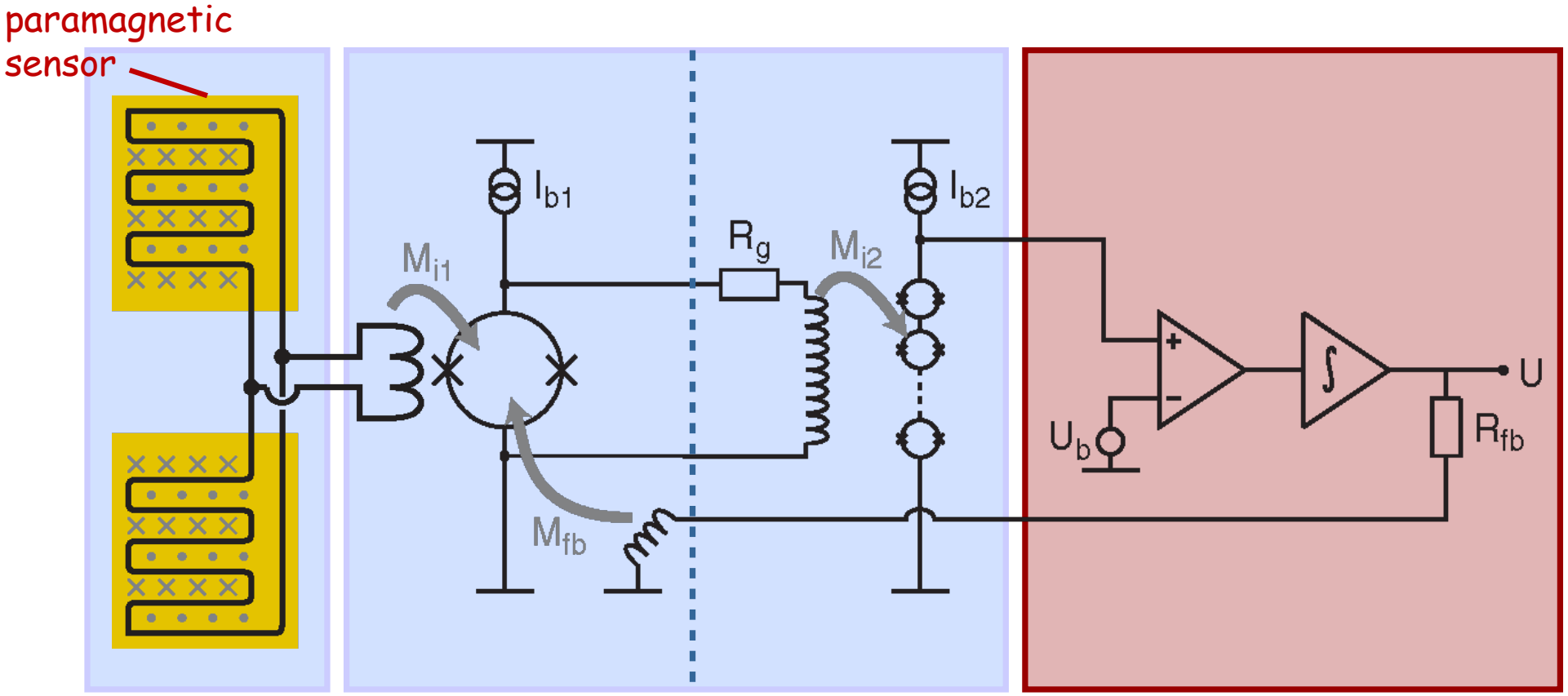

two-stage SQUID setup with flux locked loop to linearize the first stage SQUID

allows for:

- low noise (ε = 50 .. 300 $\hbar$)
- large bandwidth / slewrate
- small power dissipation on detector SQUID chip

Recent Result of a Fully Microfabricated MMC

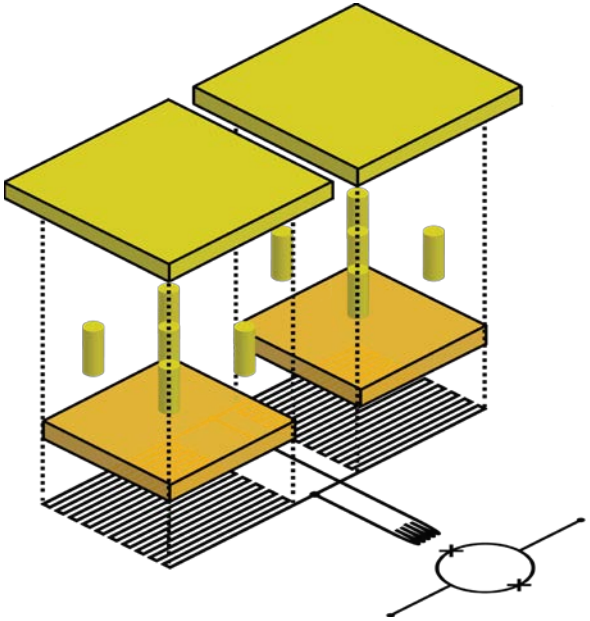

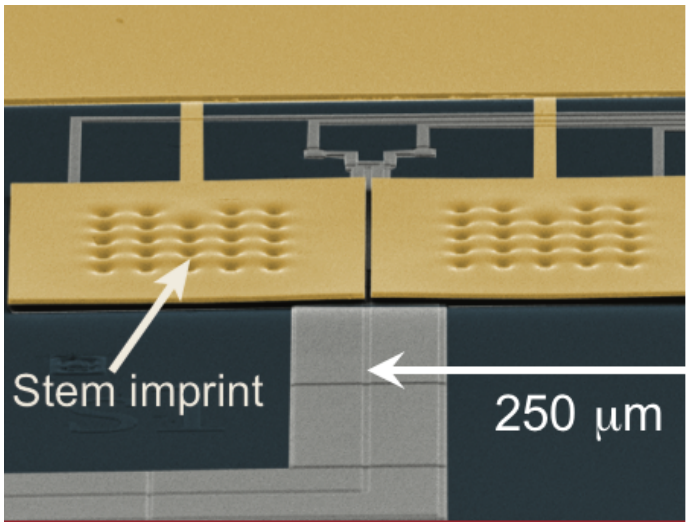

250 μm × 250 μm Gold, 5 μm thick

98% Quantum Efficiency @ 6 keV

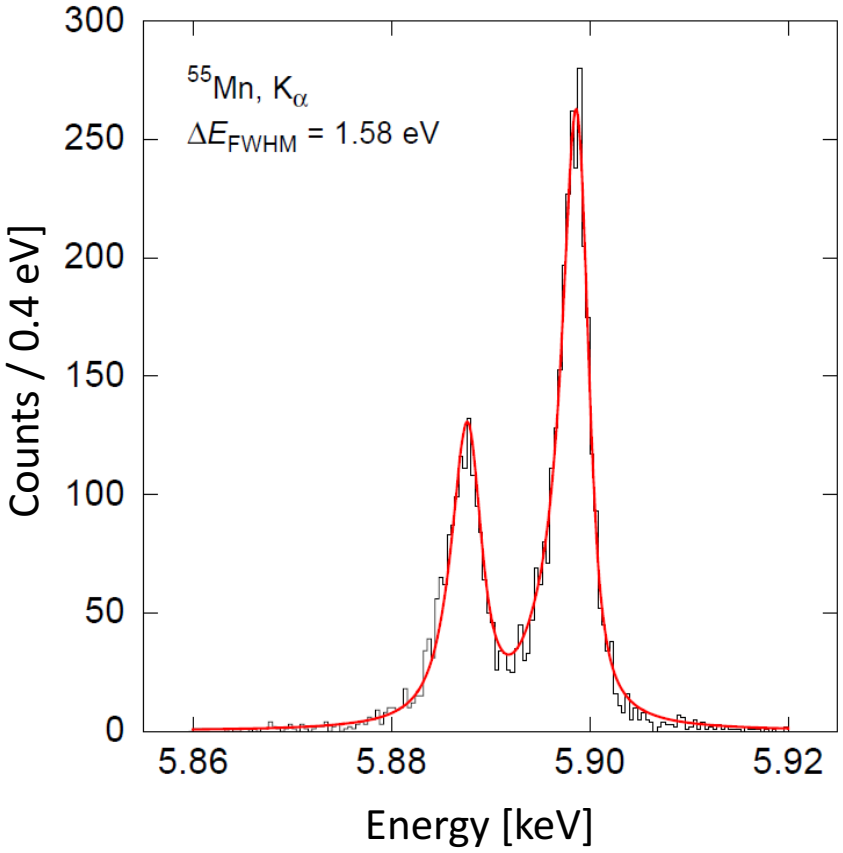

A. Pabinger et al. 2014

Operated at 20 mK (in Bluefors cryostat)

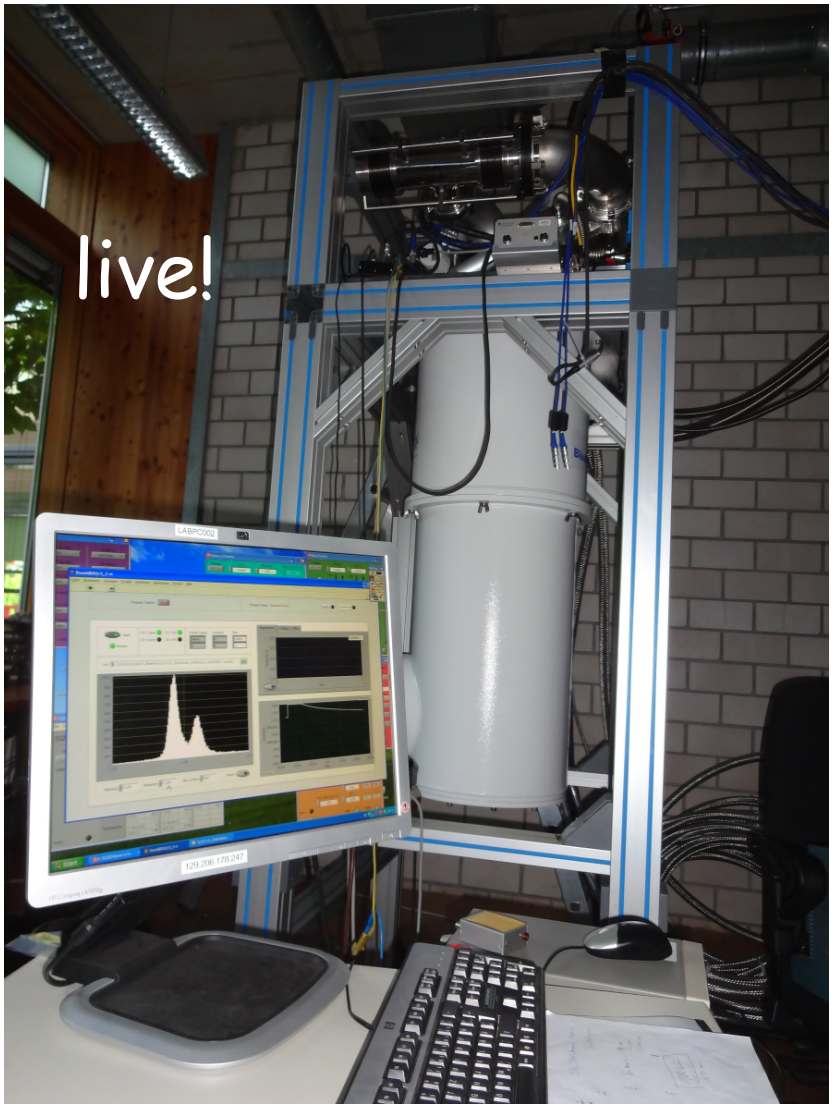

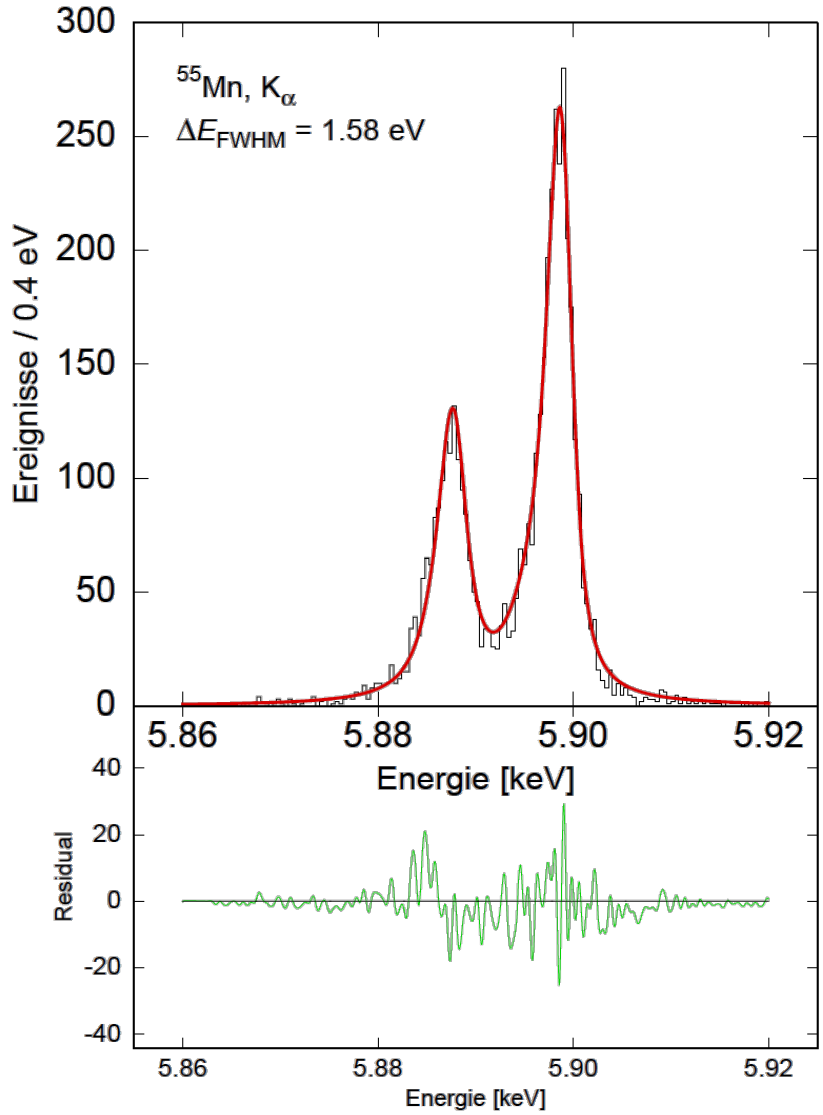

Energy Bandwidth

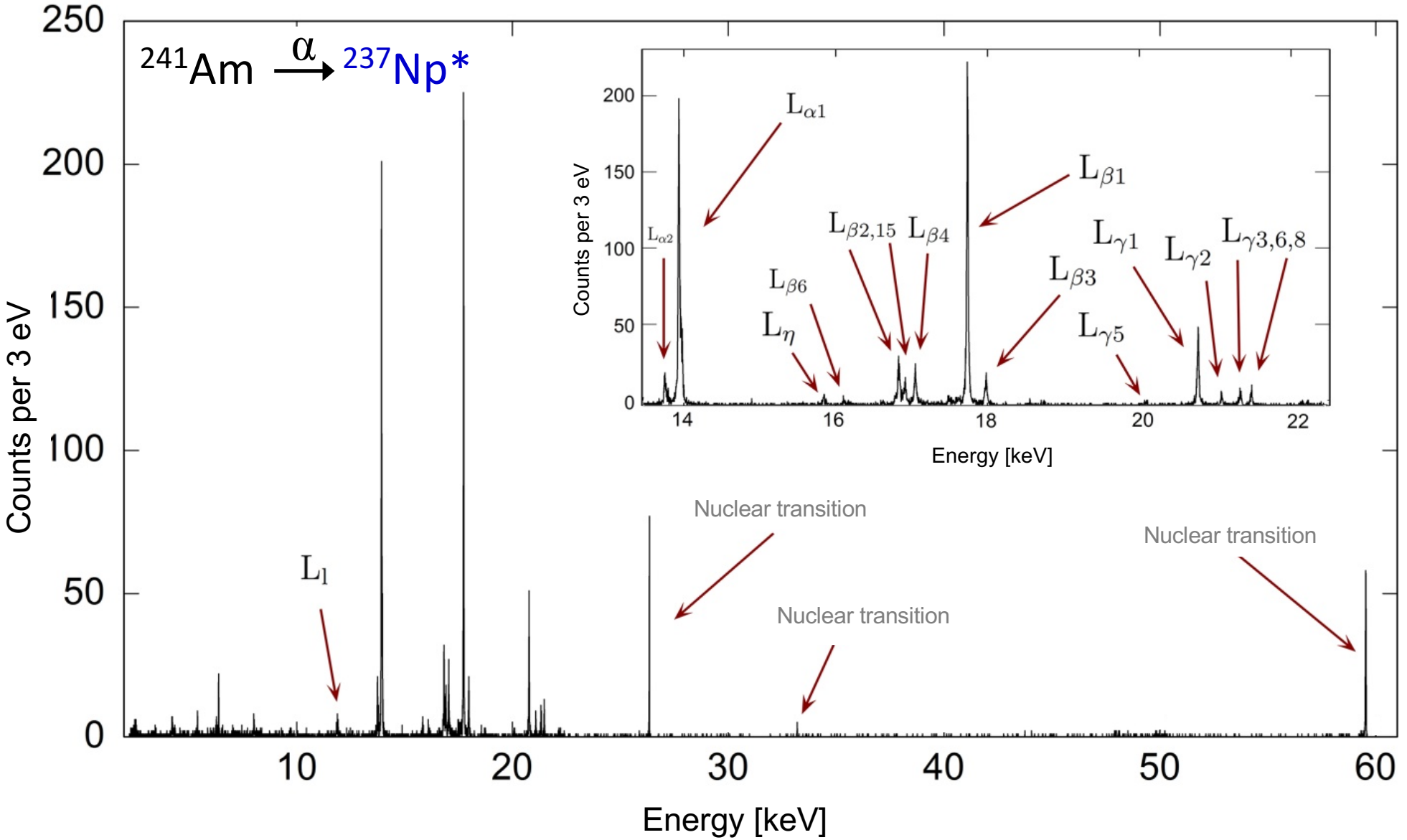

Excellent Linearity

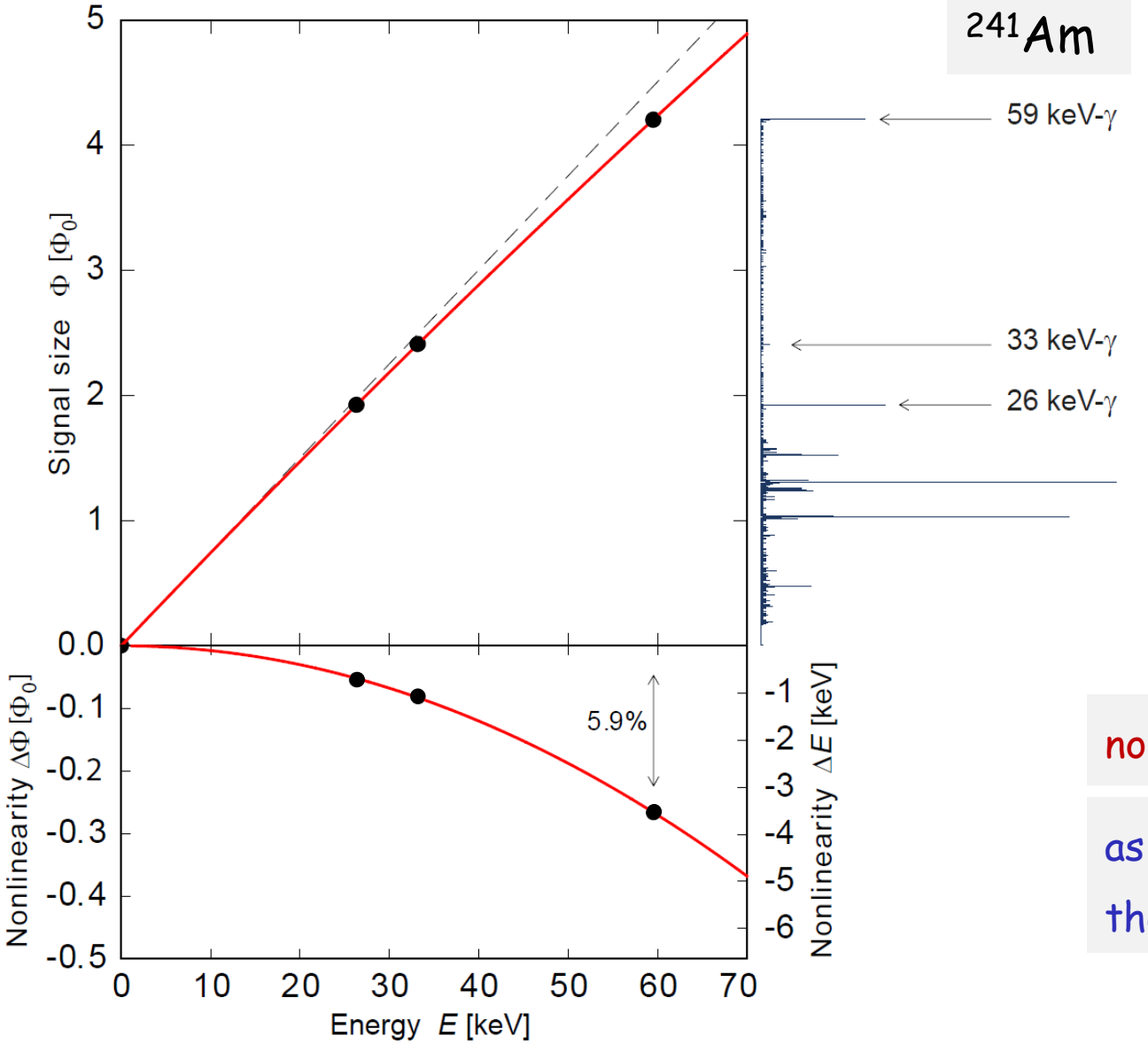

non-linearity: 6% @60 keV

as expected from thermodynamical properties

Expected Resolving Power at 60 keV

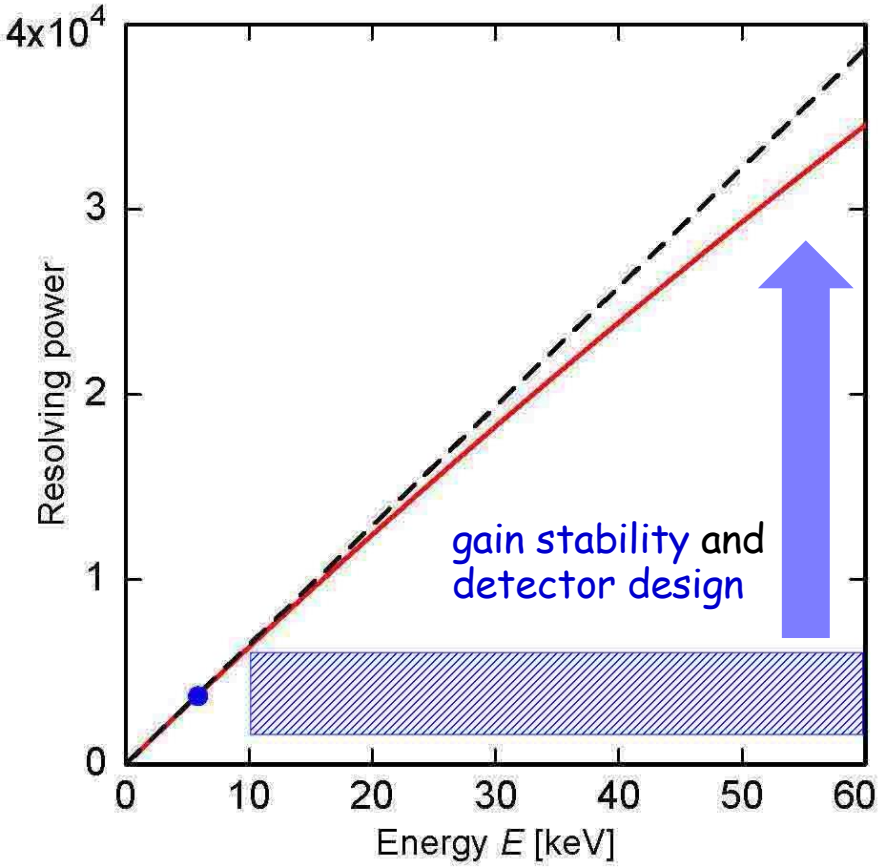

ΔE_{FWHM} = 1.6 eV @ 6 keV

non-linearity: 6% @ 60 keV

Expected resolution for 60 keV photons

ΔE_{FWHM}= 1.8 eV @ 60 keV

$E/\Delta E$ > 30 000 in reach !

Performance of maXs20 Detector at 6 keV

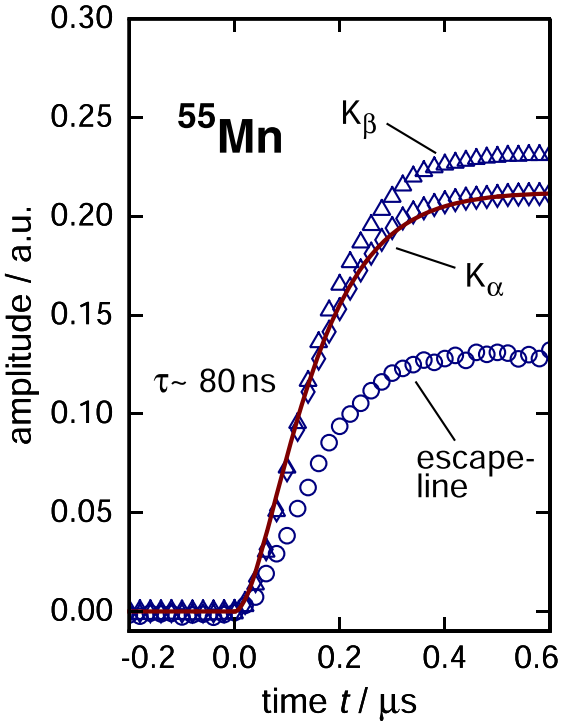

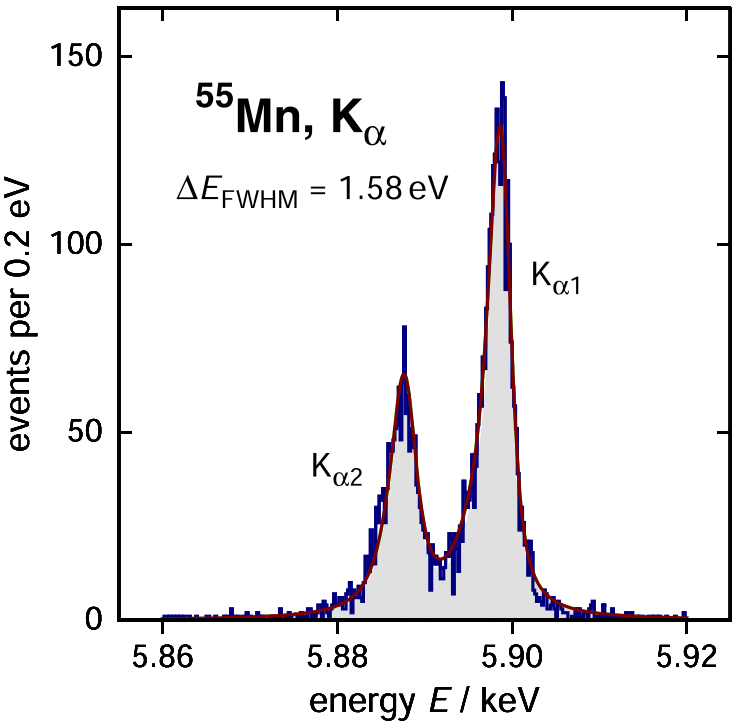

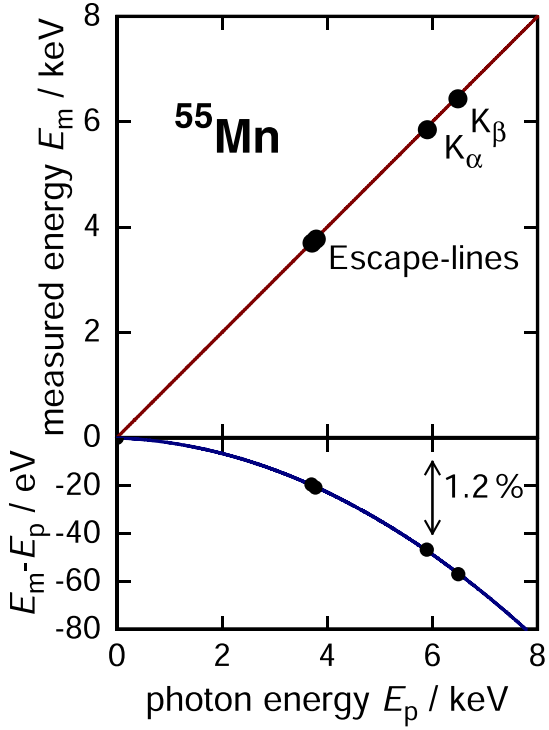

record speed

pileup identification

record resolving power

reduction of overlapping lines

record linearity

energy scale and calibration

Lamb-shift of Highly Charged Ions (SPARC)

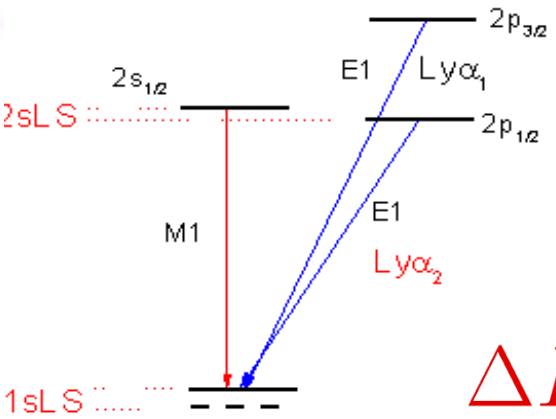

U^{91+}

$$\Delta E_{LS} \propto Z^4/n^3$$

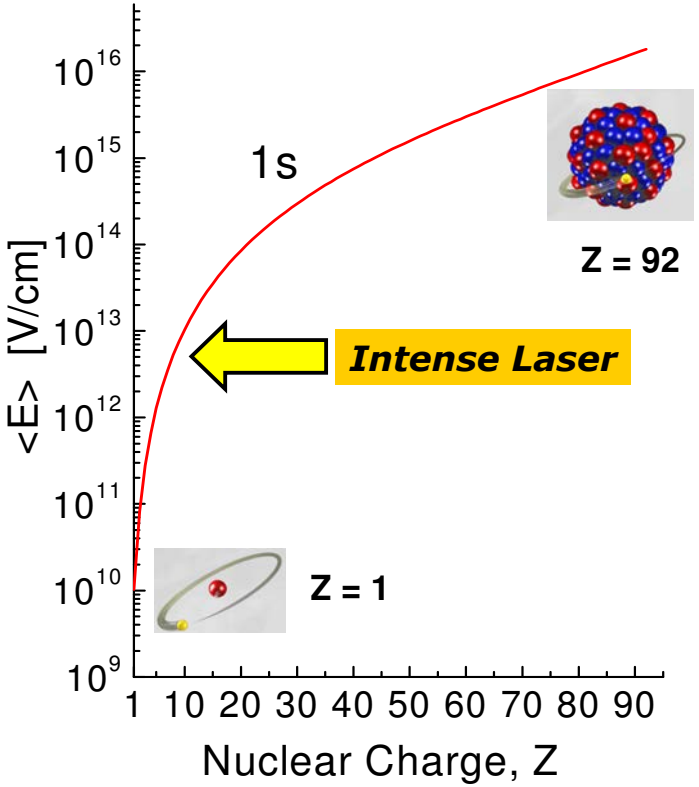

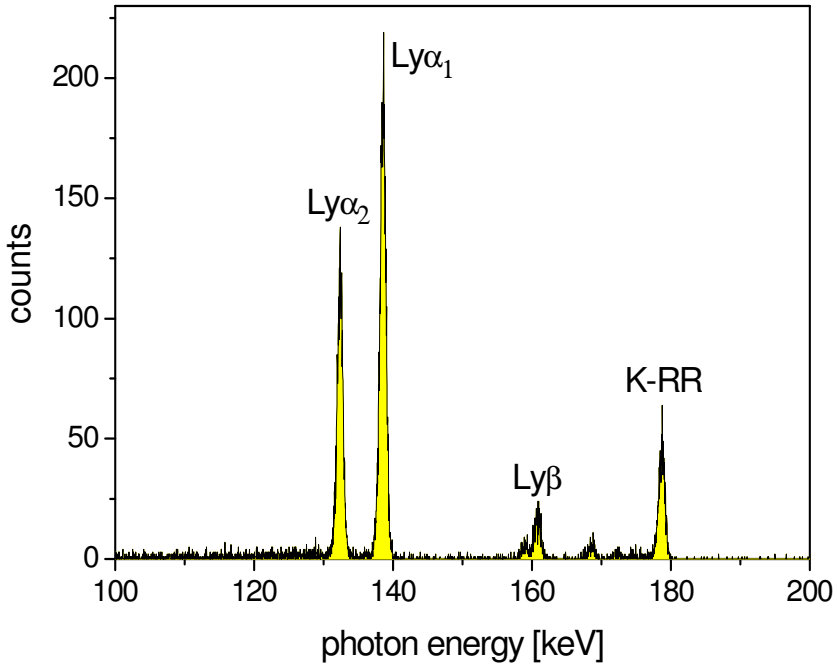

GSI Accelerator Facility

EH	Experiment hall
ESR	Experimental storage ring
FRS	Fragment seperator
SIS	Heavy-ion synchrotron
TH	Target hall
UNILAC	Linear accelerator

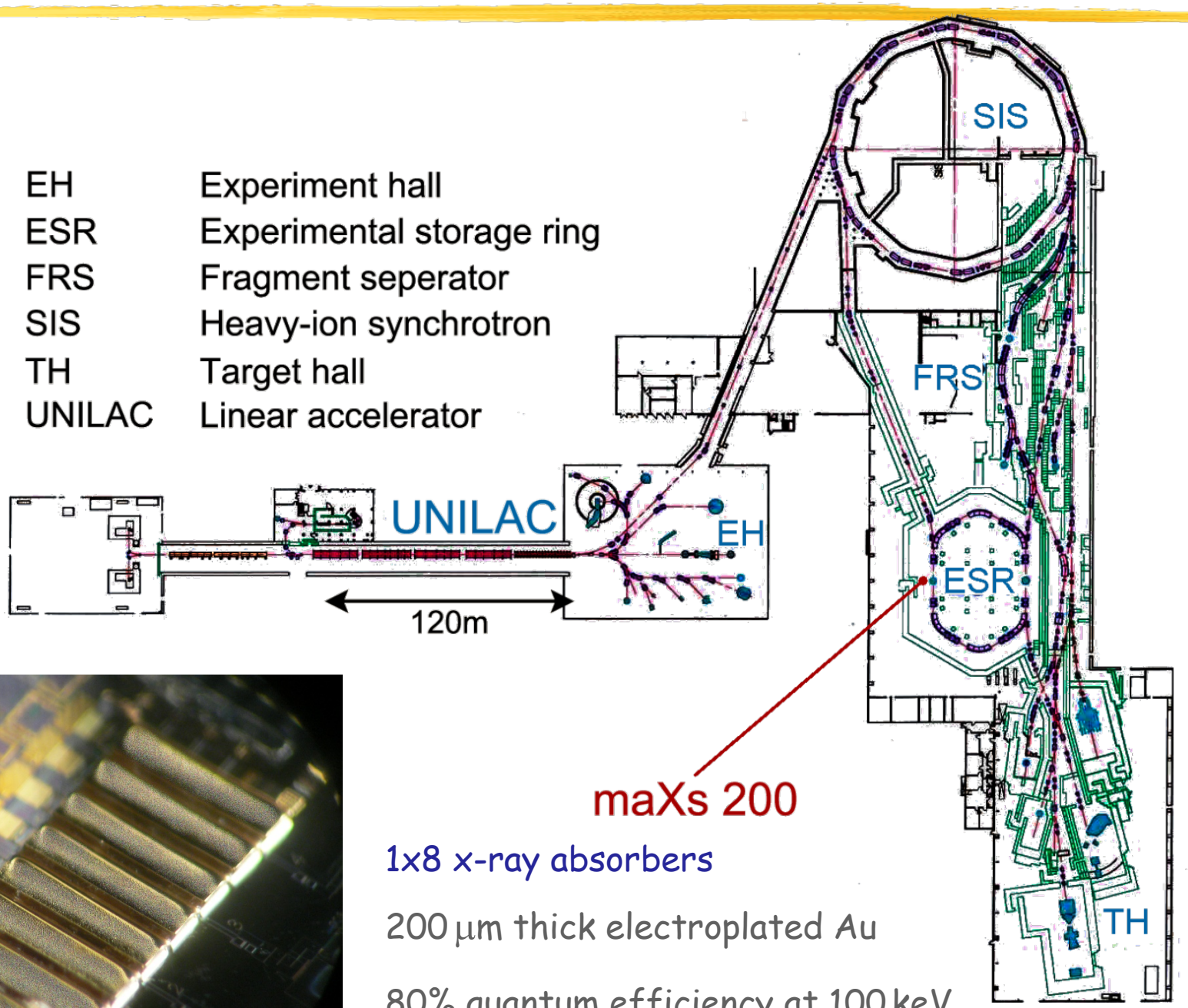

maXs 200

1x8 x-ray absorbers

200 μm thick electroplated Au

80% quantum efficiency at 100 keV

Investigation of H-like and He-like Xe at the ESR

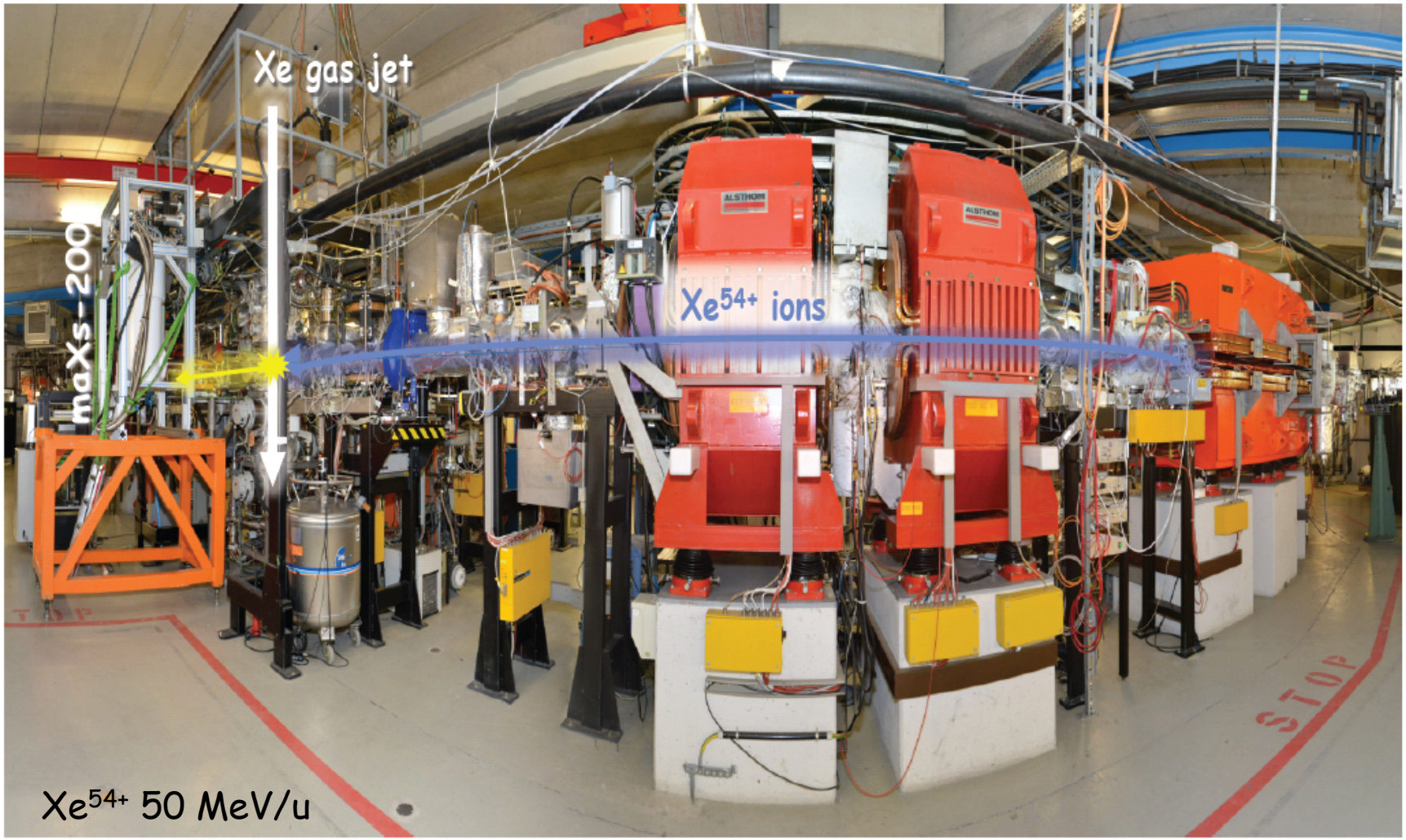

From disassembly to first pulse: 80 hours

H-like $^{53+}$Xe

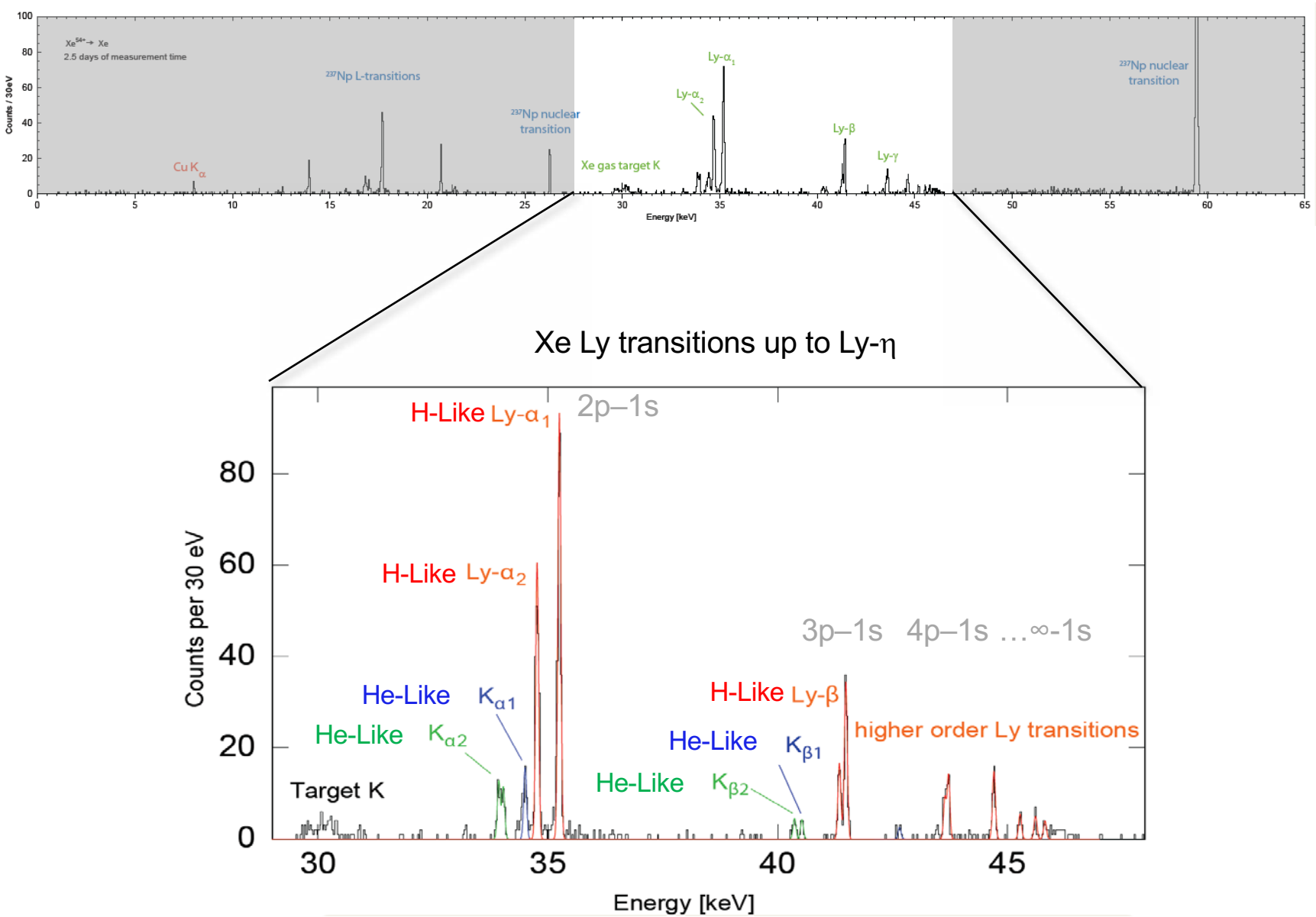

D. Hengstler, *et al.*, Physica Spripta **T166**, 014054 (2015)

maXs-30 Detector (8 x 8 Array)

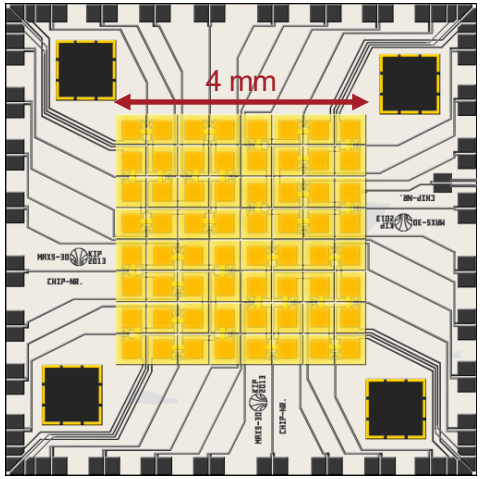

8 x 8 array of X-ray absorbers

500 x 500 µm, 30 µm thick gold

Quantum effeciency ~ 100 % @ 20 keV
80 % @ 30 keV
20 % @ 60 keV

Energy resolution $\Delta E_{FWHM} < 6$ eV

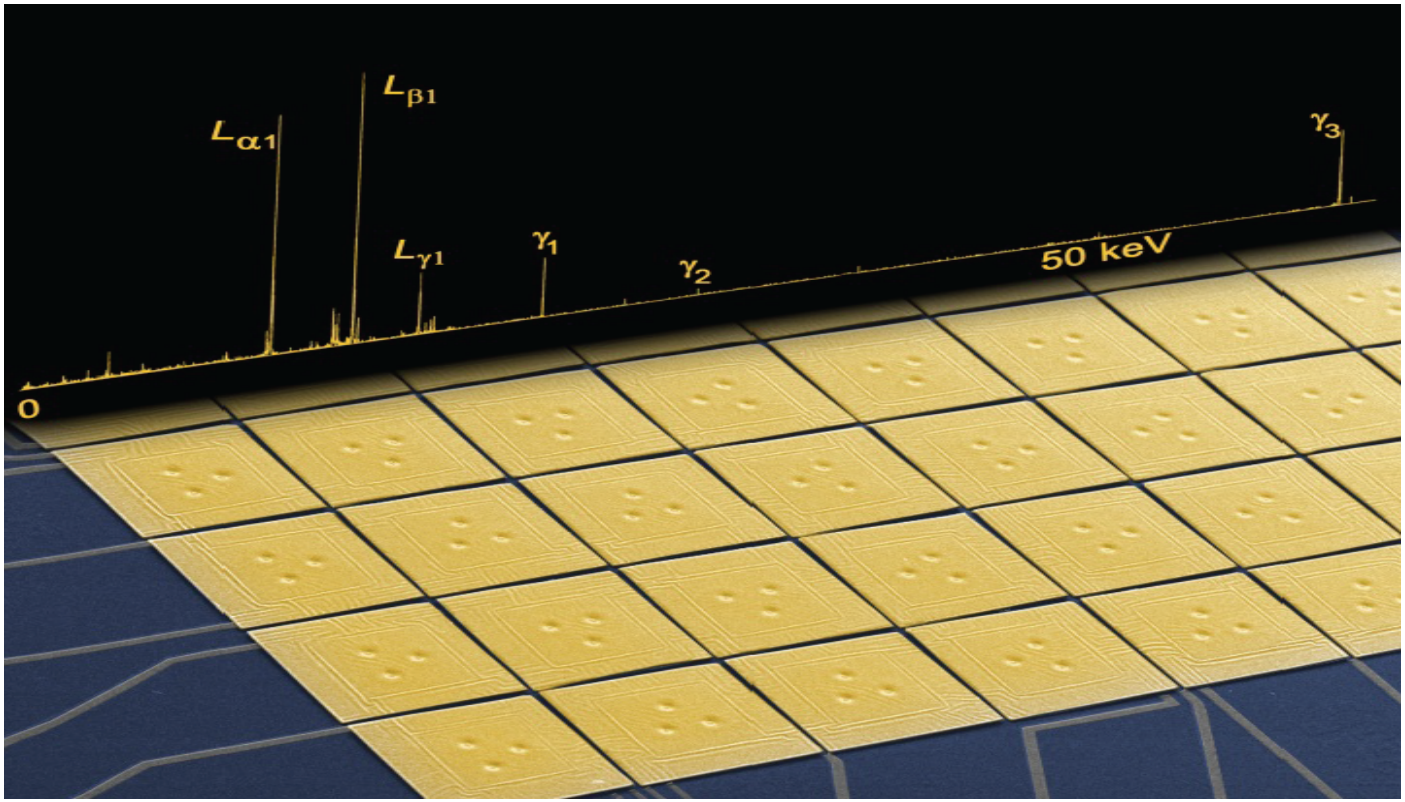

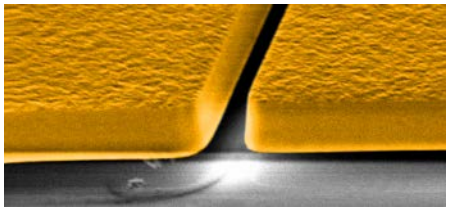

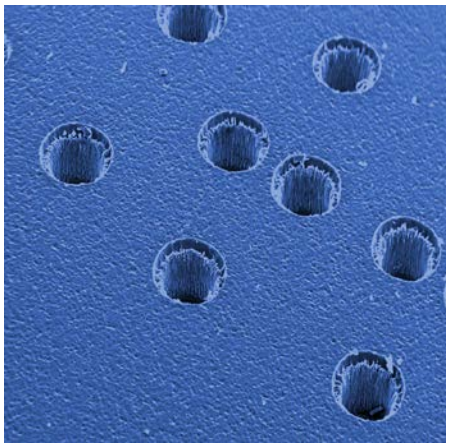

Chemistry of Interstellar Clouds

eg. Reaction rate of

$H_3^+ + e^- \rightarrow H_2 + H$

at T < 10 K (vib.-rot ground state)

Detection of Neutral
Molecule Fragments

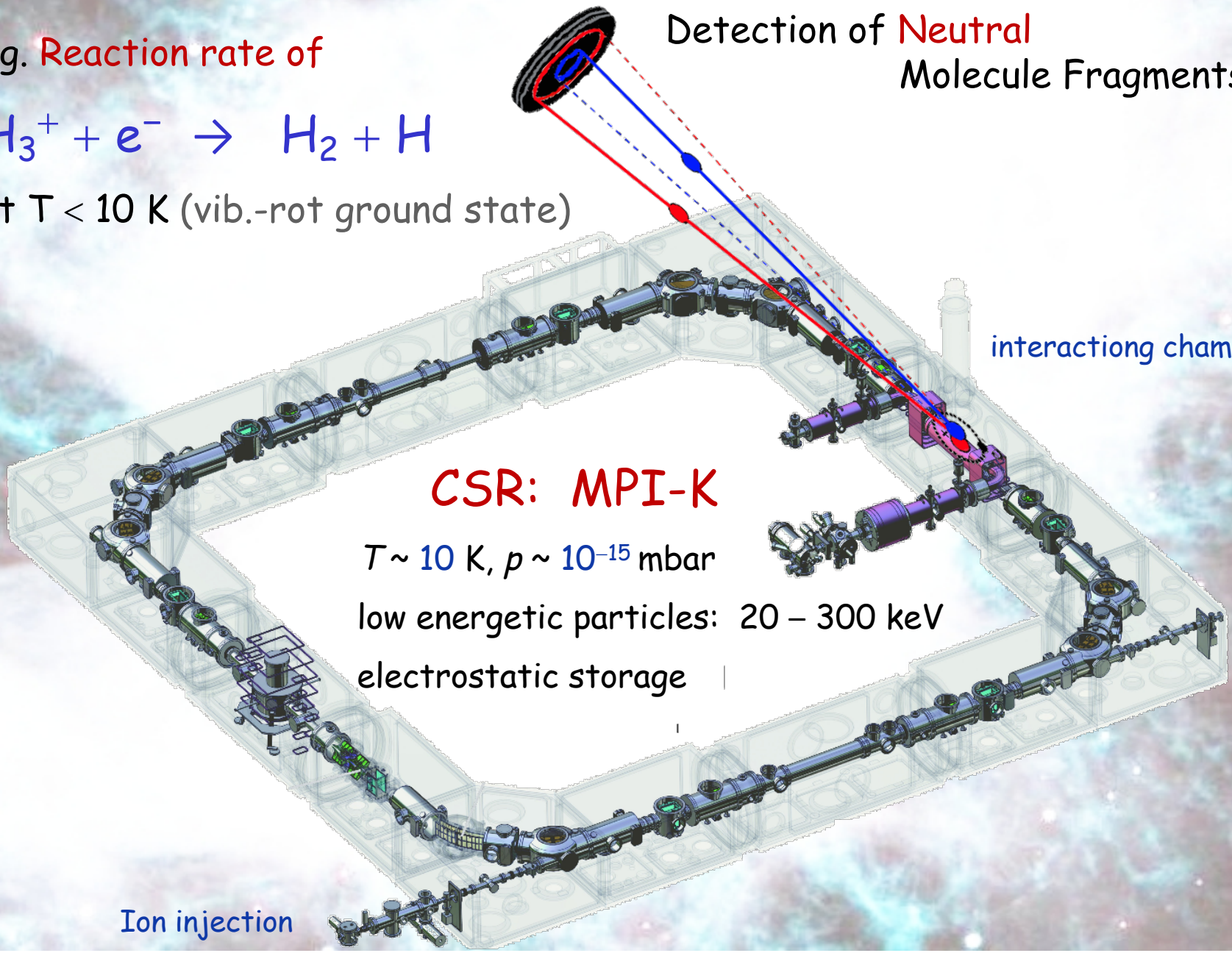

Cryogenic Storage Ring at MPI-K

K. Blaum
A. Wolf
R. v. Hahn
O. Novotny
...

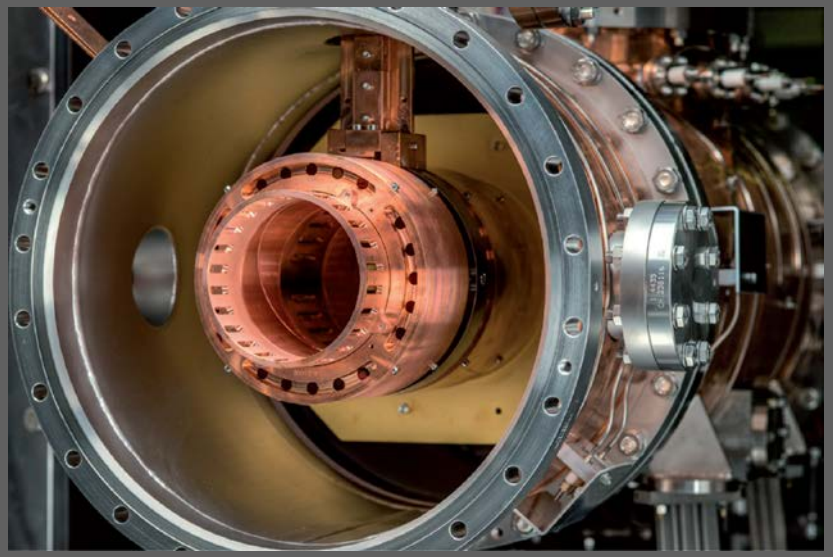

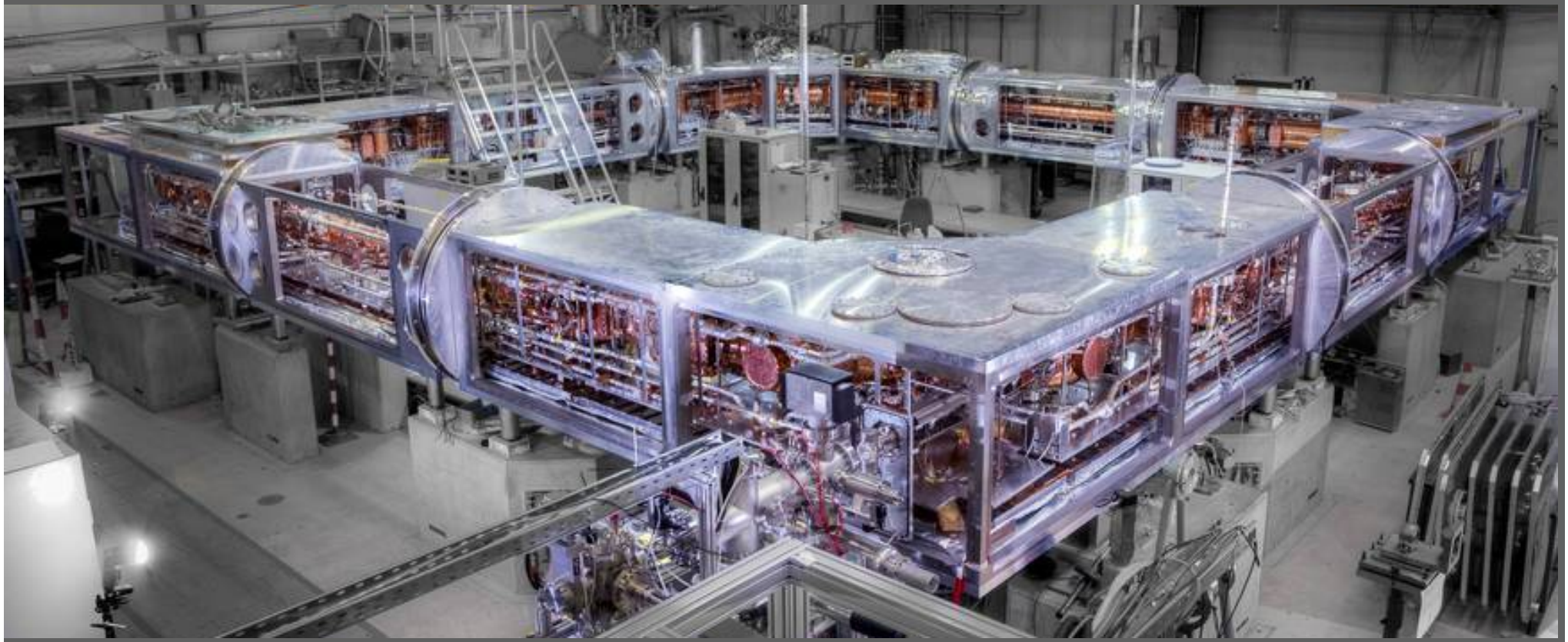

Dissociative Recombination

$$\mathrm{ABCD}^+ + e^- \rightarrow \mathrm{A} + \mathrm{BCD}$$
$$\rightarrow \mathrm{AB} + \mathrm{CD}$$
$$\rightarrow \mathrm{A} + \mathrm{B} + \mathrm{C} + \mathrm{D}.$$

Mass from kinetic energy

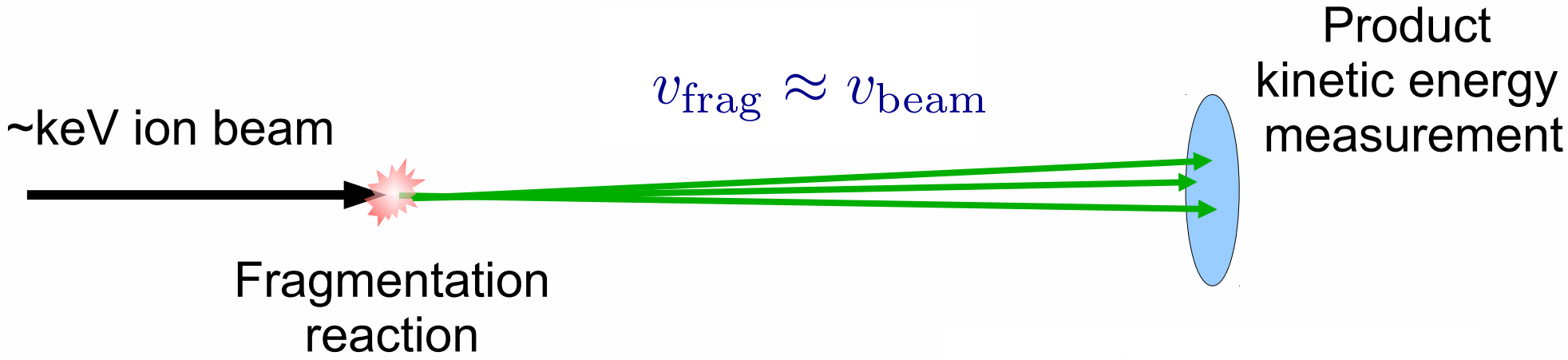

$$E_{\mathrm{kin}}^{\mathrm{lab}} \approx \frac{1}{2}\, m_{\mathrm{frag}}\, v_{\mathrm{beam}}^2$$

First Measurements at MPI for Nuclear Physics

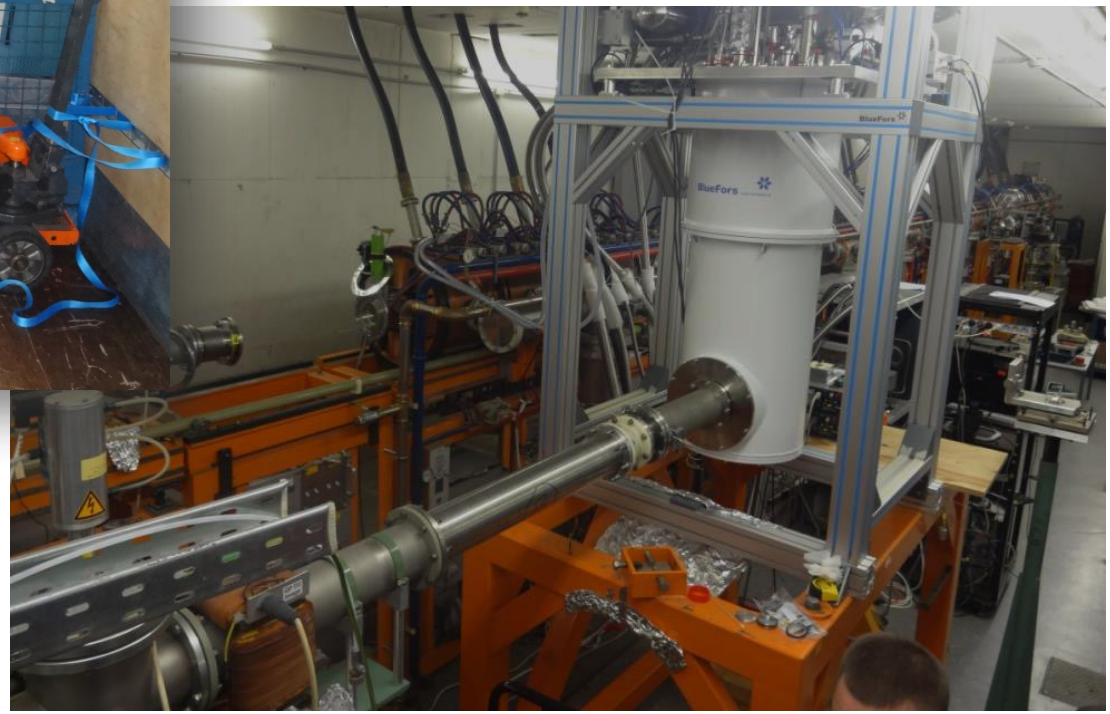

First Measurements at MPI for Nuclear Physics

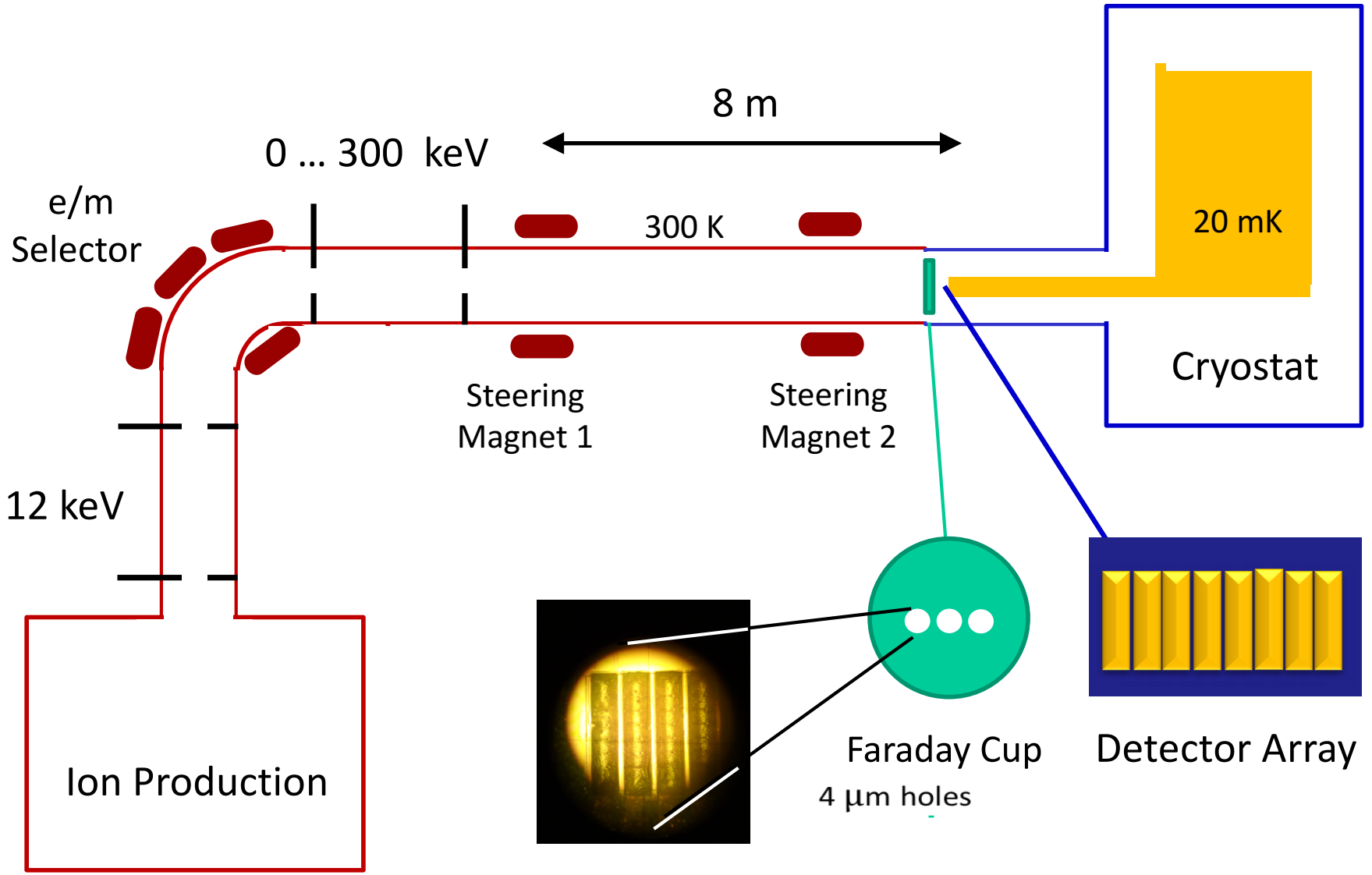

Two Days Later!

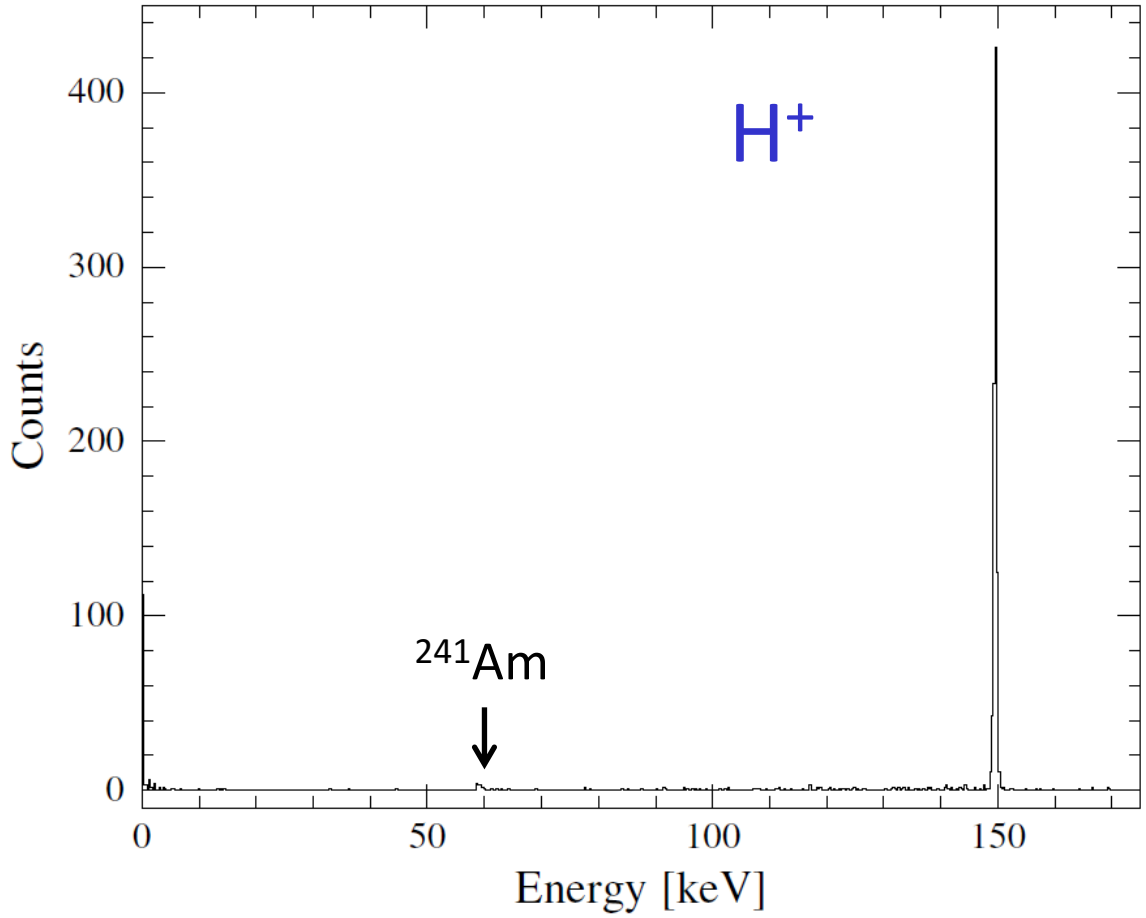

➡ sharp line with a width of about 400 eV

First Measurements at MPI for Nuclear Physics

H^+ accelerated with 14.7 keV, 52.6 keV, 89.9 keV , 151.5 keV

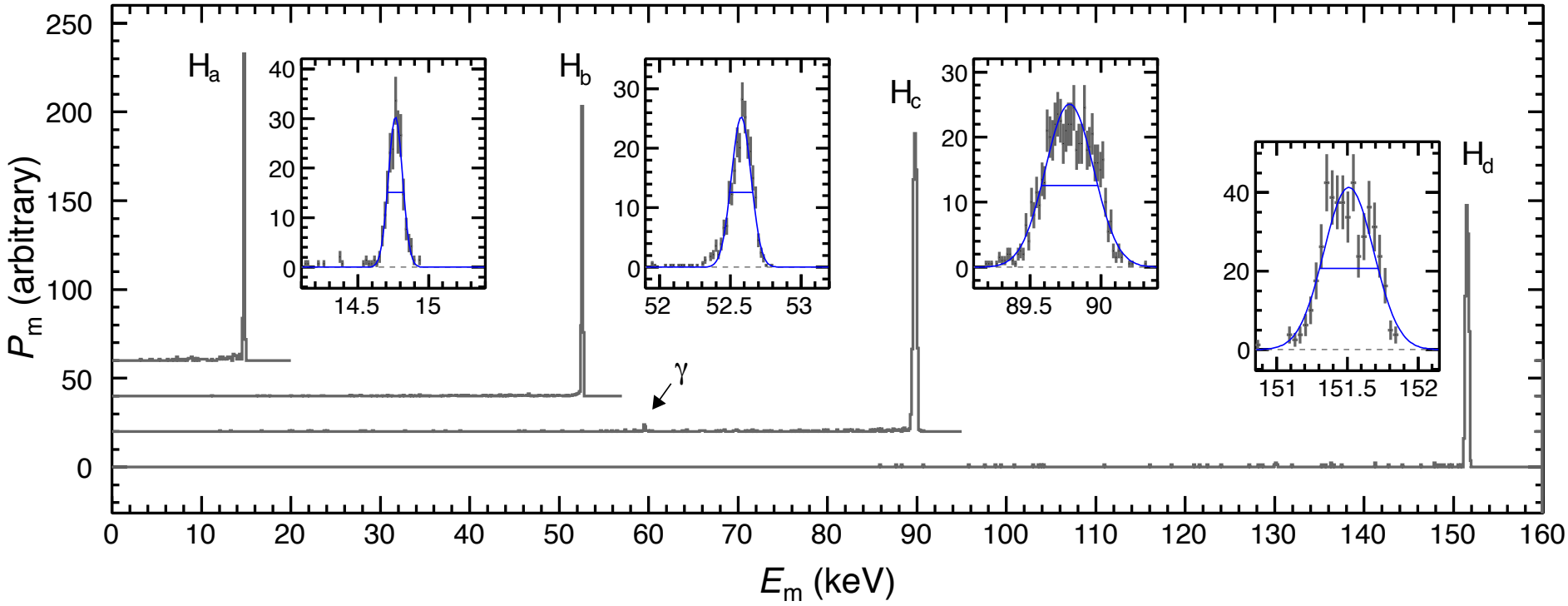

O. Novotný *et al.*, J. Appl. Phys. **118**, 104503 (2015)

Detection of Neutral Fragments

$$ABCD^+ + e^- \rightarrow A + BCD$$
$$\rightarrow AB + CD$$
$$\rightarrow A + B + C + D.$$

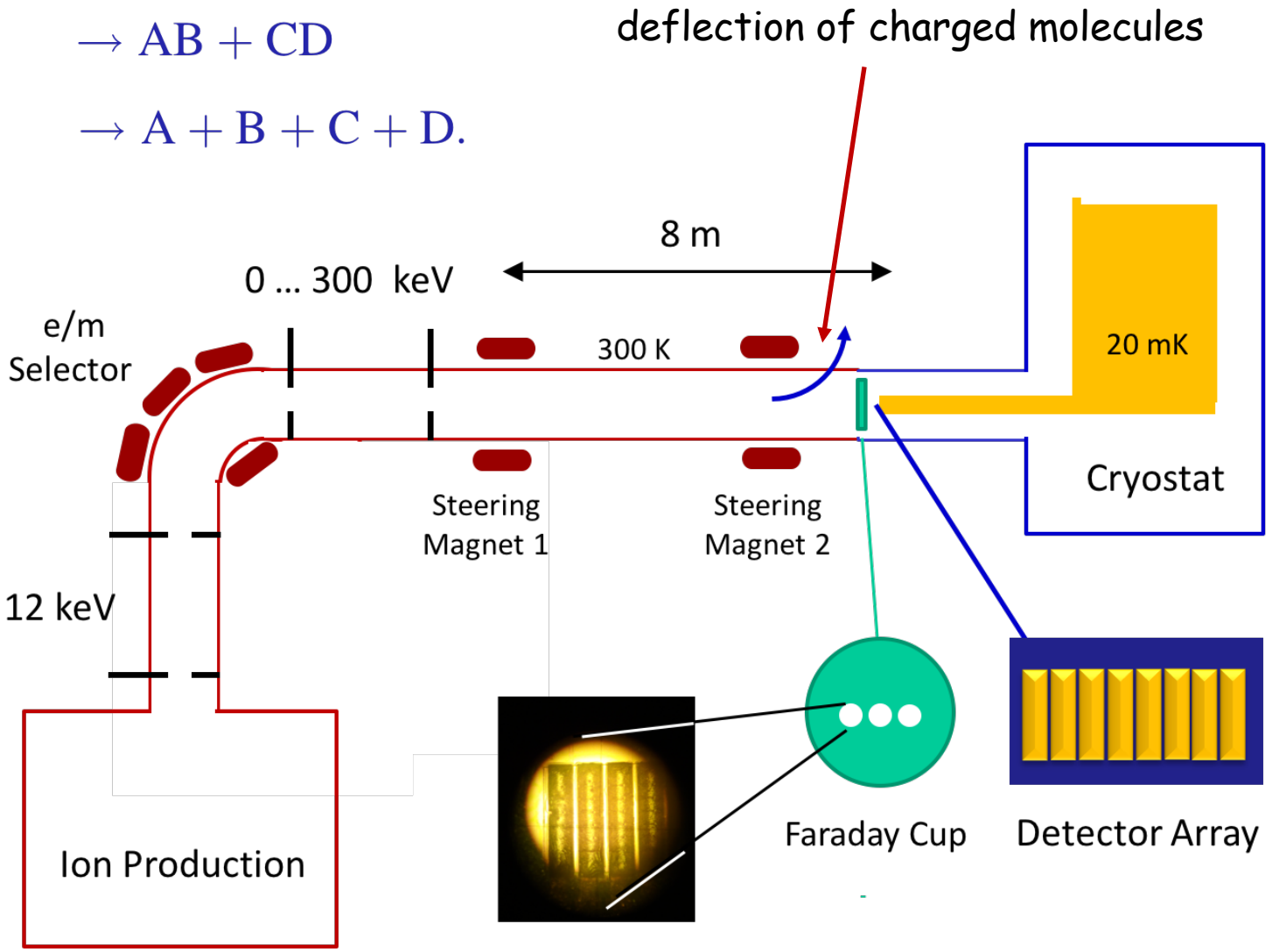

First Measurements at MPI for Nuclear Physics

$$ABCD^+ + e^- \rightarrow A + BCD$$
$$\rightarrow AB + CD$$
$$\rightarrow A + B + C + D.$$

neutral fragments of CH_3^+ accelerated with 150 keV

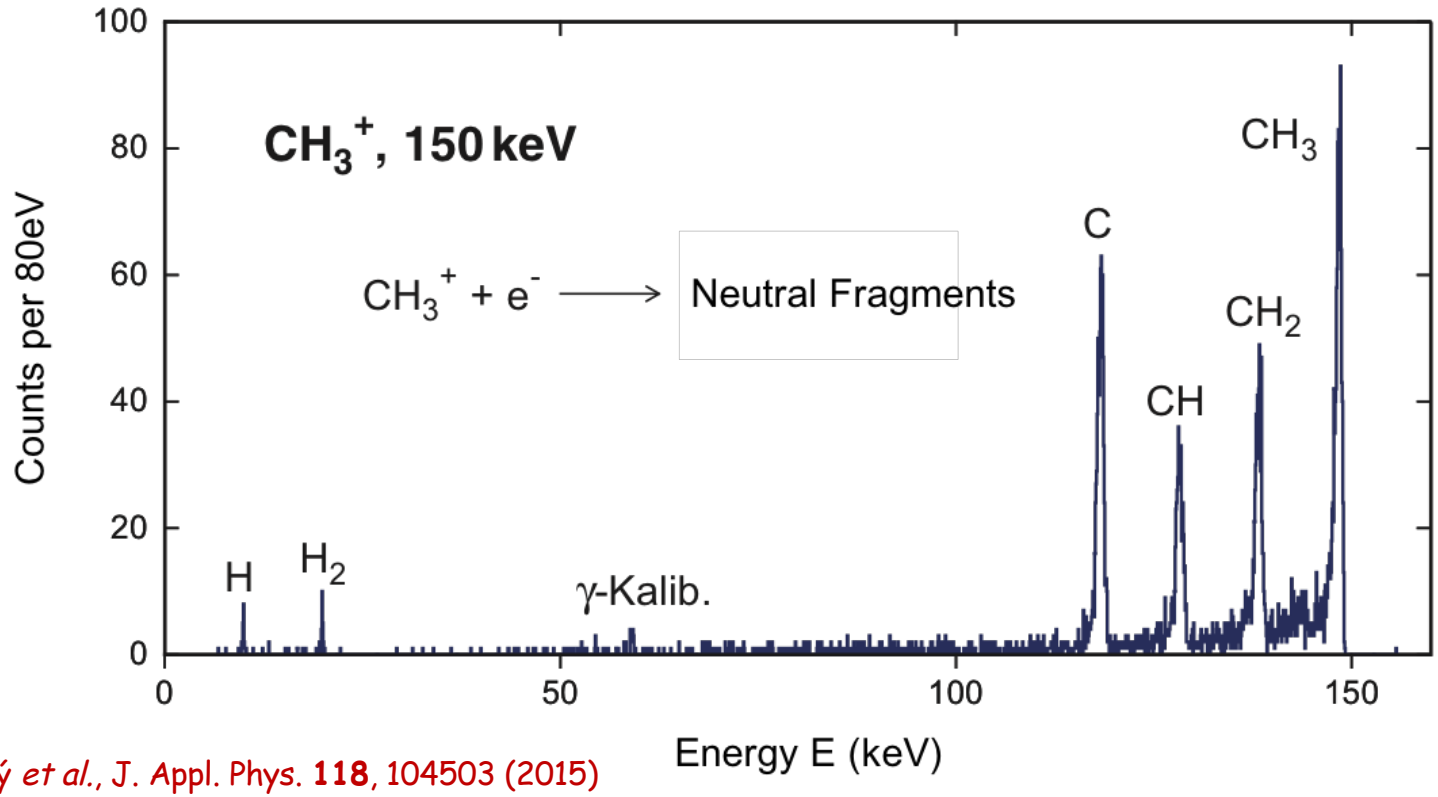

O. Novotný *et al.*, J. Appl. Phys. **118**, 104503 (2015)

MOCCA: a 4k-pixel molecule camera

64 × 64 pixels

200 eV (FWHM)

32 × 32 temperature sensors

Read out by 16 + 16 SQUIDs

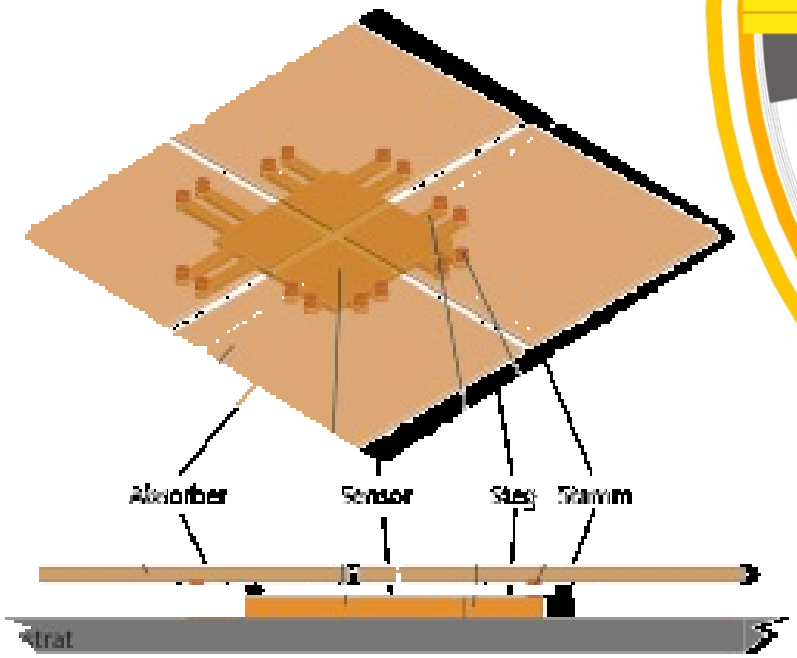

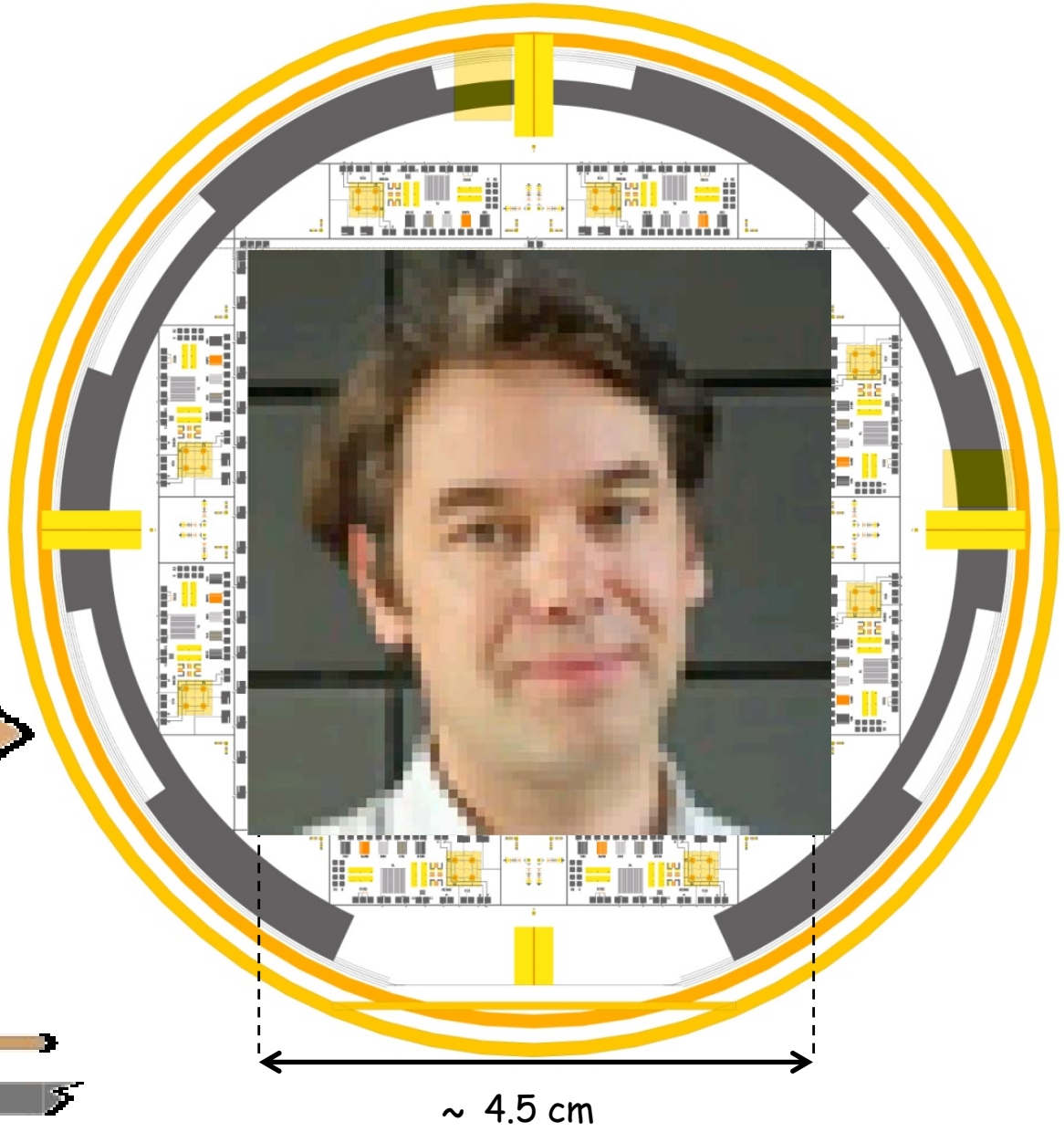

~ 4.5 cm

The Hydra Principle

As pioneered by the NASA-Group

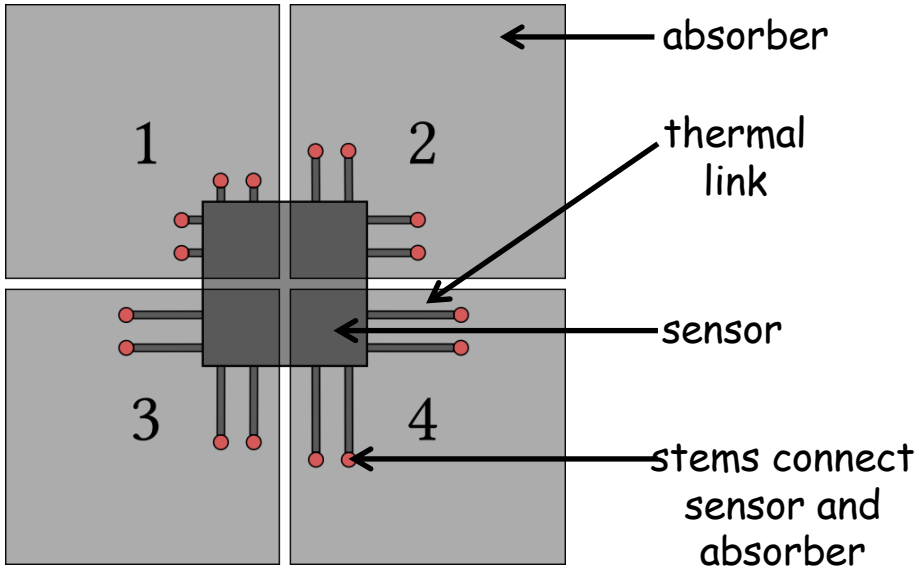

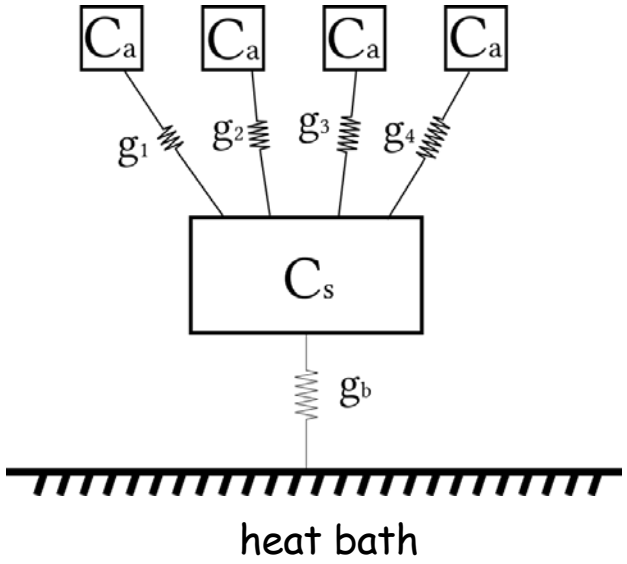

Pixel identification via rise-time of the detector signal

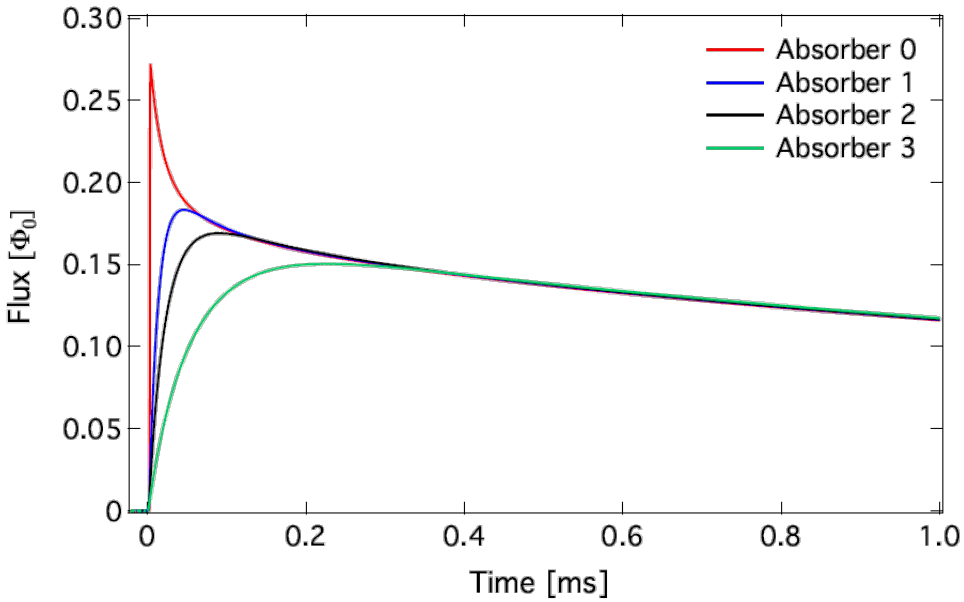

Porst *et al.*, AIP Conf. Proc. **1185** (2009) 599

Readout Scheme

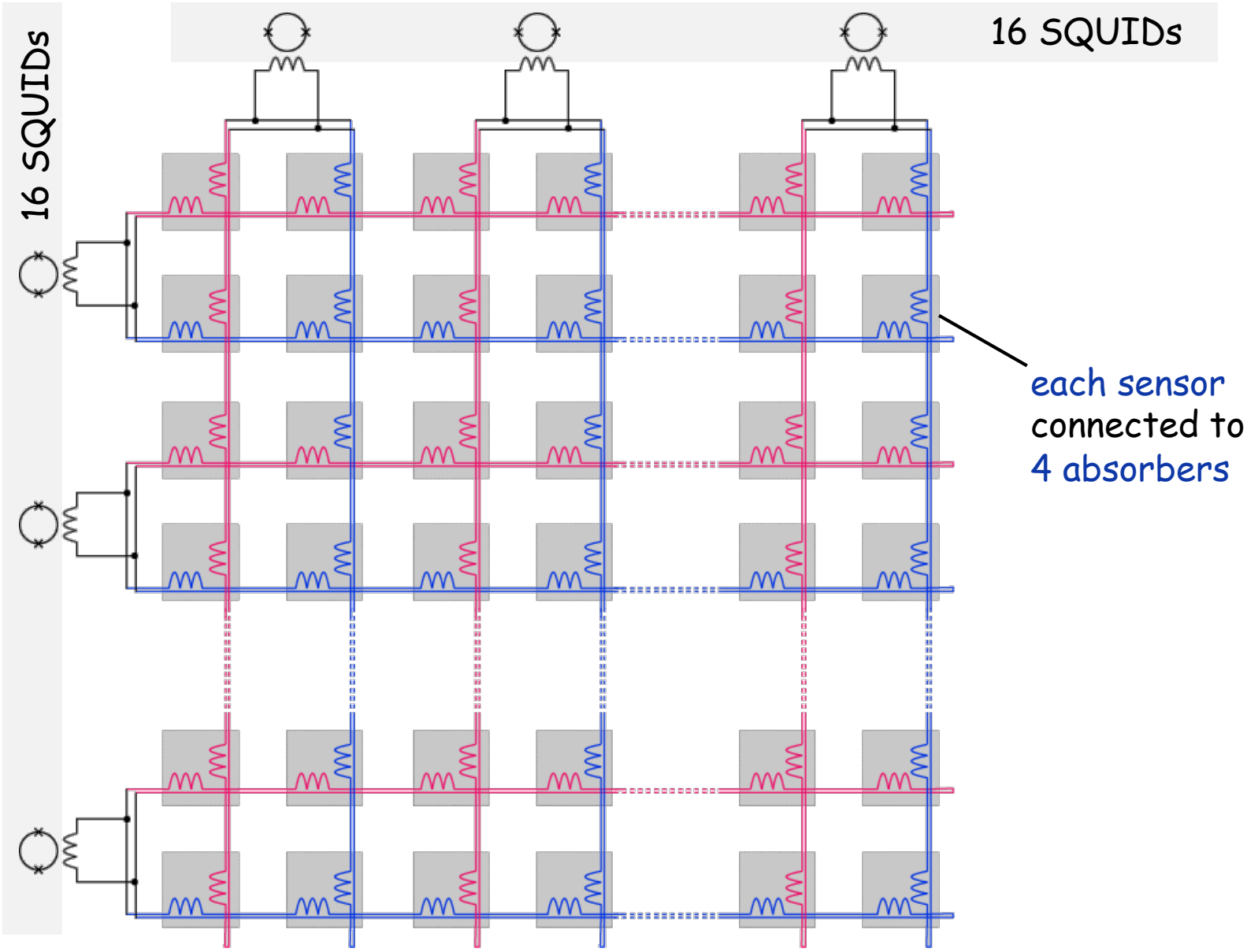

Readout Scheme

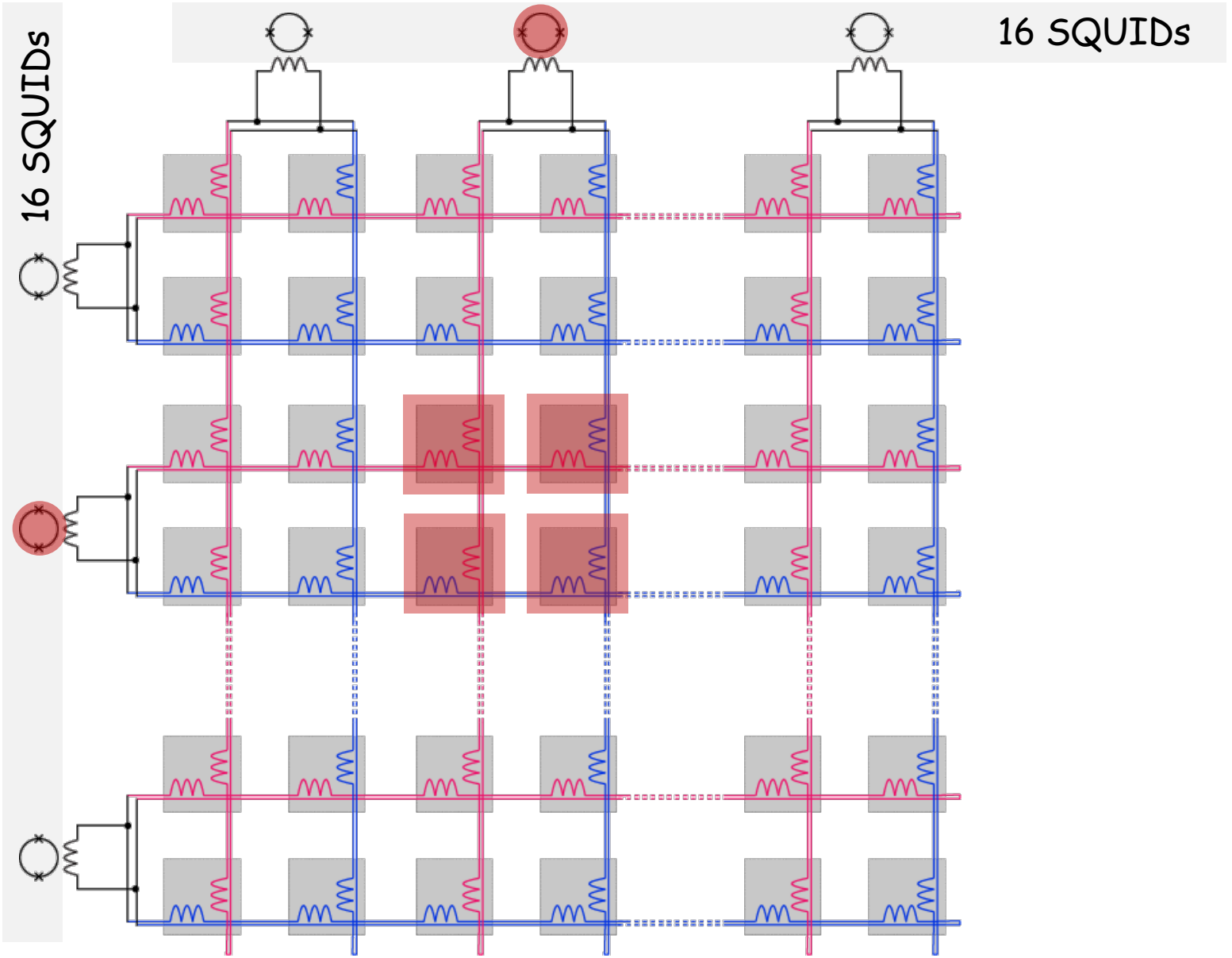

Readout Scheme

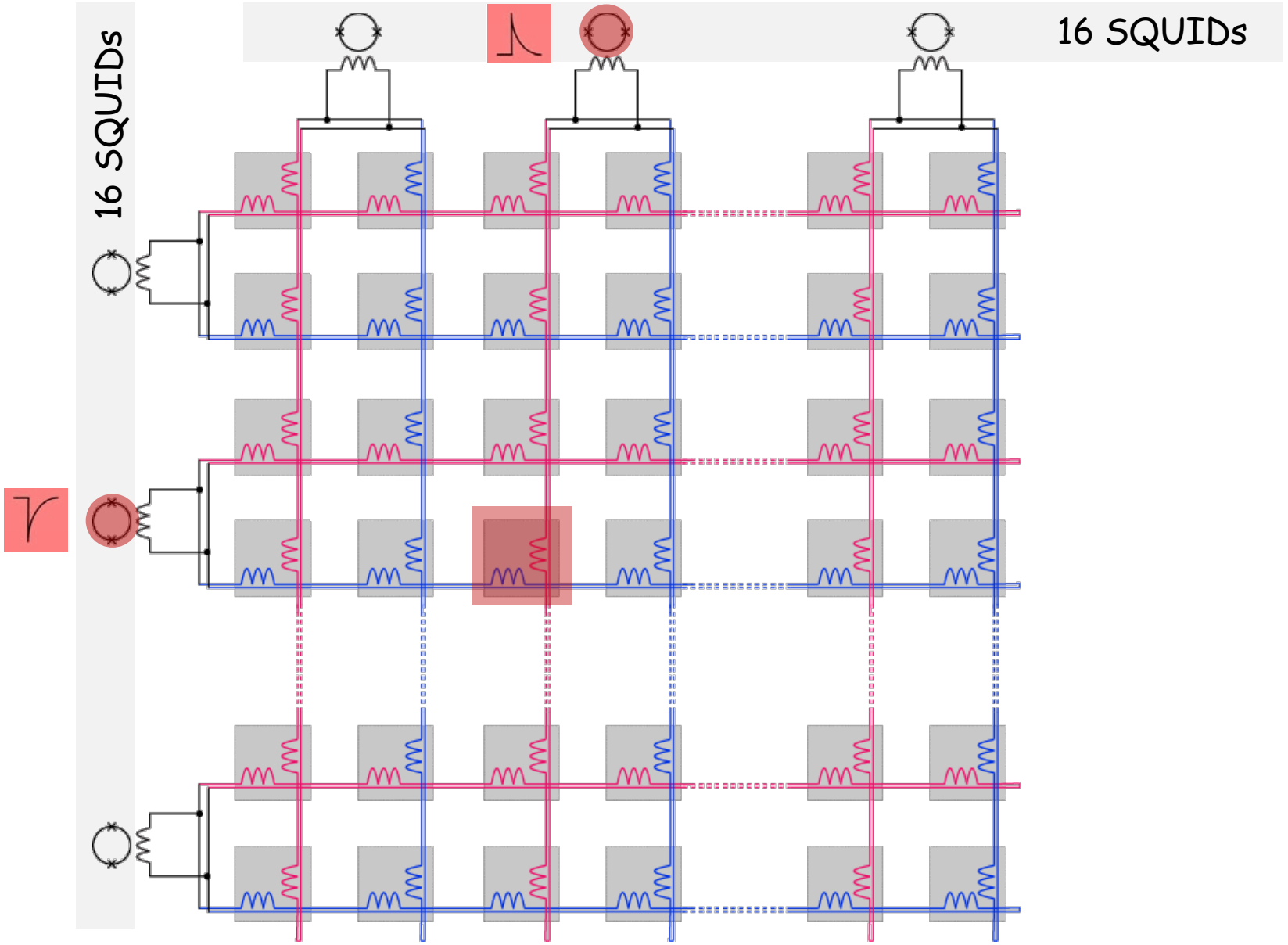

MOCCA Design and Production

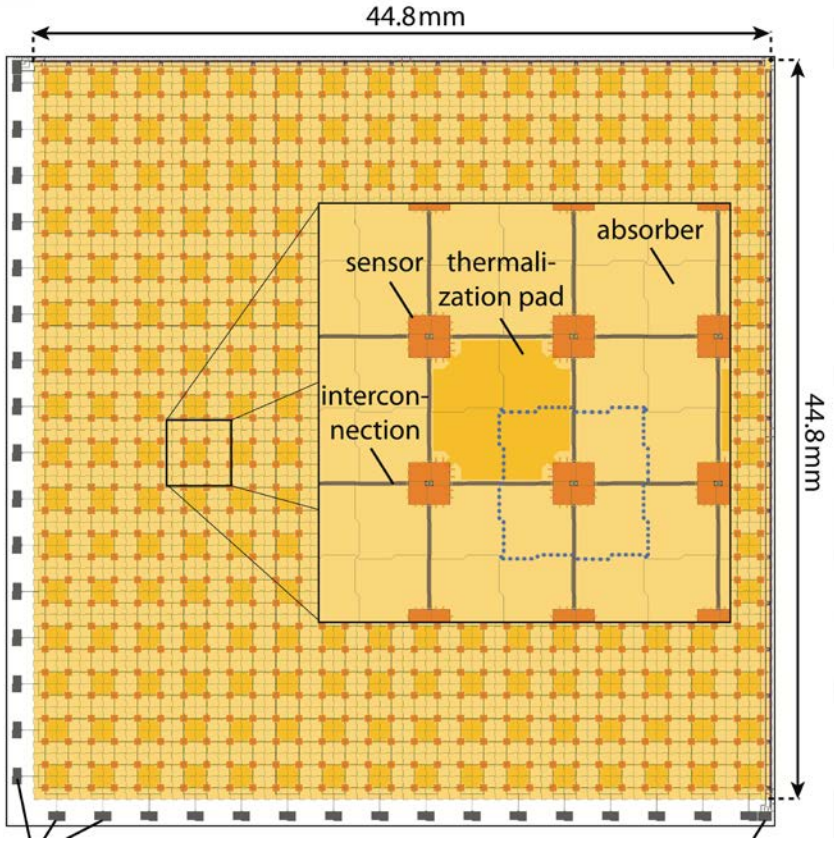

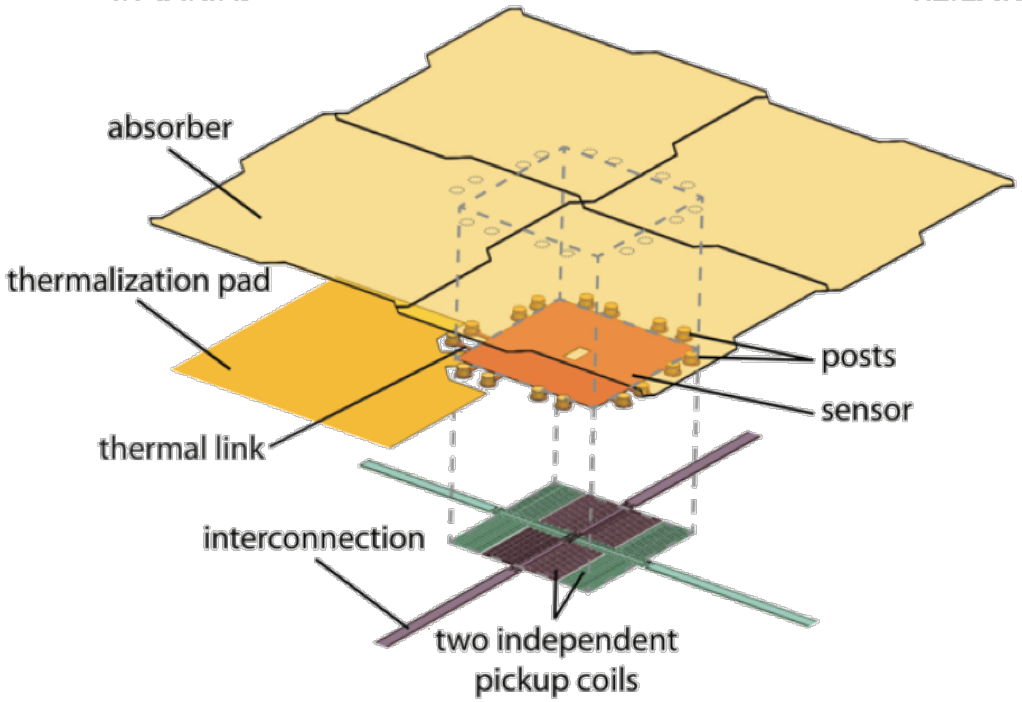

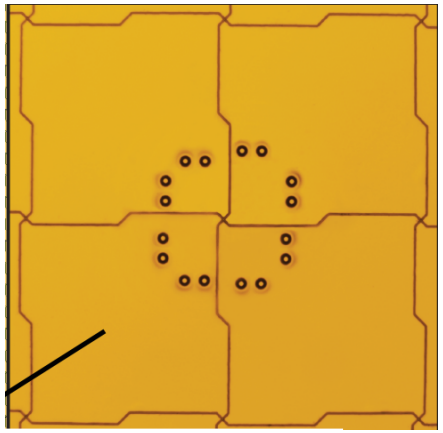

L. Gamer, *et al.*, J. Low. Temp. Phys. (2016)

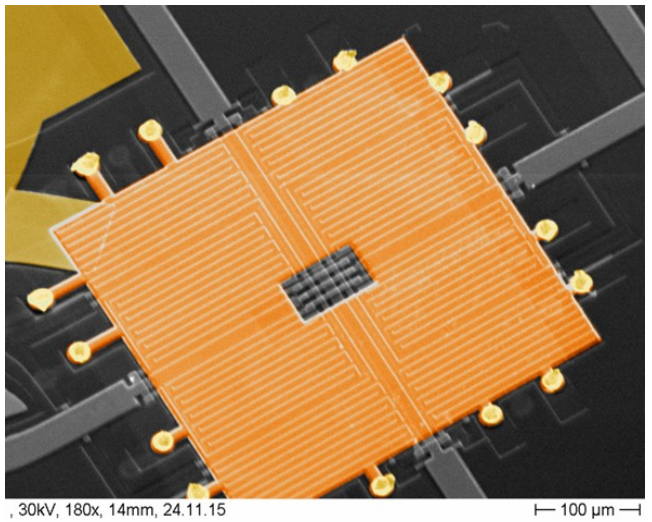

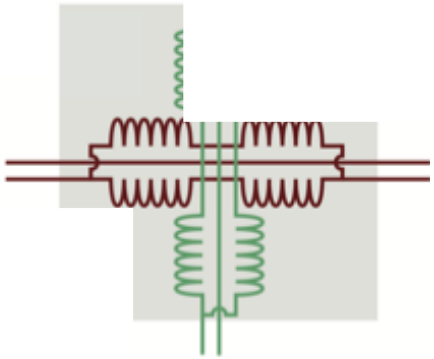

MOCCA in Production

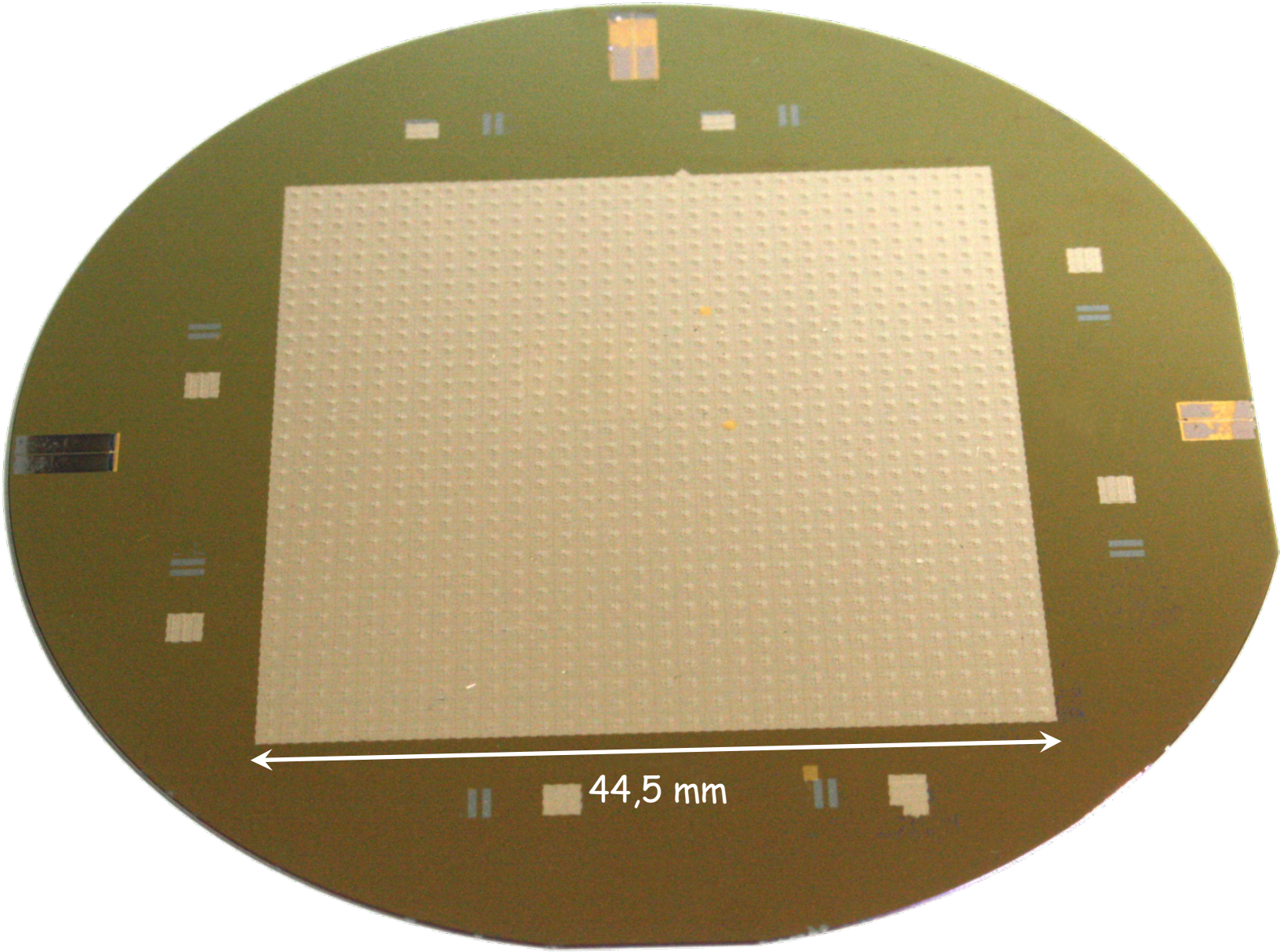

L. Gamer, *et al.*, J. Low. Temp. Phys. (2016)

Integration of MOCCA into CSR

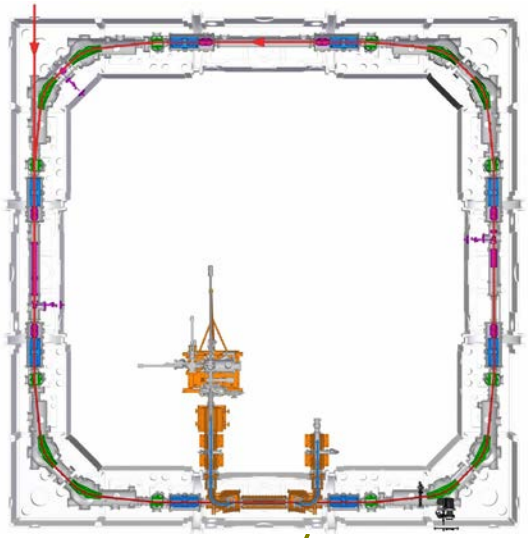

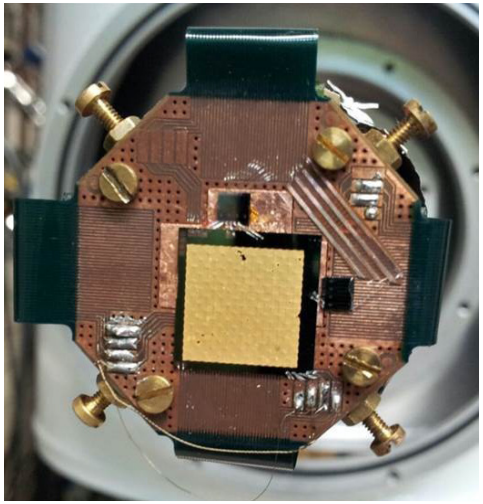

ECHo: Neutrino Mass Determination

Ultimate Goal: Direct determination of the electron neutrino mass

current best limits	$m(\bar{\nu}_e) \leq$	2 eV/c²	beta decay
	$m(\nu_e) \leq$	225 eV/c²	beta capture

Objectives in first two phases

ECHo-1k: better than 10 eV/c² within 3 years — 1 kBq total activity

ECHo-1M: better than 1 eV/c² within 6 years — 1 MBq total activity

Demonstrate the scalability of the approach → sub-eV sensitivity

Search for massive sterile neutrinos in the range up to ≈ 2.8 keV/c²

Direct Neutrino Mass Measurement

A. De Rujula, M. Lusignoli, Phys. Lett. B **118** (1982) 429

$^{163}_{67}\mathrm{Ho}$

$$p + e^- \rightarrow n + \nu_e$$

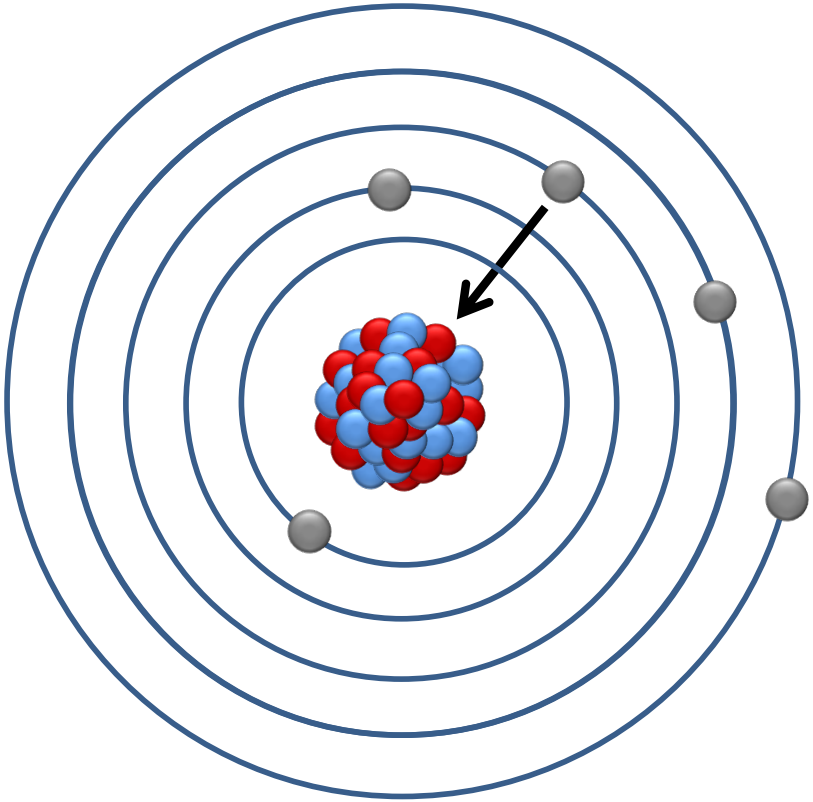

Electron Capture: ^{163}Ho

A. De Rujula, M. Lusignoli, Phys. Lett. B **118** (1982) 429

$$^{163}_{67}\mathrm{Ho} \rightarrow {}^{163}_{66}\mathrm{Dy}^{*} + \nu_{\mathrm{e}}$$

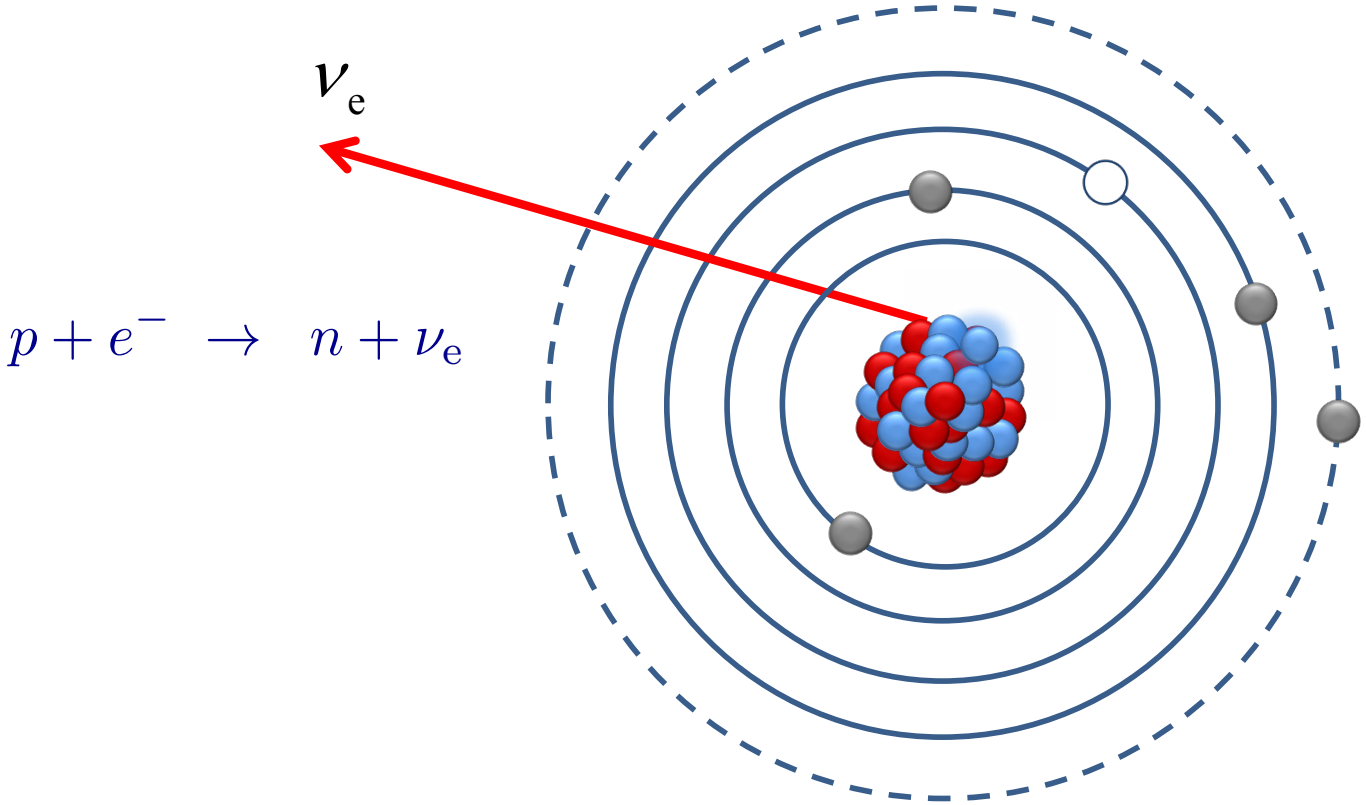

Electron Capture: ^{163}Ho

A. De Rujula, M. Lusignoli, Phys. Lett. B **118** (1982) 429

$$^{163}_{67}\mathrm{Ho} \rightarrow {}^{163}_{66}\mathrm{Dy}^{*} + \nu_{\mathrm{e}}$$

$$\hookrightarrow {}^{163}_{66}\mathrm{Dy} + E_{\mathrm{C}}$$

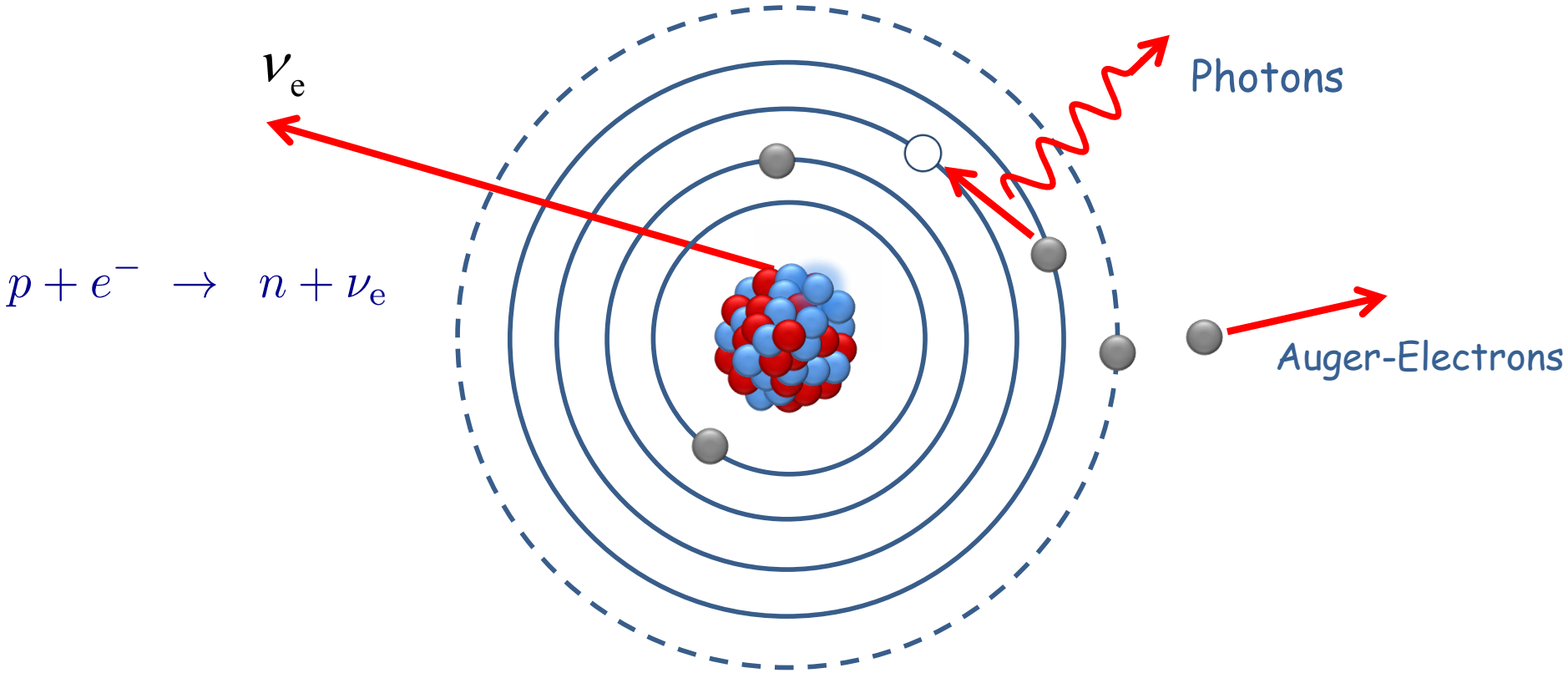

Electron Capture Spectrum of ^{163}Ho

$$\frac{\mathrm{d}N}{\mathrm{d}E_\mathrm{C}} = A\,(Q_\mathrm{EC}-E_\mathrm{C})^2\sqrt{1-\frac{m_\nu^2}{(Q_\mathrm{EC}-E_\mathrm{C})^2}}\sum_j C_j n_j B_j \phi_j^2(0)\,\frac{\Gamma_j/2\pi}{(E_\mathrm{C}-E_j)^2+\Gamma_j^2/4}$$

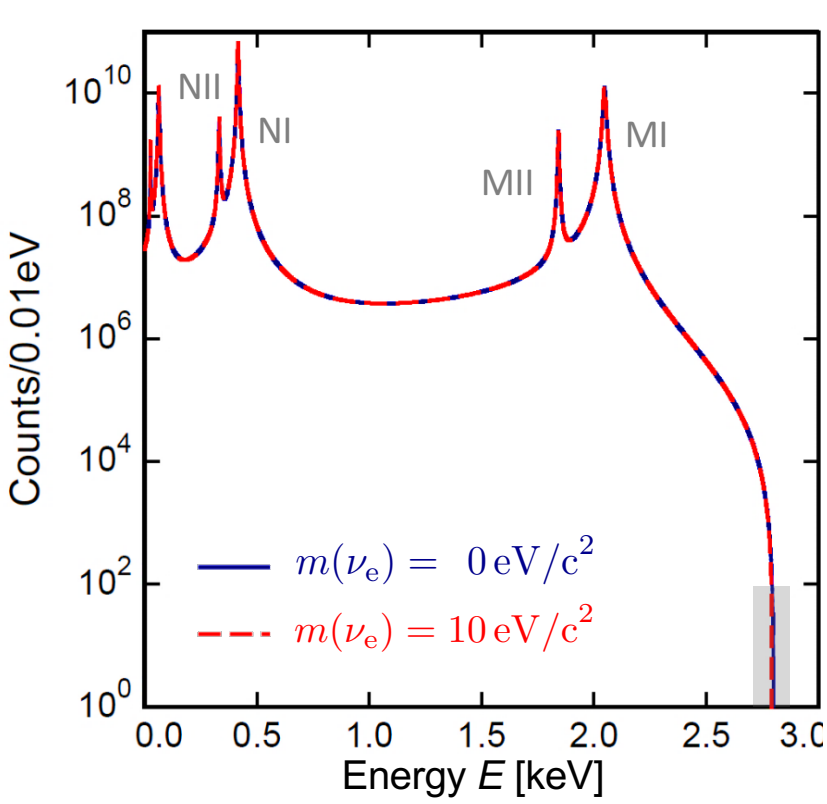

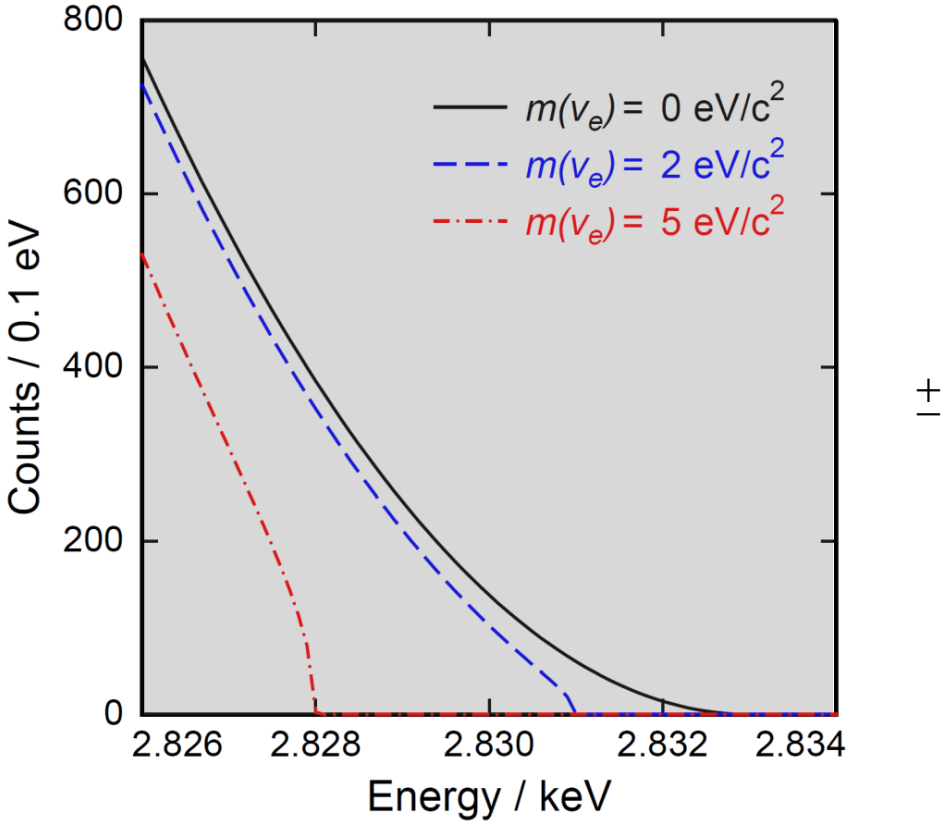

Low Q_{EC} = (2.833 ± 0,030^{stat} ± 0,015^{sys}) keV

S. Eliseev et al., *Phys. Rev. Lett.*, **115**, 062501 (2015)

Calorimetric Detection of E_C

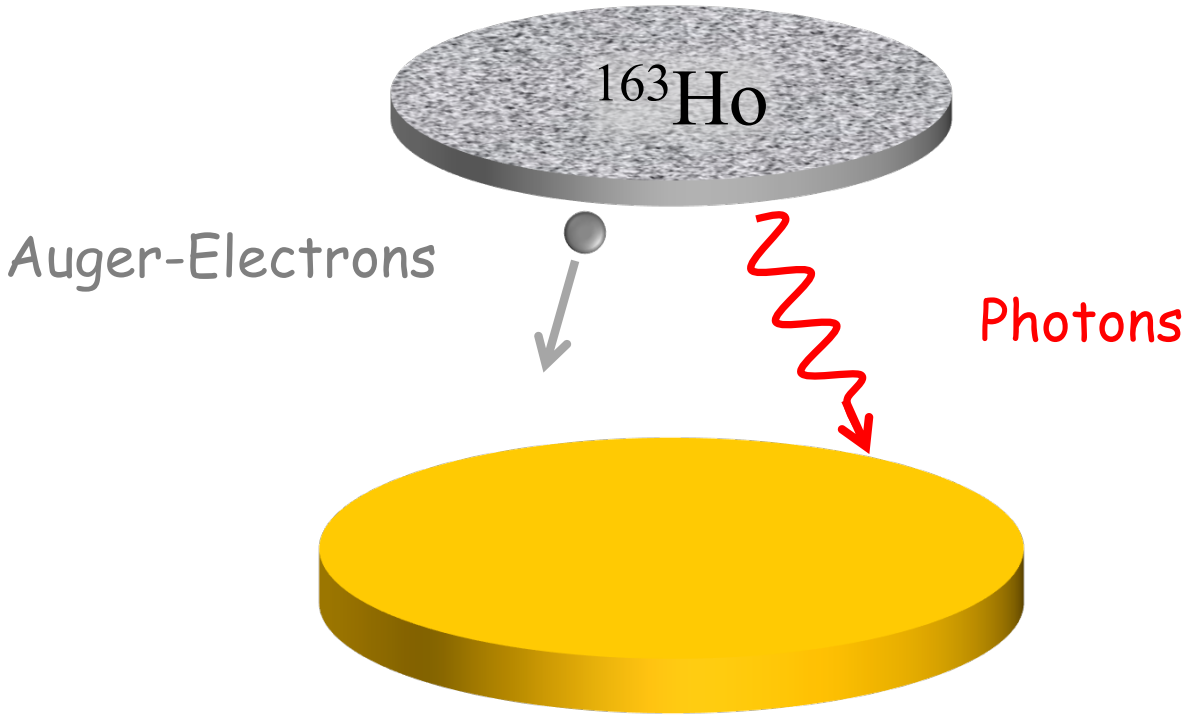

Calorimetric Detection of E_C

4π Absorber

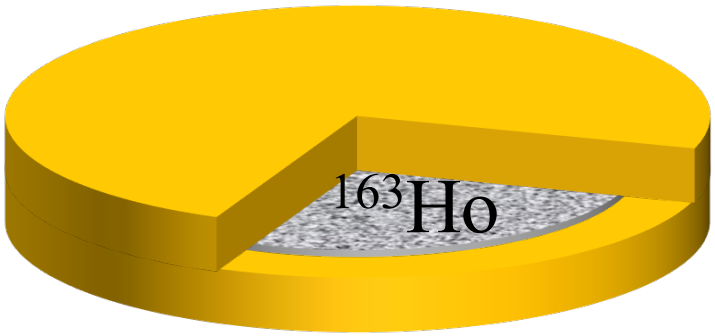

Calorimetric Detection of E_C

$$\Delta T = \frac{E}{C}$$

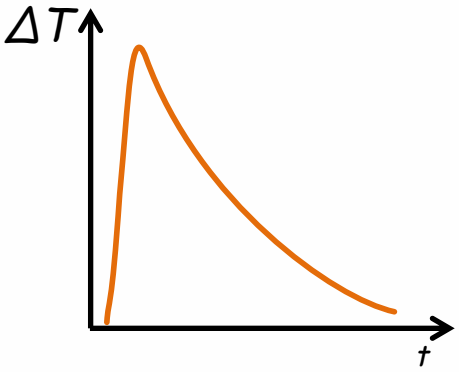

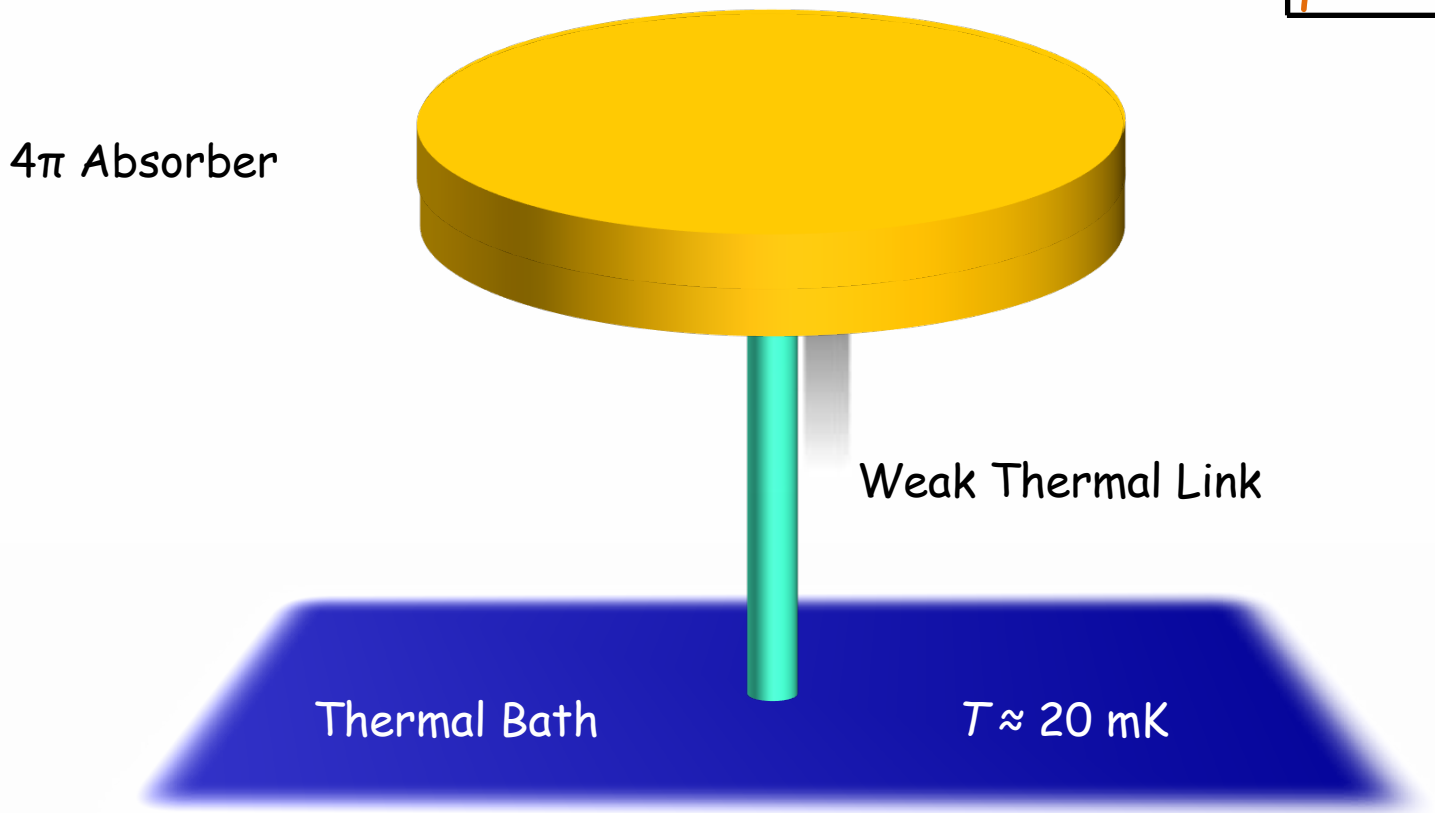

Prototype Detector

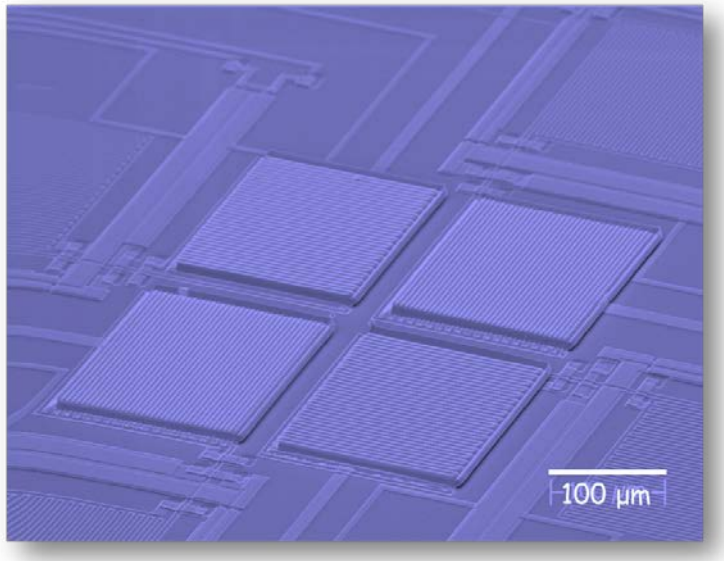

Implantation 2009 at CERN

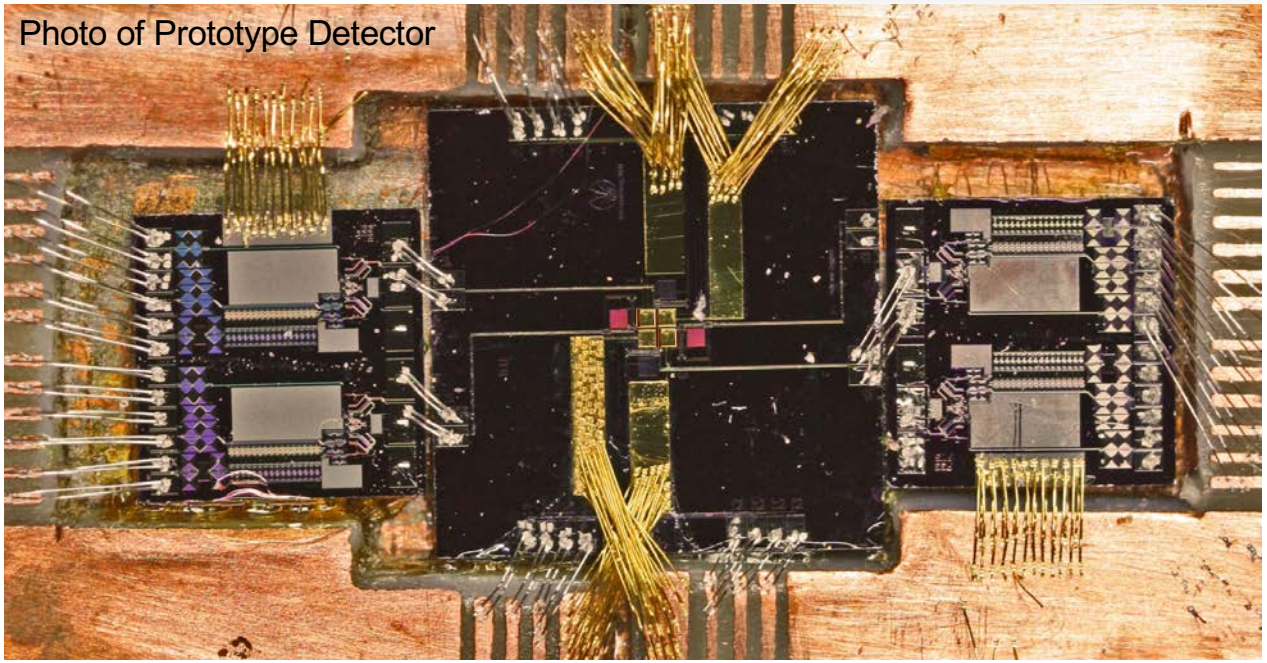

Previous Results and First MMC Measurement

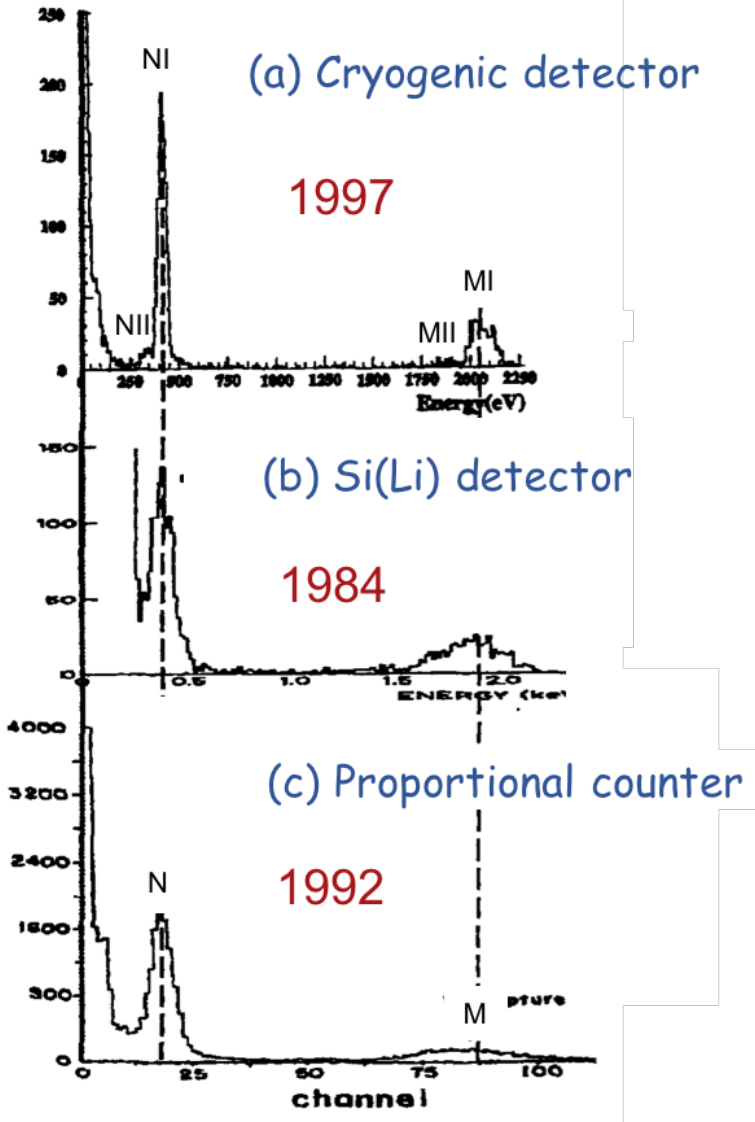

(a) F. Gatti *et al.*, Physics Letters B **398** (1997) 415-419

(b) E. Laesgaard *et al.*, Proceeding of 7th International Conference on Atomic Masses and Fundamental Constants (AMCO-7), (1984).

(c) F.X. Hartmann and R.A. Naumann, Nucl. Instr. Meth. A **313** (1992) 237.

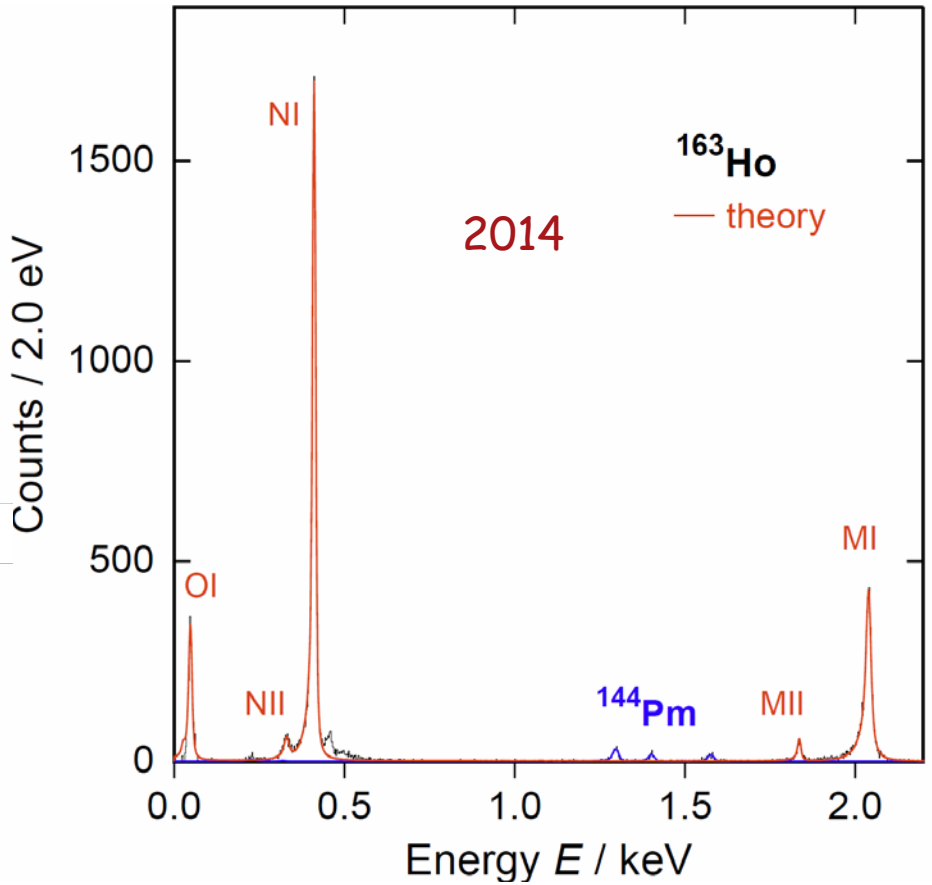

F. Gatti *et al.*, Physics Letters B **398** (1997) 415-419

arXiv:1409.0071

Requirements For Sub-eV Sensitivity: Total Number of Counts

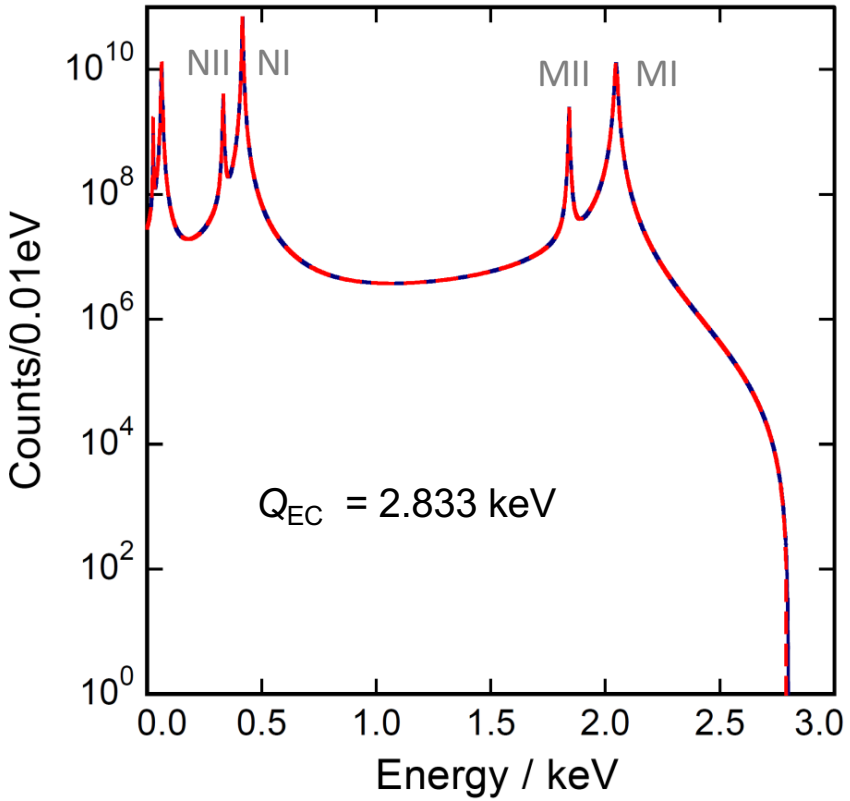

fraction of counts in endpoint region

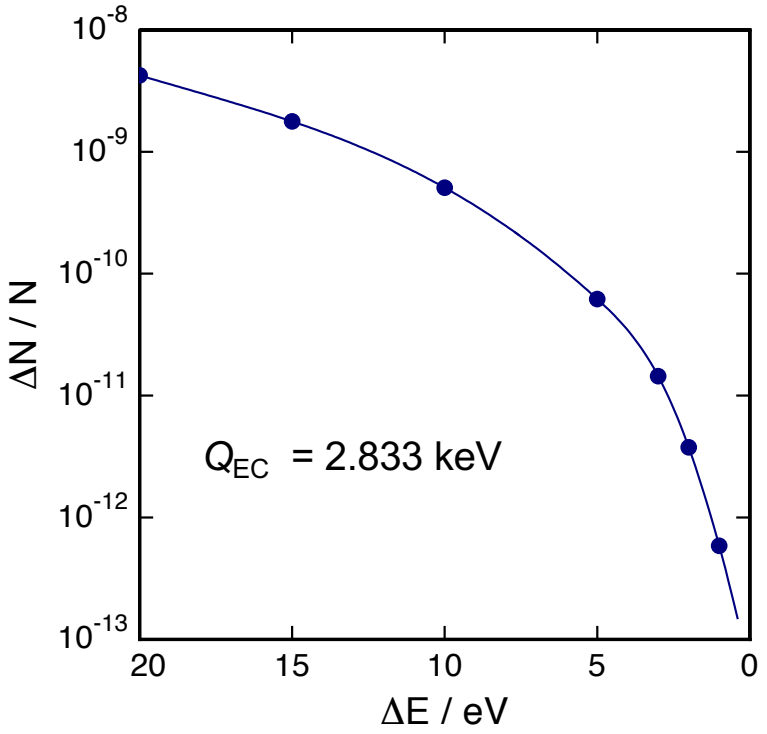

in last 1 eV interval only 6×10^{-13} counts

more than 10^{14} total number of counts needed

Expected Sensitivity for $\Delta E_{\mathrm{FWHM}} = 3$ eV and $f_{\mathrm{pu}} = 10^{-5}$

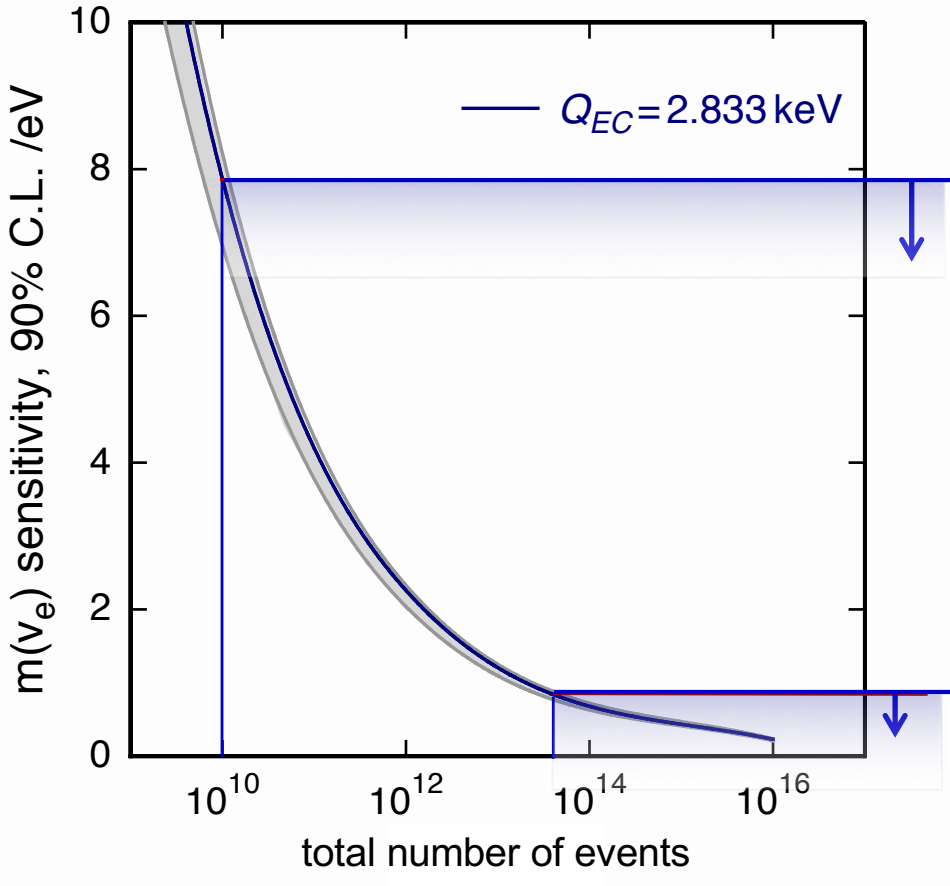

ECHo-1k

2 x 50 pixel x 10 Bq

4 months → 10^{10} events

sub 10 eV resolution

ECHo-1M

50 x 2000 pixel x 10 Bq

24 months → 6 x 10^{13} events

sub 1 eV resolution

Requirements For Sub-eV Sensitivity: Scalability

ECHo-1k: ~ 50 detectors → ECHo-1M: > 50.000 detectors → . . .

how to read out a large number of detectors ?

single channel readout:

10 wires, 2 SQUIDs, 1 electronics

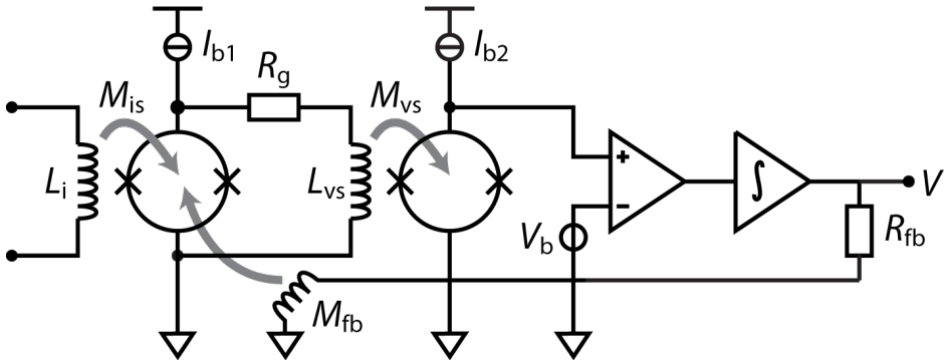

number of wires
parasitic heat load
costs
complexity
} ~ N

multiplexed readout:

~ 1000 detectors per readout cannel

possible schemes: FDM, CDM, TDM, ...

readout techology of ECHo

scalability

Frequency Domain Multiplexing

idea: detector signal is modulated on a GHz carrier

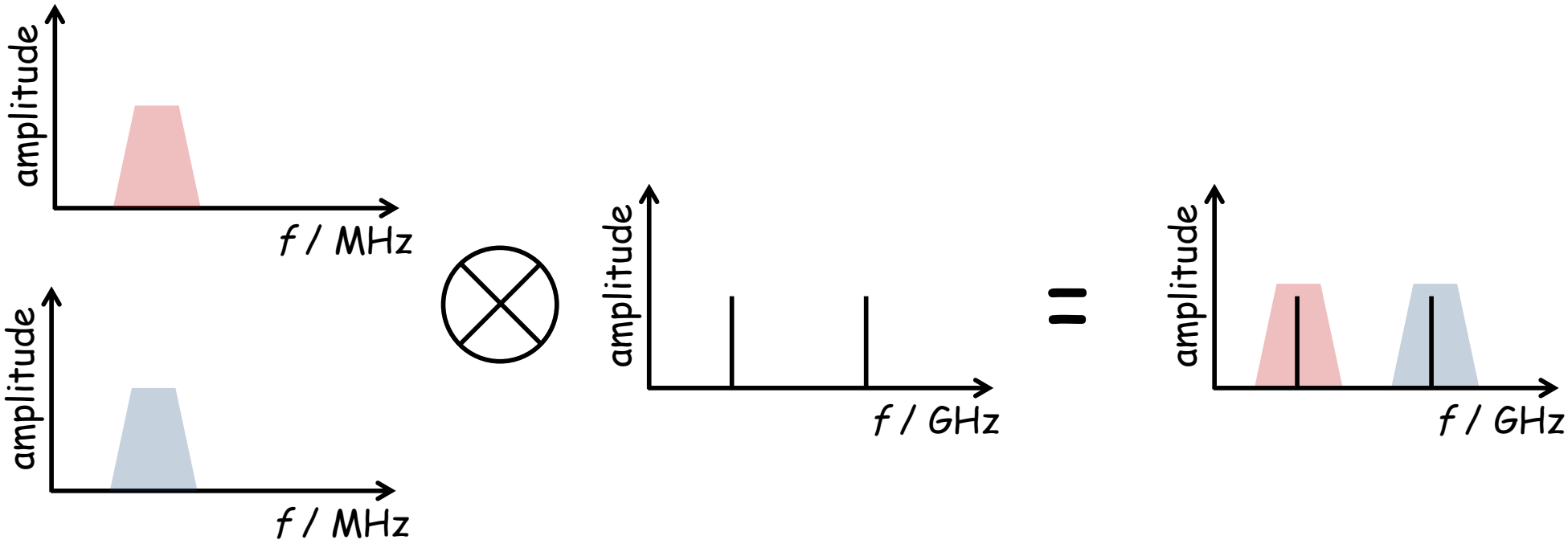

different carrier frequencies

non-linear element for mixing

Microwave SQUID Multiplexer (μMUX)

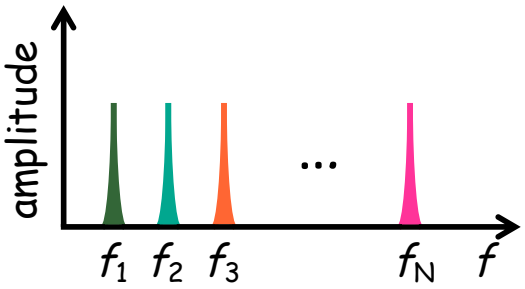

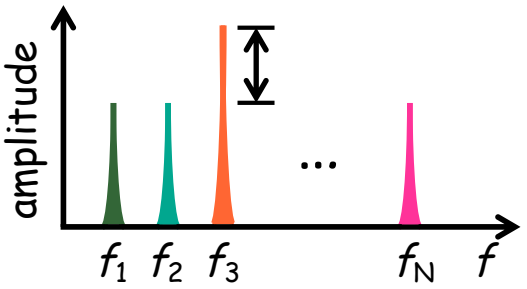

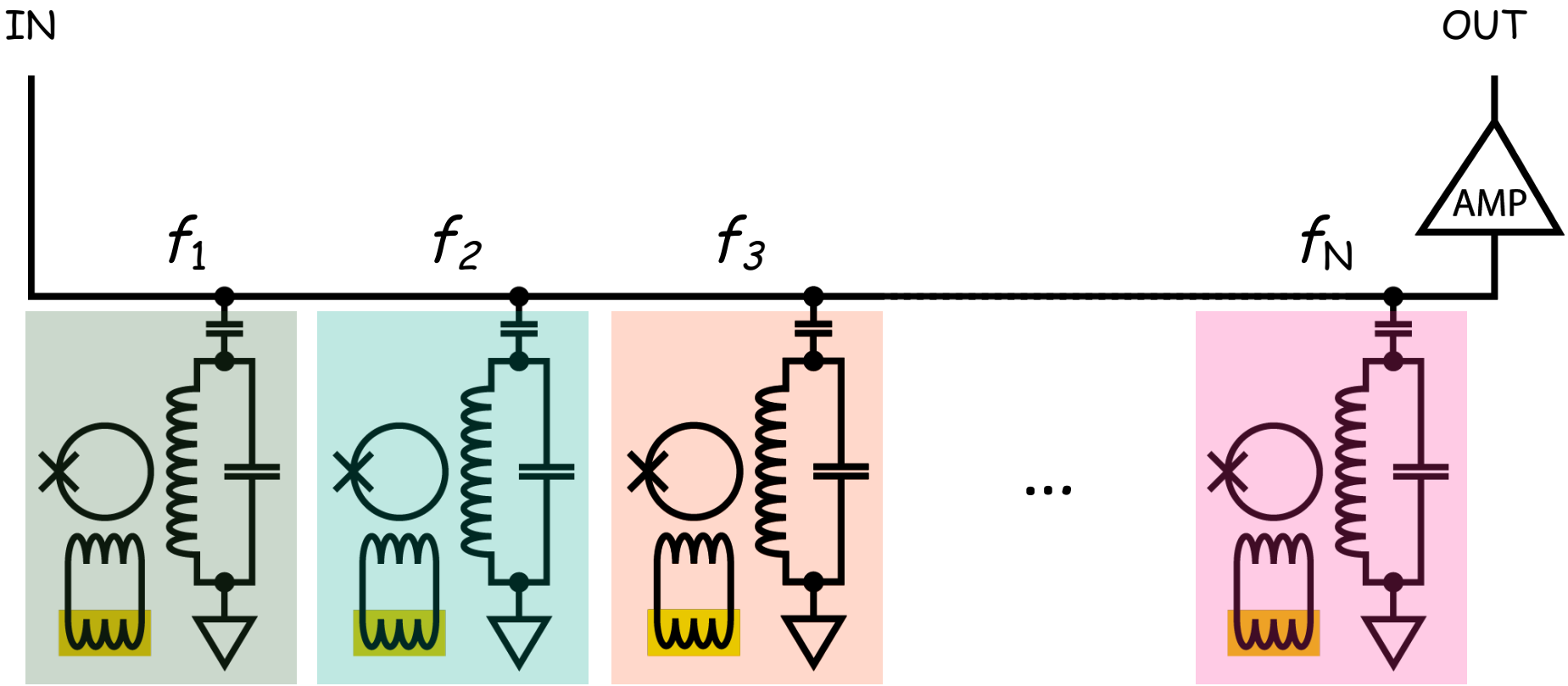

S. Kempf, *et al.*, J. Low. Temp. Phys. **175**, 850 (2014)

Frequency Domain Multiplexing: Software Defined Radio

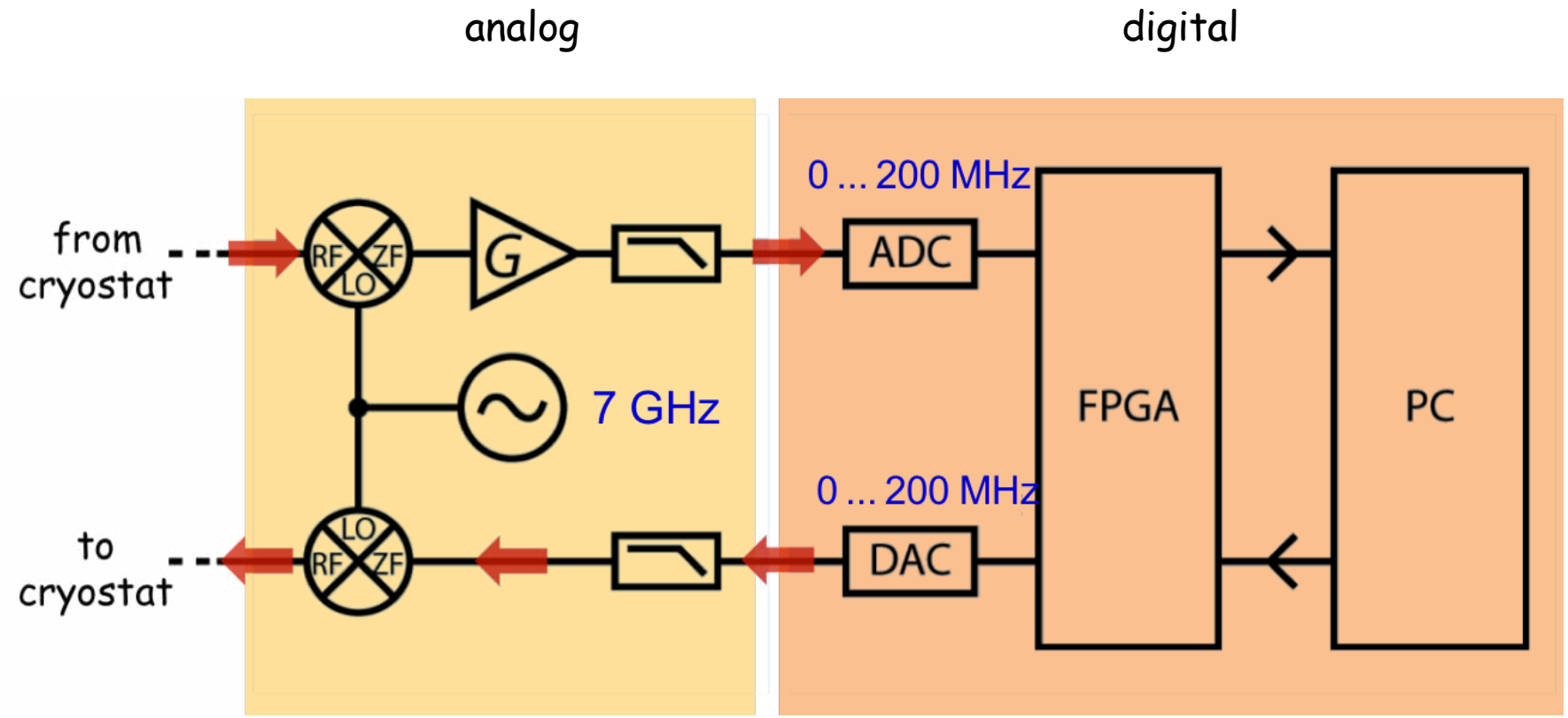

first fully functional system expected in 4 to 6 months

Joint development with
M. Weber, (KIT)
J. Becker (KIT)
U. Kebschull (Uni Frankfurt)

Frequency Domain Multiplexing: First Results

μMUX64: 64 pixel microwave muxing prototype

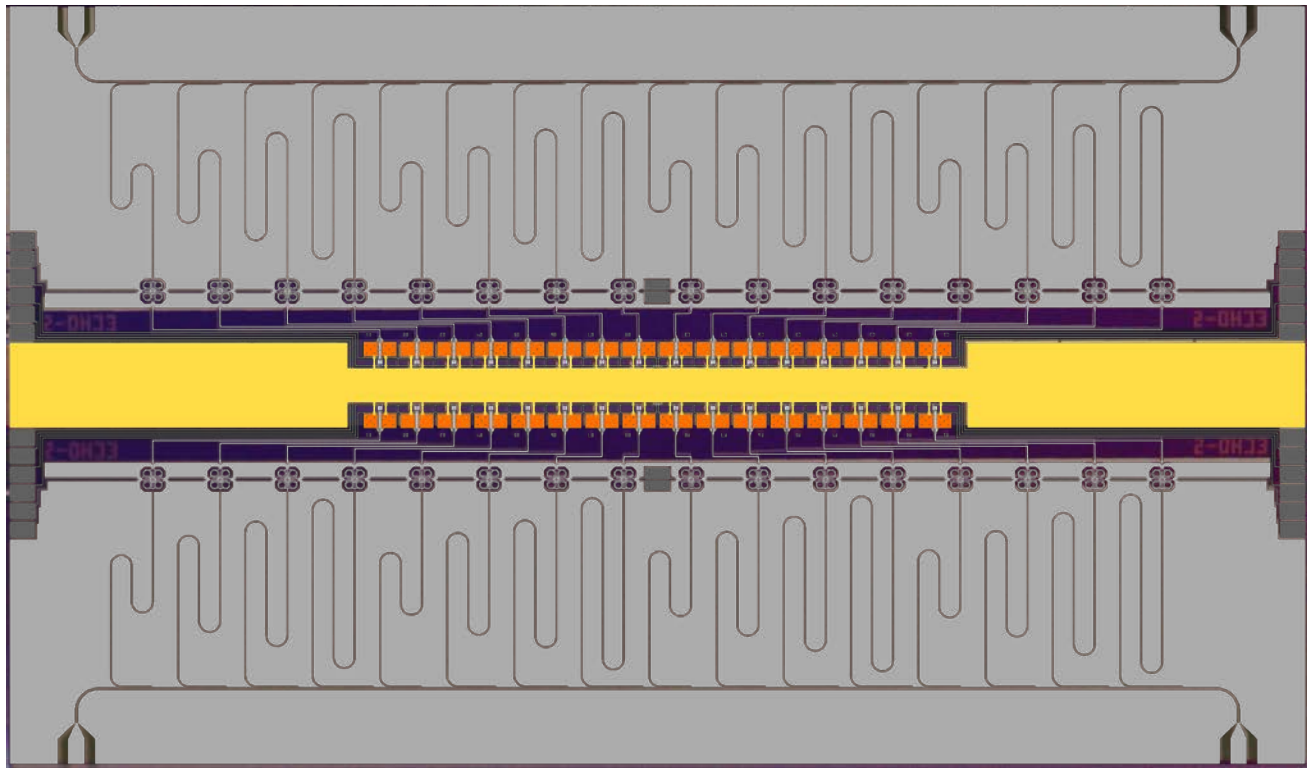

18 photolithographic layers

Frequency Domain Multiplexing: First Results

μMUX64: 64 pixel microwave muxing prototype

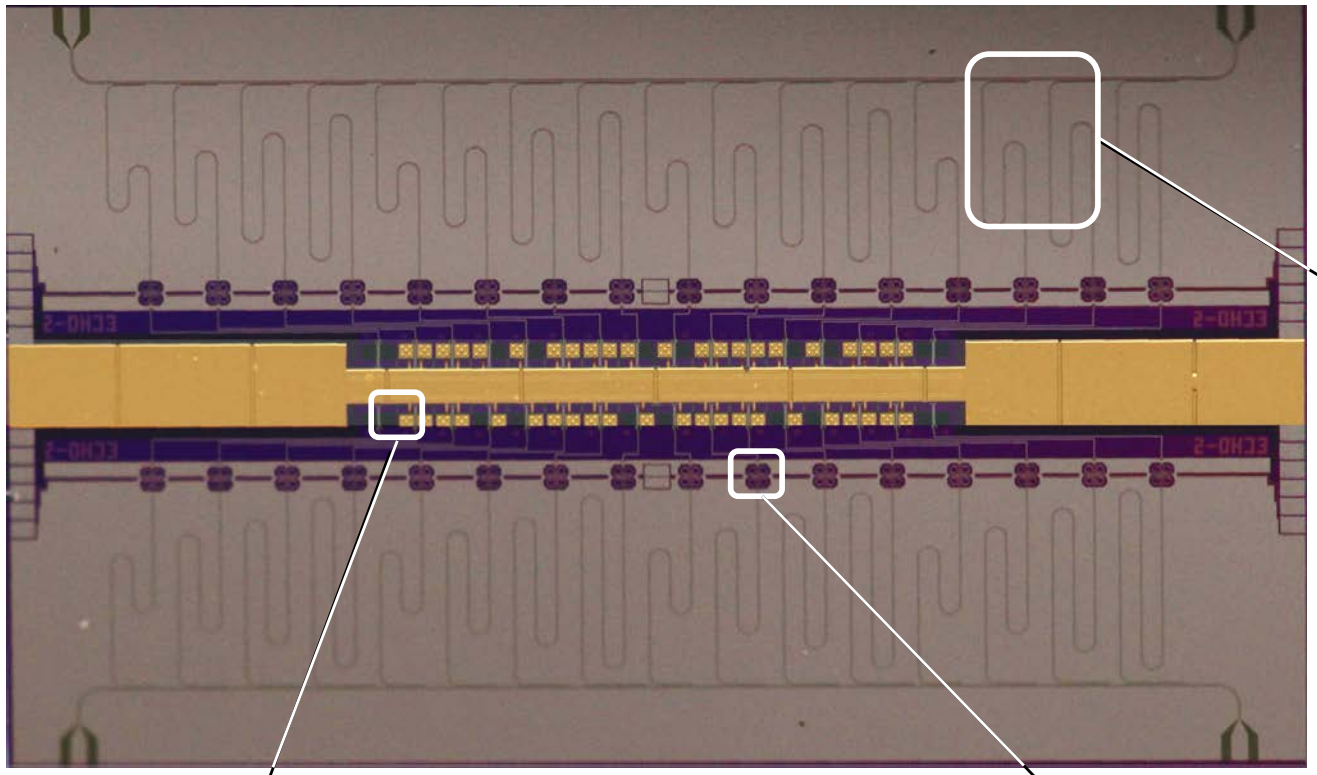

λ/4 resonantors

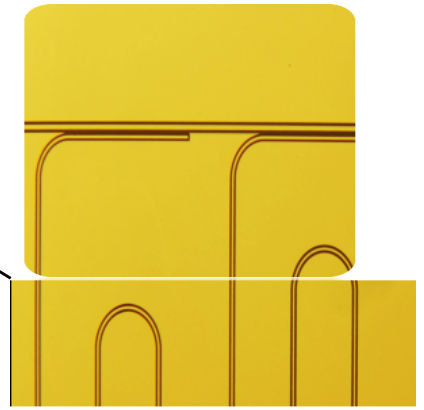

18 photolithographic layers

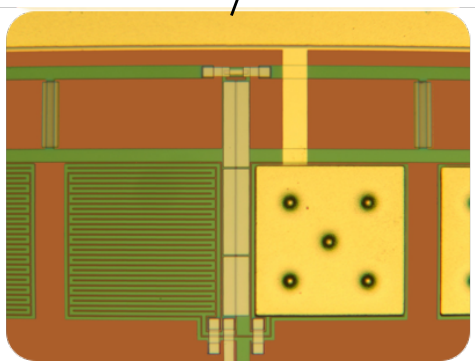

MMC
meander detector

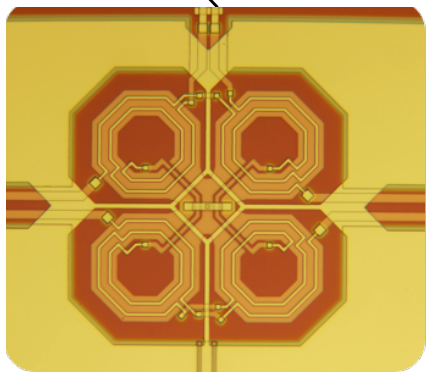

un-shunted rf-SQUID